Drainage Timescale Estimates and Storage Change Analysis on a Basin Scale

A THESIS
SUBMITTED TO THE GRADUATE SCHOOL
OF THE UNIVERSITY OF MINNESOTA
BY

Xiang Li

IN PARTIAL FULFILLMENT OF THE REQUIREMENTS
FOR THE DEGREE OF
MASTER SCIENCE

Dr. John L. Nieber

June 2020

Acknowledgement

Thanks to the Legislative Citizen Commission of Minnesota Resources (LCCMR) for funding this work. The principle investigator, Dr. John Nieber, who is also my advisor, put trust in me and offered me this valuable research opportunity. I would like to express my deepest appreciation to Dr. John Nieber for his instruction throughout my master career. My pursuit of academic interest in both hydrology and computer science will not have been possible without his generosity and support to allow me take courses in those fields for my master degree. I'm also extremely grateful to his patience, instructive guidance. It is really an honor for me to investigate the classic and popular baseflow recession analysis approach in this thesis, which was first proposed by Dr. John Nieber and his advisor Dr. Wilfried Brutsaert in 1977. He opened this fantastic hydrology world to me and I am hooked forever.

I would like to extend my sincere thanks to my committee members, Dr. Bruce Wilson, Dr. Diana Karwan and Dr. Vipin Kumar for their insights and suggestions to this thesis and my career development. I am also grateful to the hydrologist Jared Trost for his perfect and seamless collaboration. Many thanks to the assistant scientist Kerry Holmberg, phD student Francisco Lahoud, both of whom were in the research team and helped me during the research.

Finally, I would like to give my very profound gratitude to my parents. Their emotional support and encouragement have always been accompanying me throughout years of study. Without their education and efforts for shaping my confident, optimistic and endurant personalities, I would never accomplish what I have done so far. Thank you.

Abstract

The groundwater travel time depicts the characteristic timescale of the catchment drainage process and is therefore also known as drainage timescale (*K*). Catchment drainage timescale can be estimated empirically from recession flow analysis as well as from hydraulic theory. Applicability of K is critical in groundwater hydrology, such as, estimation to groundwater storage change. The groundwater storage change estimation allows to assess risks for potential flood and droughts and to provide action guidelines for water managers to adjust water needs under increasingly intense population pressure. On account of the importance of K in catchment hydrology, it brings the necessity for the research on *K*. This thesis conducts two analyses for K for 17 HUC-8 watersheds in central Minnesota. First, the unknown agreement between empirically obtained drainage timescales and the groundwater theory is confirmed statistically. From theoretical analysis, K is dependent on geomorphic features and hydrological conditions from the contributing unconfined aquifer, such as watershed area, stream length, saturated thickness, aquifer slope, hydrologic conductivity. A satisfactory statistical result and the interpretation are obtained showing the general agreement of the K obtained from the recession analysis and the groundwater theory expression. Although the aquifer thickness' contribution to regression results are inexplicit, the relationship strength of stream length, watershed drainage area, aquifer slope and aquifer transmissivity against K is characterized by statistical coefficients and signs. Second, applicability of K in annual groundwater storage change estimate is validated with a unique approach, which computes groundwater storage change by interpolating water tables' temporal deviations (WT method). An overall agreement regarding the magnitude of order and the trend confirms the applicability of K in annual groundwater storage change analysis. We identify 3 watersheds where the groundwater storage change estimated from K does not conform to the storage change prediction from the WT method. An attempt to explain this observed

discrepancy is based on the quality and seasonal completeness of discharge data, which impacts the recession analysis. But the comparison consistency is observed for the remaining watersheds in the study area. Among them, for 4 watersheds, the storage change estimated from K correlates very well with that calculated from WT method, which is indicated by the correlation coefficient over 0.7.

Contents

List of Figures

List of Tables

1. Introduction

Surface hydrology has been frequently investigated to study precipitation, evapotranspiration and streamflow under various climate situations (Shiklomanov 2003), but research into groundwater systems is more limited due to the sparseness of historical observations. The intrinsic spatial heterogeneity of both the vadose zone and the phreatic zone also makes it difficult to quantify groundwater storage (Rupp and Selker 2005; Troch et al. 2013). Nevertheless, as a large portion of global freshwater resources, groundwater is the most critical component of the terrestrial water budget. It outstrips other hydrological components in magnitude and practical availability (Brutsaert 2008).

Groundwater contributions to streamflow are of crucial importance for studying regional hydrological responses. The streamflow hydrograph, including rising limb and recession limbs, records the temporal discharge variation and hence presents a powerful analytical technique for catchment studies (Thomas, Vogel, and Famiglietti 2015). Generally, the recession curve, at least part of which is maintained from aquifer storage, tells about the interaction between surface water and groundwater. Accordingly, it serves as a valuable tool for both aquifer behavior studies and other areas of water resource management, such as irrigation management and hydroelectric power production (Arciniega-esparza et al. 2017).

Classic baseflow recession analysis is essential for quantifying and understanding groundwater drainage processes (Tallaksen 1995). Characteristic drainage timescale (denoted as K), also denoted as groundwater travel time, is derived from baseflow recession analysis empirically. One of its potential applications is long term groundwater storage change analysis, which has been applied worldwide (Brutsaert 2010; Gao et al. 2015; Zhang et al. 2014). However, the validation is performed by comparing the calculated long-term groundwater storage change against monitoring well's water level heights due to the difficulty of obtaining the 'observation' data of groundwater storage. This thesis examines the groundwater storage change analysis by yielding an actual groundwater storage

volume based on regional water table interpolation scheme. It is the first purpose of this thesis to validate the power of *K* in annual groundwater storage change estimation. Application of this analysis has also facilitated the temporal downscaling of the current long-term groundwater storage change estimate approach to the annual scale. As groundwater resources are in lack of observation data, estimation of annual groundwater storage change serves to improve current groundwater monitoring systems and water resources management.

In addition to the application of *K*, the insight into *K* itself is of great importance for studying catchment drainage properties. But the research into *K* remains difficult due to collective behaviors of the drainage process on a catchment scale. Both temporal and spatial variability observed in drainage events obstruct a comprehensive view of *K*. The intriguing question of *K* in groundwater drainage modeling becomes "What are the influential and dominant catchment characteristics that could not only elaborate the mechanisms behind *K* but also interpret the variability of *K* across watersheds?". The second purpose of this thesis is to preliminarily answer this question by validating the consistency between empirical recession analysis and groundwater theory in an attempt to discover controlling factors for *K* on a basin scale. This is of interest because investigating *K* on a basin scale allows the systematic understanding about hydrological responses from the complex groundwater drainage system, accounting for the regional spatial heterogeneity in drainage properties and hydrogeological conditions. If the validation procedure confirms the existence of controlling factors about *K*, an alternative becomes possible to estimate *K* from these controlling factors for basin studies.

2. Literature Review

Catchment scale hydrological processes are difficult for modeling as the complex catchment system is hard to characterize. Hydrologic response from both the unsaturated and saturated zone are complicated due to the intrinsic spatial heterogeneity of soils, vegetation and aquifers (Biswas, Das Majumdar, and Banerjee 2014; Johnson, E.A. and Dils 1956; Patnaik et al. 2015). Furthermore, groundwater movement pathways are not directly observable and are very difficult to predict. This constitutes the uniqueness of investigating groundwater drainage as we cannot identify subsurface water flow (Skaugen and Mengistu 2016). Nevertheless, groundwater discharge dynamics becomes somewhat observable in regions where water table interacts with the landscape, such as lakes and streams. Surface water fluctuation in these areas, where groundwater discharges into, allows the potential to study drainage characteristics. Particularly, for the discharge fed mainly from the drainage of the riparian aquifer in the upper basin, an approach to investigate basin groundwater dynamics is developed, which is baseflow recession analysis (Brutsaert and Nieber 1977). Although the classic baseflow recession analysis gains its popularity from its simplicity, the analysis performance relies on the quality of low flow data, which in reality is commonly affected by hydrological processes in addition to groundwater discharge, including overland flow, shallow subsurface flow and evapotranspiration (Brutsaert and Nieber 1977). But the influence of these other processes may be ignored when baseflow recession analysis is evaluated based on theoretical groundwater discharge, derived under the framework of groundwater hydraulic theory. Analytical solutions to the Boussinesq equation are available for expressing groundwater discharge without the impact of other concurrent hydrologic processes.

2.1. Groundwater Hydraulic Theory

M.J. Boussinesq presented a landmark contribution to derive the groundwater discharge to streams (Boussinesq 1868). The Boussinesq equation is built upon the Dupuit-Forchheimer assumptions, which neglect the capillary effect

above the water table and form a free surface with atmospheric pressure (Brutsaert 1994). Groundwater flow is assumed to be proportional to the slope of the water surface and it is assumed that the flow is parallel to the bottom of the aquifer. Adopting the Dupuit-Forchheimer assumption allows to simplify the groundwater flow as the one-dimensional outflow from an unconfined rectangular aquifer overlying on an impermeable layer. Due to the difficulty to derive analytical solutions to the Boussinesq equation, other assumptions are made in terms of aquifer slope, initial conditions such as aquifer saturated thickness (Troch et al. 2013), and other spatial heterogeneity of hydraulic parameters (Rupp and Selker 2005). While a majority of researchers consider the horizontal aquifer for investigating the Boussinesq equation (Brutsaert 1994; Brutsaert and Nieber 1977; J.-Y. Parlange and Govindaraju 2000; Troch et al. 2013; W. L. Hogarth 1999), solutions considering a sloping aquifer are less common (Rupp and Selker 2006).

2.1.1. Horizontal aquifer

When a horizontal aquifer is considered, the expression for the flow per unit width is derived after vertically integrating Darcy's law over the saturated thickness.

$$q = -kh\frac{\partial h}{\partial x} \qquad (1)$$

where q is expressed as the flow rate per unit width of aquifer in the x direction, $h = h(x,t)$ is the saturated thickness, and k is the hydraulic conductivity parallel to the impermeable layer. The continuity equation applied to this situation is

$$\varphi\frac{\partial h}{\partial t} = -\frac{\partial q}{\partial x} + R \qquad (2)$$

where φ is drainable porosity, and R is the recharge rate. Both drainable porosity and recharge rate are assumed to be spatially constant for simplicity. The flow rate expression could be inserted into the continuity equation and yields the Boussinesq equation for a horizontal aquifer as shown in equation (3) (Boussinesq 1868).

$$\frac{\partial h}{\partial t} = -\frac{k}{\varphi}\frac{\partial}{\partial x}\left(h\frac{\partial h}{\partial x}\right) + \frac{R}{\varphi} \qquad (3)$$

Approximate analytical solutions are found with linearization approaches. Assuming h changes relatively negligibly in the x direction, h is taken out of the derivative term and is given as a constant equivalent to $p_B D$, where p_B is a weighting constant between 0 and 1 while D is initial saturated thickness of the aquifer. The Boussinesq equation is therefore linearized as in equation (4). Although other linearization methods are applicable (Brutsaert and Ibrahim 1966), substituting h with $p_B D$ is the most common linearization operation and has been widely adopted.

$$\frac{\partial h}{\partial t} = -\frac{k p_B D}{\varphi}\frac{\partial^2 h}{\partial x^2} + \frac{R}{\varphi} \qquad (4)$$

Analytical solutions for equation (3) and (4) are derived under various assumptions. The recharge term R is 0 since the discussion scope is limited to the groundwater flow without recharge. Initial and boundary conditions constrain the temporal duration of groundwater system, spanning from early time domain, intermediate time domain and late time domain. Details on the analytical solutions of the Boussinesq equation are beyond the thesis scope, but a review about general characteristics of Boussinesq equation analytical solutions are summarized below.

For horizontal aquifers, Boussinesq offered a solution assuming an initially saturated horizontal aquifer with an abrupt water table drawdown to the channel. The initial and boundary conditions are below:

$$\begin{aligned} &h = D_c, x = 0, t \geq 0 \\ &\frac{\partial h}{\partial x} = 0, x = B, t \geq 0 \\ &h = D, 0 \leq x \leq B, t = 0 \end{aligned} \qquad (5)$$

where B is the width between the stream channel and the aquifer boundary, and D_c is the water depth within the stream. For the Boussinesq system, the original linear partial differential equation (equation (4)) is solved by the Fourier method to obtain the analytical solution as a summation of infinite series as follows.

$$q(t) = \frac{2kp_B D^2}{B} \sum_{n=1,3}^{\infty} \exp(-\frac{n^2\pi^2 kp_B Dt}{4B^2\varphi}) \quad (6)$$

where $B = \frac{A}{2L}$ is the breadth of the aquifer, D is the aquifer thickness, φ is the drainable porosity, k is the hydraulic conductivity. If only the first term within the summation part is preserved, this analytical solution represents the groundwater outflow during late time period as shown in equation (7).

$$q(t) = \frac{2kp_B D^2}{B} \exp(-\frac{\pi^2 kp_B Dt}{4B^2\varphi}) \quad (7)$$

Another analytical solution to the Boussinesq equation is specified when assuming that D_c in the water channel is 0. Initial water table shape is approximated by an inverse incomplete beta function. The groundwater outflow is expressed in equation (8) (Brutsaert and Ibrahim 1966; Brutsaert and Nieber 1977). This case corresponds to groundwater outflow in the intermediate and late time domain.

$$q(t) = \frac{0.862kD^2}{B}[1 + (\frac{1.115kD}{\varphi B^2})t]^{-2} \quad (8)$$

Polubarinove-Kochina proposed another analytical solution to equation (3) considering a similarly horizontal aquifer but its width is semi-infinite (Polubarinova-Kochina 1962).

$$\begin{aligned} &\frac{\partial h}{\partial t} = 0, x \to \infty, t \geq 0 \\ &h = D, x > 0, t = 0 \end{aligned} \quad (9)$$

Boussineq equation is reduced to an ordinary differential equation via the Boltzmann's transformation and yields an approximate analytical solution (Polubarinova-Kochina 1962). It is obtaind by applying the Blasius equation to the Boussinesq equation (Heaslet, M. A. 1961; Polubarinova-Kochina 1962; W. L. Hogarth 1999). The solution is valid when the discharge through the aquifer can proceed, as if the phreatic zone is semi-infinite wide (i.e., $B \to \infty$). Consequently, it is also referred to as the solution under short time domain as shown in equation (10).

$$q(t) = 0.3321(k\varphi)^{\frac{1}{2}} D^{\frac{3}{2}} t^{-\frac{1}{2}} \qquad (10)$$

Other approximate solutions to the Boussinesq equation are developed regarding different boundary and initial conditions as well as hydrologic characterization of the saturated zone (Daly and Porporato 2004; J.-Y. Parlange and Govindaraju 2000). When the effect of having the hydrologic conductivity decrease with the depth is explored, previous analytical solutions are extended by Rupp and Selker to refine the homogeneous aquifer. The power law function between the hydraulic conductivity and the height above bedrock (equation (11)) is inserted into equation (4) and solved for both early time domain and late time domain respectively (Rupp and Selker 2005).

$$k(d) = (k_D - k_0)(\frac{d}{D})^n + k_0 \qquad (11)$$

where *k(d)* is the depth varying hydrologic conductivity, *d* is the vertical depth, k_D and k_0 are upper and lower bounds of *k*, k_D is the hydrologic conductivity at depth *D*, while k_0 is *k* in the water table surface, and *n* is the assumed power term constant between depth and *k*. The solution for q under early time domain and late time domain is expressed below. For the early time outflow,

$$q(t) = \frac{1}{2}[\frac{1-2\mu}{(1-\mu)(n+2)(n+1)} k_D \varphi D^3]^{\frac{1}{2}} t^{-\frac{1}{2}} \qquad (12)$$

where μ is a constant specified within an approximate function satisfying homogeneous aquifer assumption during the derivation process to obtain $q(t)$ (Lockington 1997).

For the late time transient case,

$$q(t) = \frac{B_n k_D D^2}{(n+3)(n+1)B[1+\frac{B_n^2}{2(n+3)}\frac{k_D D}{\varphi B^2} t]^{\frac{n+2}{n+1}}} \qquad (13)$$

where B_n is the beta function in a form of

$$B_n = Beta(\frac{n+2}{n+3}, \frac{1}{2}) = \int_0^1 t^{\frac{n+2}{n+3}-1}(1-t)^{\frac{1}{2}-1}dt \quad (14)$$

2.1.2. Sloping Aquifer

Let α denote the aquifer slope when a sloping aquifer is considered. The Dupuit-Forchheimer assumption assumes that water flow is parallel to the underlying impermeable layer (Jacob Bear 1972). The integrated Darcy equation becomes

$$q = -kh(\cos\alpha \frac{\partial h}{\partial x} + \sin\alpha) \quad (15)$$

Inserting the flow rate expression into the continuity equation yields the Boussinesq equation for a sloping aquifer. Adopting the linearization assumption that h varies little along x, and substituting h with $p_B D$ yields the linearized form of the Boussinesq equation for a sloping aquifer.

$$\varphi \frac{\partial h}{\partial t} = kp_B D\cos\alpha \frac{\partial^2 h}{\partial x^2} + k\sin\alpha \frac{\partial h}{\partial x} + R \quad (16)$$

Under the condition specified in equation (5), Brutsaert gives the solution to equation (16) in a summation form of infinite series (Brutsaert 1994).

$$q(t) = \frac{2DV\varphi}{L^3} \sum_{s=1,2,\ldots}^{\infty} \frac{z_s^{\,2}[(2e^{-aL}\cos z_s) - 1]\exp[-V(\frac{z_s^{\,2}}{L^2} + \frac{U^2}{4V^2})t]}{(\frac{z_s^{\,2}}{L^2} + \frac{U^2}{4V^2} + \frac{U}{2VL})} \quad (17)$$

where $V = \frac{kp_B D\cos\alpha}{\varphi}$, $U = \frac{k\sin\alpha}{\varphi}$, $a = -\frac{U}{2V}$. As the phase term dependent on L (Brutsaert 1994). z_s is the sth root of the equation $\tan(z_s) = \frac{z_s}{aL}$.

2.2. Recession Flow Analysis

Recession flow analysis is the analysis to study catchment characteristics based on recession flow (Brutsaert and Nieber 1977; Kirchner 2009; Shaw and Riha 2012; Stoelzle, Stahl, and Weiler 2013; Tallaksen 1995). It leverages the recession period in hydrograph (Lyon et al. 2015; Tallaksen 1995; Troch et al. 2013). This

approach is defined by a non-linear storage-discharge relationship assumption, which underlies the theoretical basis to derive *K*. The well-known function to reveal relationships between recession rate and discharge is the dominant principle behind the recession analysis.

$$-\frac{dQ_b}{dt} = f(Q_b) \qquad (18)$$

where Q_b is the recession baseflow while f is an arbitrary function. Low flow characteristics are capable to reflect the groundwater storage as the flow observation is fed by upstream riparian aquifer outflows. Connecting equation (18) with water storage is essential to the catchment hydrological analysis. Considering a water balance equation

$$\frac{dS}{dt} = P - ET - Q \qquad (19)$$

where S is water storage, P is precipitation, ET is evapotranspiration and Q is discharge. Coupling equation (18) and (19) indicates the application potential of recession analysis for watershed storage analysis under a storage discharge framework. Particularly, when recharge events are absent, baseflow recession analysis can be applied to infer basin drainage characteristics.

The history of recession flow analysis can be traced back to the 19th century (Boussinesq 1868), when theoretical groundwater flow was first considered for analysis due to the difficulty to distinguish flows from various resources. Based on Darcy's law and the Dupuit-Forchheimer assumption, the Boussinesq equation is difficult to solve due to its non-linearity.

Bypassing pure mathematical and physics aspects of recession flow, graphical methods, another recession analysis regime based on hydrograph data since the early 20th century, are applied to study recession by constructing a master recession curve. Graphical methods are commonly referred to the correlation method (Langbein 1937), the strip method (Toebes, C. 1964) and the tabulating method (Johnson, E.A. and Dils 1956). The correlation method examines the

correlation between Q_t and Q_{t+N} on natural scales. Q_{t+N} is the discharge N days later than *t*. It assumes the data points fit a simple exponential equation, from which recession characteristics are derived (Langbein 1937). The strip method superimposes individual recession curves collectively, from which the master recession curve is constructed. A group of individual recession curves are adjusted horizontally for the sake of maximal overlapping among every single recession. The mean line crossing a majority of overlapped recession points is the master recession curve (Toebes, C. 1964). Similar to the strip method, the tabulating method evaluates the individual recession event in the tabulator format. Individual recessions are recorded in the column and are adjusted vertically until they approximate with each other. The master curve is obtained by averaging all individual recessions horizontally (Johnson, E.A. and Dils 1956).

Combining the mathematical aspect from recession studies and historical graphical methods, in late 20th century, Brutsaert and Nieber made a landmark contribution to advance the recession analysis technique (Brutsaert and Nieber 1977). A general form of f in equation (18) could be expressed as the power law relationship.

$$-\frac{dQ_b}{dt} = \frac{Q_b^{\,b}}{K} \qquad (20)$$

where K is referred to as the drainage timescale, *b* is recession parameter. K is a function of geomorphic and hydraulic properties on a basin scale. *b* varies under different recession event duration circumstances. Many studies have confirmed the existence of the power law relationship indicated by equation (20) for watersheds under various geological settings (Brutsaert 1994; Troch et al. 2013). For the sake of understanding subsurface hydrological processes, parameters in equation (18) are applied for catchment analysis, such as long term groundwater storage change inference (Brutsaert 2008) and aquifer behavior investigation (Biswal and Nagesh Kumar 2014, 2015).

The advantage and innovation of this method is the elimination of the recession time reference. Instead of overlapping individual recession curves to fit a master recession curve, the data cloud in the space framed by $-\frac{dQ_b}{dt}$ and Q_b is explored for recession behavior examination. Since then, Brutsaert and Nieber (1977) recession analysis has been widely adopted for recession studies (Biswal and Marani 2014; Biswal and Nagesh Kumar 2015; Brutsaert 2008; Jachens et al. 2020; Lyon et al. 2015; Roques, Rupp, and Selker 2017; Rupp and Selker 2006; Shaw and Riha 2012).

2.3. Recession Parameters Discussion

Equation (18) and (20) are the general form for the recession flow analysis. Employing solutions to linearized Boussinesq equations, the exponent b and catchment travel time K could be expressed theoretically under specific conditions (Rupp and Selker 2006; Troch et al. 2013).

Rewriting the groundwater outflow after late time period (equation (7)) into the form of equation (20) yields with $b=1$. Equation (8), where an initially curvilinear (inverse beta function) water table surface is assumed, is substituted into equation (20) and yields $b=\frac{3}{2}$. For an infinitely wide aquifer, $b=3$ is derived when conducting recession analysis on the theoretical groundwater discharge as expressed in equation (10). Adopting the assumption of a heterogeneous aquifer where depth decreasing k is considered, the range of b is similar to homogeneous aquifer cases. For the late time transient case, $b=\frac{2n+3}{n+2}$ is determined by inserting equation (13) into equation (20). These derivations are obtained under an assumption of the horizontal aquifer. For the sloping aquifer assumption, a similar range of b is yielded from recession analysis. For late time domains, equation (17) is reduced to the first term, recession analysis in a form of equation (20) yields with $b=1$. Investigating the recession behavior of equation (17) in the early time yields

with $b = 3$ (Brutsaert 1994; Rupp and Selker 2006; Troch et al. 2013). These different *b* values rely on the time domain of groundwater outflow analytical solutions. It means that *b* in equation (20) is not a constant but dependent on the duration of groundwater drainages.

K could be expressed from numerous approximate analytical solutions of the Boussinesq equation in the recession analysis in the form of equation (20). For scenarios of the late time domain during recessions for horizontal aquifers, taking the first derivative of equation (7) and substituting it into equation (20) for investigating theoretical recession characteristics yields the *K* expression for a horizontal aquifer (equation (21)). Similarly, *K* expression for the sloping aquifer is derived as shown in equation (22). *K* is a lumped parameter variable dependent on basin geomorphic features and other hydraulic parameters. These expressions of *K* reflect the assumptions adopted for deriving Boussinesq solutions.

$$K = \frac{\varphi A^2}{\pi^2 p_B k D L^2} \qquad (21)$$

$$K = \frac{\varphi A^2}{\pi^2 p_B k D L^2 \cos\alpha [1 + (\frac{D}{\pi p_B})^2]} \qquad (22)$$

As indicated by equation (21) and (22), hydraulic theory assists for providing a comprehensive view into *K*. The complicated drainage system could be simplified to approximate analytical solutions for certain flow scenarios. The groundwater theory to derive *K* yields its physical and hydrologic interpretation explicitly. Nevertheless, as stated in the introduction section, the intriguing question for *K* nowadays is "What are the influential and dominant catchment characteristics that could not only elaborate the mechanisms behind *K* but also interpret the variability of *K* across watersheds?" Accordingly, analysis and modeling to answer this intriguing question of *K* is essential to progress the systematic understanding of groundwater drainage systems.

Among numerous controlling factors for *K*, recent catchment modeling contributions prove the ability of catchment geomorphological properties to influence hydrological responses (Biswal and Marani 2010, 2014; Biswal and Nagesh Kumar 2015). Distinct from the Boussinesq model, which models the drainage events based on physical interpretations, Biswal proposed ADN (Active Drainage Network), a conceptual process-based framework to study basin drainage processes based on quantitative comparisons against recession analysis results (Biswal and Marani 2010, 2014; Biswal and Nagesh Kumar 2014). Focusing on the spatial organization of basin streams, this ADN model incorporates the temporal evolution of the drainage network into the basin drainage study and discovers that these geomorphic features connect well to recession event parameter. Although the intriguing question is not completely answered by the ADN model, it exhibits the impacts to basin drainage behaviors from catchment geomorphic features.

2.4. Application in Groundwater Storage Change Analysis

K is critical for regional groundwater system analysis as it characterizes the dynamic recession events. It could be applied for regional water supply planning and water quality management. The universal storage discharge relations are described in a power law equation

$$S = Kq^m \qquad (23)$$

where S is the storage while q is the discharge. m and K are constants depending on the catchment physical properties. m ranges from 0.5 to 1. An objective determination for the unbiased estimate of m is difficult regarding the spatial heterogeneity as well as the temporal duration of the storage discharge relationship. Even though, the assumption of $m = 1$ has witnessed remarkably applicable results of the field data in drought flow analysis. An exponential decay of discharge is confirmed under this assumption. Consequently, most literature and research substitute the power law relation with the linear relationship between storage and discharge (Brutsaert 2008).

For regions where groundwater storage measurements are sparse, a reliable inference of groundwater storage change based on streamflow records is critical. As first proposed in 2008, Brutsaert proposed a recession based method to analyze groundwater storage change from streamflow recession characteristics and *K*. The long term change of the groundwater storage is estimated based on K as exhibited in equation (24).

$$\frac{dS}{dt} = K\frac{dy_{L7}}{dt} \qquad (24)$$

where y_{L7} is the annual lowest seven-day flow obtained from drought flow statistics. Specifically, a long-term groundwater storage change estimate could be yielded from K. This method is advantageous as it only needs the stream flow data for deriving groundwater storage change without acquisition of groundwater data. At present, streamflow data are abundant, including gauging station measurements, numerical simulation data from hydrological models and satellite data. These data recourses and advanced stream flow data collection techniques provide opportunities for implementing the Brutsaert method for estimating groundwater storage change. The applications in two Illinois states' watersheds has witnessed successful trend estimation agreements (Brutsaert 2008). This methodology has also been applied worldwide to catchments in Australia (Zhang et al. 2014), China (Gao et al. 2015) and eastern United States (Brutsaert 2010). Spanning a nearly 40 to 80 years' long period, in Australia, in the Loess Plateau in China as well as in the United Sates east of the Rocky Mountains, most selected catchments were estimated to have a negative storage trend. The observed general agreement between the drought flow statistics based approach and historical observation wells' records proves its applicability of K for deriving long term groundwater storage change although occasional disagreements are identified without detailed explanations (Brutsaert 2008, 2010). Testing the Brutsaert method lacks sufficient data to represent the groundwater storage change. Usually the estimated groundwater storage is underrepresented by the water level data for comparison purposes

(Brutsaert 2008, 2010; Gao et al. 2015), which motivates to test the applicability of Brutsaert method by calculating the actual groundwater storage change from water level data.

3. Hypothesis

This thesis conducts the research over testing the application of K in estimating storage change and the scientific discovery about basin drainage system characteristics. Two specific hypotheses are tested.

The first hypothesis is that the annual groundwater storage change estimate from the Brutsaert method matches the groundwater storage change computation. Although the applicability for the groundwater storage change has been confirmed on a longer term (Brutsaert 2010; Gao et al. 2015; Zhang et al. 2014), the validation on an annual basis has not been performed. Besides, previous research compared storage change estimation against groundwater level evolution instead of actual groundwater storage changes (Brutsaert 2008, 2010; Gao et al. 2015). Previous studies have shown that the long-term groundwater storage change and the corresponding water table elevation change are significantly correlated in the eastern United States (Brutsaert 2010), Australia (Zhang et al. 2014) and the Loess Plateau in China (Gao et al. 2015). The inferred long-term groundwater storage is confirmed to be correlated with the increasing or decreasing trend of water table regardless of the magnitude of the actual ground storage trend. The uniqueness of our proposed test is that it evaluates the estimated groundwater storage change by comparing against the groundwater storage change calculated from the spatial interpolation of water table and drainable porosity. This comparison is refined to the annual scale. To our knowledge, the groundwater storage calculated from the spatial interpolation approach serves as a refined validation to the Brutsaert method in terms of the storage change estimation magnitude, which is closely related with K and stream discharge.

The second hypothesis is that the relation between variables included in the physically-based derived expression for K could be examined by the data on a catchment scale. It furthers the understanding of K on a basin scale. The K derived from empirical recession analysis is hypothesized to have the same relation with watershed parameters as formed in the theoretical equation. The relation will be

evaluated statistically. Guided by the theoretical expression of K, the variables' contribution to the catchment drainage is investigated and quantified from multivariate analysis. Other research also inspires the selection of variables. Biswal and others discovered and justified the geomorphic controls over the basin recession events and drainage system (Biswal and Marani 2010; Biswal and Nagesh Kumar 2014, 2015). Therefore, this geomorphic control over basin drainage argument supports the inclution of A, L and D into the multivariate analysis. D (aquifer thickness), φ (drainable porosity), k (hydraulic conductivity), A (basin area) and L (stream length) impact K, the extent to which is hypothesized to approximate to what equation (21) and (22) indicate.

4. Methods

The two hypotheses outlined in chapter 3 focus on the parameter *K*. This chapter describes the method to test the two hypotheses. The explanation to derive *K* from recession analysis is given in section 4.1. Section 4.2 introduces the multivariate analysis to understand *K* on a catchment scale with the guidance of groundwater hydraulic theory (equation (21) and (22)). For the groundwater storage change analysis, the proposed validation method to compute groundwater storage based on water table elevation interpretation is introduced in section 4.3.

4.1. Recession Analysis

The recession analysis is based on stream flow data. The discharge at the watershed outlet collects the surface and subsurface runoff as well as groundwater discharge from the drainage area enclosed by the outlet gauging station and basin boundary. Preprocessing the discharge data is necessary and these steps are explained below. Following the 'Preprocess Discharge Data' section is the description of the Brutsaert-Nieber recession analysis.

4.1.1. Preprocess Discharge Data

A drainage network complicates the hydrological analysis on a basin scale especially for watersheds drained and intersected by an intricate river network. Particularly, high order streams originate from headwater catchments to the watershed mouth, fed by tributaries along the water course where multiple gauging stations are located for monitoring stream discharges. The gauging station in the main channel monitors an integration of upstream runoff, which includes tributary and headwater. However, this monitoring framework is not appropriate for a nested hydrologic analysis since the discharge from a small sub catchment might be of research interest but is not directly provided. In our study, the watersheds intersected by the Mississippi River is used as an illustration for an explicit problem definition (Figure 1).

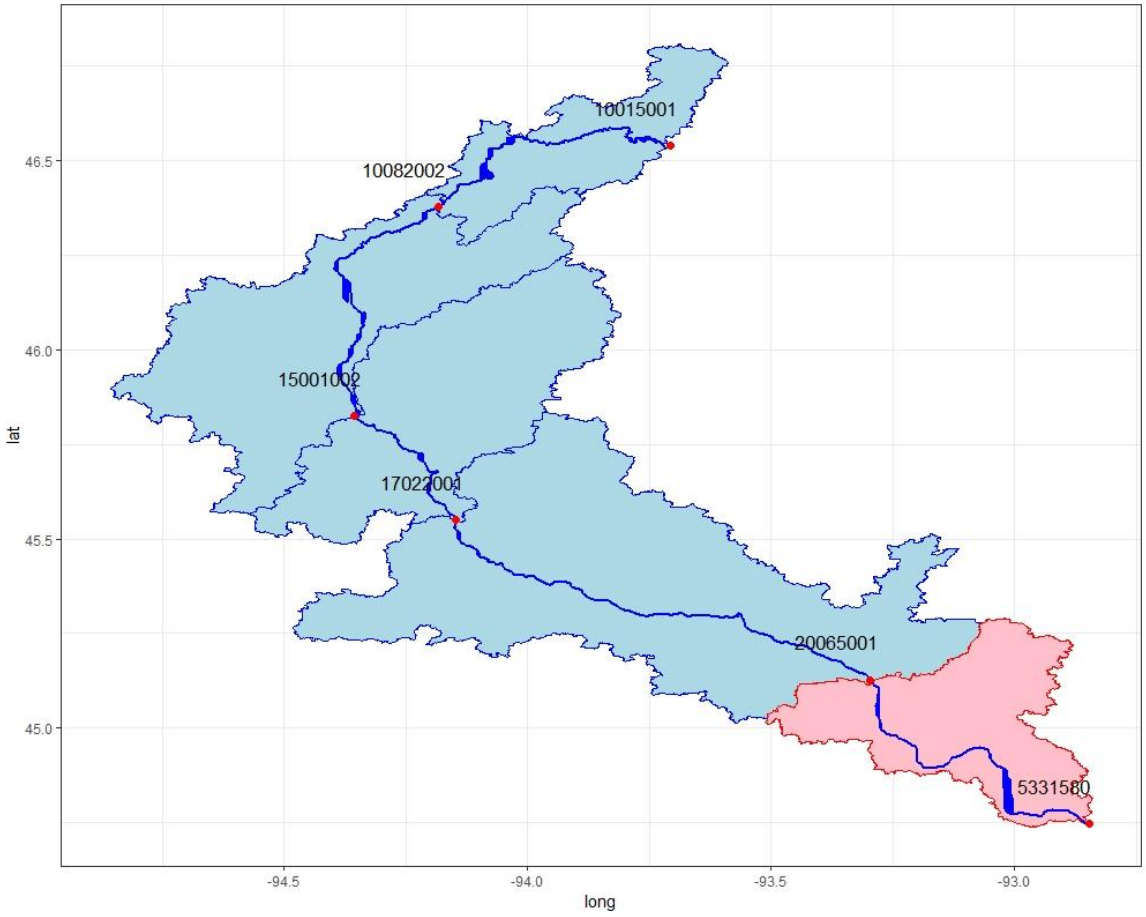

Figure 1. Upstream discharge contribution, illustrated by the watersheds intersected by the Mississippi River. Blue line is the Mississippi River. Gauging stations are represented by red dots. The target catchment is colored and outlined by red with downstream gauging station 5331580.

For the 5 watersheds crossed by the Mississippi River, the corresponding gauging station located at a specified pour point record both the discharge flux in the local Mississippi River segment channel, which is defined as the channel between the specific pour point gauging station and its nearest upstream gauging station, as well as the runoff from the upstream Mississippi River segment. For instance, the sub catchment with gauging station 5331580 is the target catchment, which is colored in red in Figure 1. Flow from the station 20065001 contributes to gauging station 5331580. Accordingly, the discharge monitored at 5331580 records the flow contributed by the target red area and the drainage area spanning from the Mississippi headwater to its nearest upstream gauging station 20065001. If the discharge data recorded at gauging station 5331580 is fed directly to the recession analysis, the inferred drainage characteristics will respond to an aggregation of catchments drained by the upstream Mississippi River, the course of which is scaled from the Mississippi River headwater to the gauging station 5331580. However, it is inconsistent with the spatial scope of the target red catchment. Therefore, removing the discharge contribution at gauging station 2006501 from the discharge at gauging station 5331580 will confirm that the drainage scope indicated by the discharge is consistent with the target catchment boundary, which is colored in red in Figure 1.

However, removing the upstream discharge is not straightforward. Considering the case at gauging station 5331580 and 20065001, calculating the discharge difference between those two gauging stations at the same date is hydrologically naïve since the temporal lag caused by surface water travel time is not negligible. The discharge at station 20065001 does not flow to the station 5331580 instantaneously. Accordingly, estimating the stream travel time from the stream velocity data is critical to remove redundant upstream runoff. A two-step procedure to remove redundant upstream runoff is proposed and explained below.

4.1.1.1. Surface water travel time estimate

For consistency, the watershed whose outlet gauging station is 5331580 is used for illustration purposes as shown in Figure 2. Let *P* denote the upstream gauging station and *R* denote the downstream gauging station. *Y* is the stream segment length between site *P* and *R*.

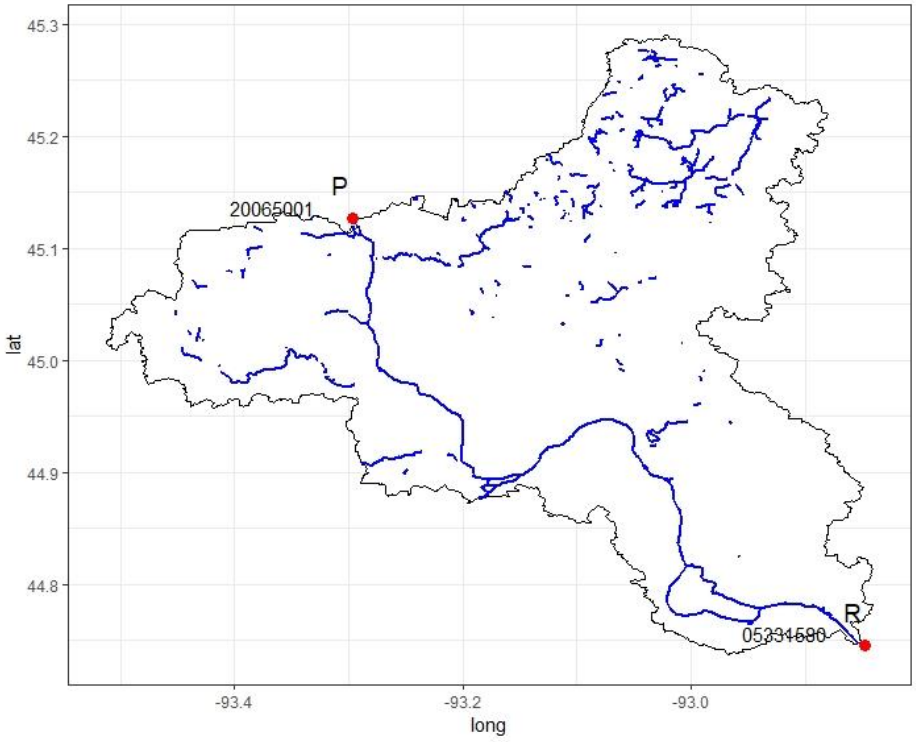

Figure 2. Redundant stream flow elimination illustration at the gauging site 5331580

Assumptions are made that the stream velocity is uniform along the river segment. It is also assumed that the stream velocity between upstream and downstream gauging stations is the average of stream velocities quantified at the two gauging stations. These two assumptions simplify the surface water travel time estimation remarkably.

Let v_{P_t} denote the stream velocity at gauging station *P* at time t and v_{R_t} denote the stream velocity at gauging station *R* at time t. The subscript t denotes a fixed date. The subscript $t+\Delta t$ denotes the date that upstream discharge at point *P* at time t arrives at gauging station *R*. Δt is the surface water travel time estimation. The problem is defined as that 'given a time series of v_{P_t} and v_{R_t}, what is the surface water travel time Δt at any given date t ?'. The travel time needs to be determined iteratively (Figure 3). For any given t an initial guess is made for Δt based on the flow at point P. This then determines the value of the discharge at point *R* to use in the flow averaging process. The value of Δt is then updated and the iterative process continues until the calculation steps converge on a final value of Δt. A user specified threshold ζ is used to determine when convergence is satisfied. In our case, ζ was set to 0.0001.

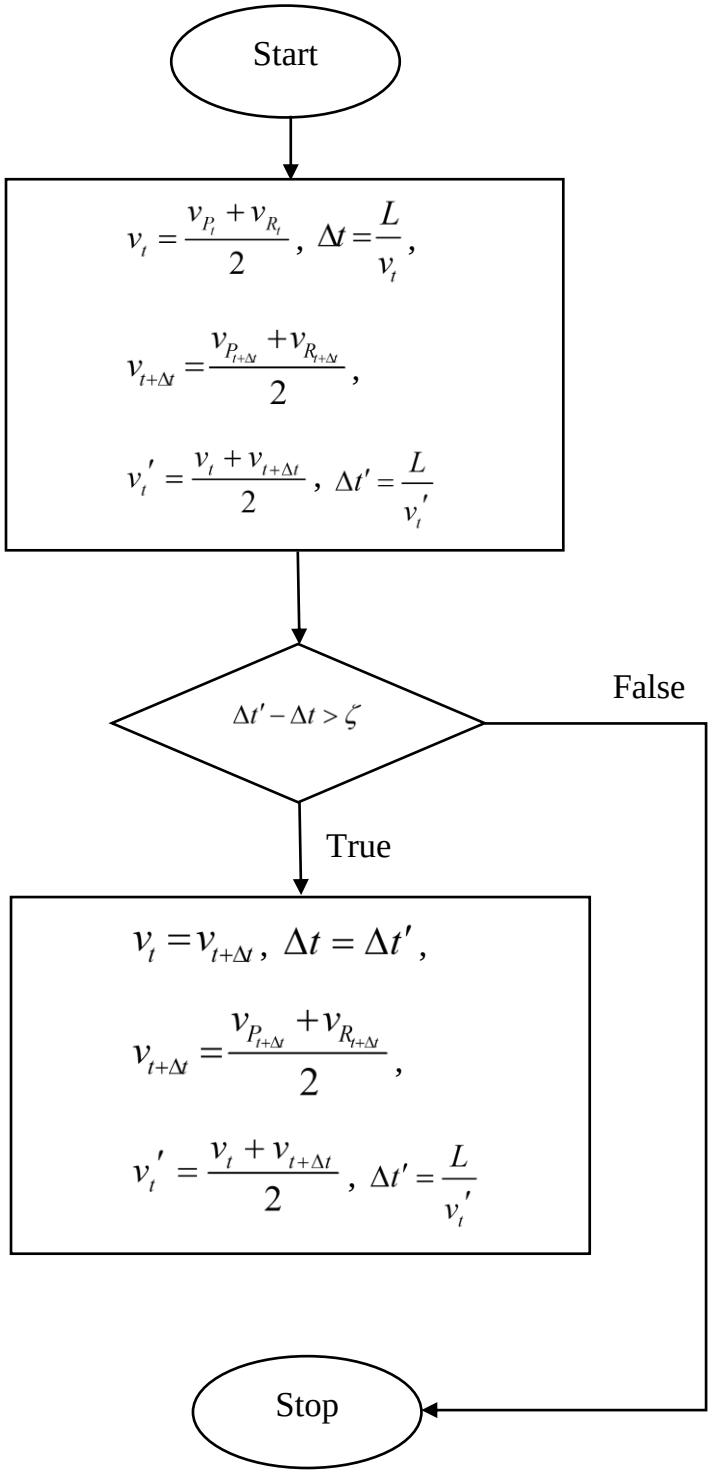

Figure 3. Flowchart showing the coding and application of the algorithm. The proposed approach iteratively estimates the surface water travel time between two gauging stations.

The typical magnitude for surface water travel time found in the analysis here ranged from 2 to 8 days. Δt is heuristically initialized as $\frac{L}{v_t}$, assuming the discharge from station *P* arrives at station *R* are the same in the initial guess. v_t is the average of stream velocities quantified of the gauging station *P* and *R* at time *t*. Δt is updated iteratively until the date for computing the mean velocity between upstream and downstream station is in accordance with the derived surface water travel time.

The stream velocity data was acquired from the USGS database. But the stream velocity data is sparser than the stream discharge. To remedy this sparseness of the stream velocity data, a linear regression between the discharge and the stream velocity was constructed for each gauge site. For one specific gauging site, in dates when both discharge data and stream velocity data were available, the linear regression model was built to predict stream velocity based on streamflow data. This linear regression model was applied for the same gauging station on dates for predicting stream velocity when streamflow data were available but velocity data were absent with the intention to complete the stream velocity data record. The linear models for 11 sites whose data were used for the upstream discharge elimination were all statistically significant. The regression performance for one specific gauging station, 12039001, is exhibited below (Figure 4). The R^2 was between 0.8 and 0.9 for all gauging stations except for the site 17022001, whose R^2 was 0.4.

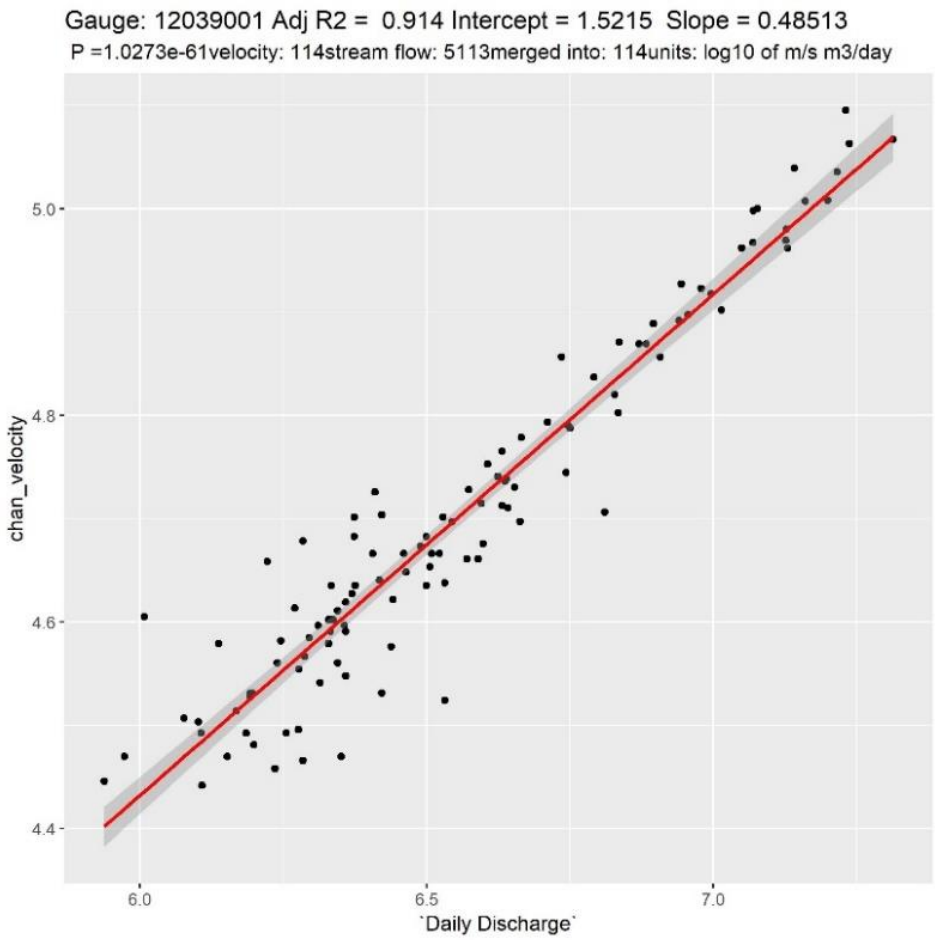

Figure 4. Linear regression between gauging station's discharge and stream velocity. The regression performance at site 12039001 is exhibited. Stream flow data is complete from 2002 January 1st to 2015 December 31st, which spans 5113 dates. But stream velocity data are present for only 114 dates. It should be noted that the regression is executed on logarithmic scale. Both p value and R^2 proves that the linear model is statistically significant and explains a large portion of the system variance.

4.1.1.2. Upstream discharge elimination

The upstream discharge that contributes to the watershed downstream outlet discharge on a certain date is traced back after the travel time $\Delta t'$ is determined (equation (26)). At the catchment outlet, point *R*, drainage area with respect to the corrected outlet discharge Q'_{R_t} is the watershed area. If travel time $\Delta t'$ is not an integer, $Q_{A_{t-\Delta t'}}$ is linearly interpolated between the discharges at two consecutive days, in which $t-\Delta t'$ lies. Let $t_0 \le t-\Delta t' \le t_1$ where t_0 and t_1 are two integers that are the lower bound and upper bound of $t-\Delta t'$ respectively. The linear interpolation is explained in the equation (25).

$$Q_{P_{t-\Delta t'}} = Q_{P_{t_0}} + (Q_{P_{t_1}} - Q_{P_{t_0}}) * (t-\Delta t'-t_0) \qquad (25)$$

$$Q'_{R_t} = Q_{R_t} - Q_{P_{t-\Delta t'}} \qquad (26)$$

The Mississippi River and other tributaries drain through the five watersheds whose gauging IDs are 10082002, 15001002, 17022001, 20065001 and 5331580. The reference to the gauging station map is Figure 8 in the section 5.1. These tributaries join with the Mississippi River at the confluence before reaching the watershed mouth. Especially for higher order tributaries whose flow route spans several watersheds, which is similar to what Figure 1 illustrates, their upstream discharge is necessary to remove from the watershed mouth gauging station since the recession analysis requires flow contributed by the associated watershed only. Accordingly, the upstream discharge elimination scheme is adopted for high order rivers in addition to the main stem of the Mississippi River. For the gauging station 5331580, upstream discharge recorded from the gauging station 20065001 (Mississippi River) and 5330920 (Minnesota River) is removed. For the gauging station 20065001, upstream discharge recorded from the gauging station 17022001 (Mississippi River) and 5280000 (Crow River) is eliminated. For the remaining 3 watersheds mentioned above, only the upstream discharge in the Mississippi River is removed.

Using the procedure described above the Q'_{R_t} values for the gauging station were calculated. Irrational negative discharges were observed to occur occasionally on certain dates (Figure 5). The discharge correction scheme applied to sites 5331580, 15001002 and 20065001 yielded very satisfactory results because the irrational negative discharge appeared to occur infrequently. The discharge correction for sites 17022001 and 10082002 yielded a greater number of negative discharges. For all cases the negative discharge values were set to zero to rationalize the discharge.

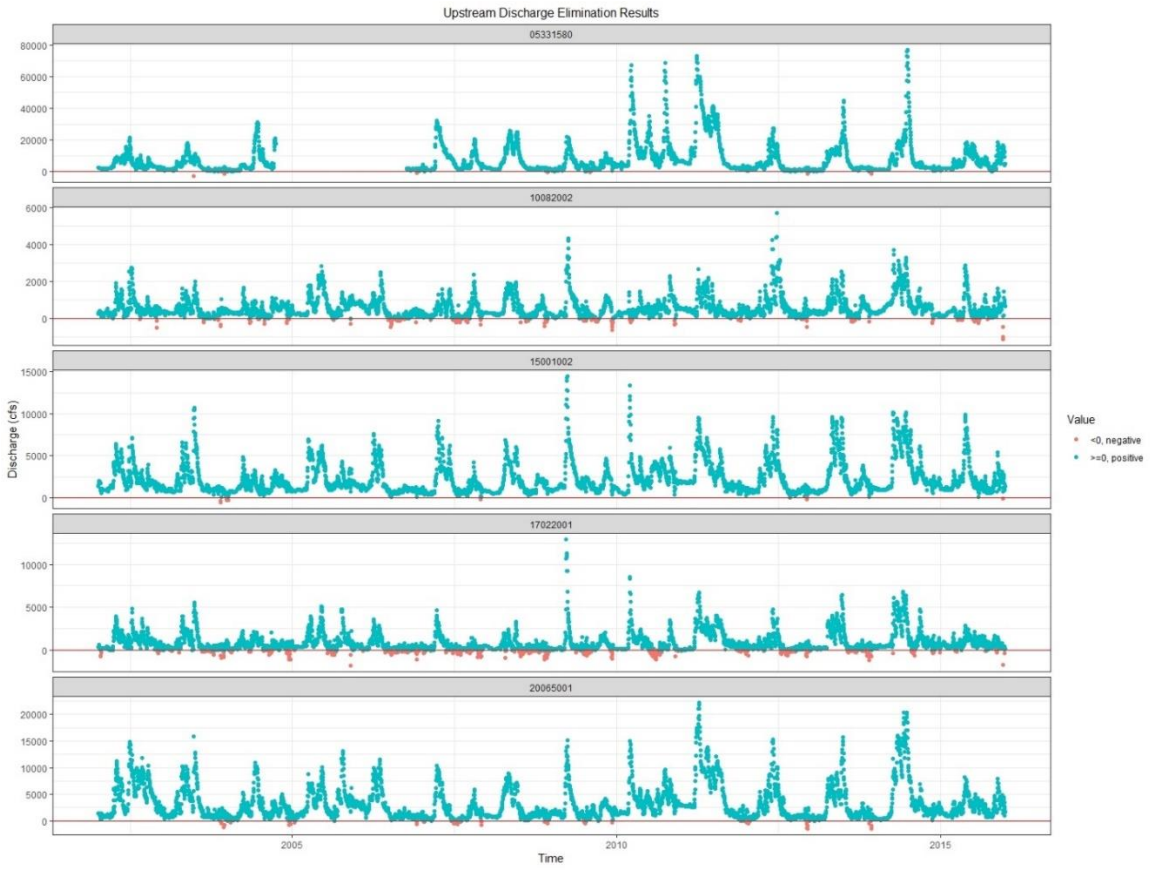

Figure 5. Discharge correction for five sites crossed by the Mississippi River, whose pour points IDs are 10082002, 15001002, 17022001, 20065001 and 5331580

4.1.2. Brutsaert-Nieber method

The Brutsaert-Nieber method is a classic recession analysis approach that's been widely adopted since the late 1970's. It is a two-step procedure involving filtering discharge data from the recession period and drawing log-log plot of -dQ/dt versus Q to fit the relationship quantified by equation (20). It gains advantage by removing time references among abundant recession events (Brutsaert and Nieber 1977). In equation (20), K and m are two constants that describe the aquifer behaviors, whose hydrologic interpretations could be also given under the context of the storage and discharge relationship as indicated by equation (23). A typical magnitude for K is 45 ± 15 days in large river basins (Brutsaert 2008). In order to depict the catchment behavior without recharge event impacts, the recession flow should be drought flow ideally, which means that storm runoff is absent. However, obtaining accurate baseflow from discharge data is difficult. Especially in large basins, the recharge events could not be fully captured by rain gauge networks.

The criterion for selecting recession flows from streamflow are complex (Brutsaert 2008; Kirchner 2009; Shaw and Riha 2012; Stoelzle et al. 2013). Vogel (Vogel and Kroll 1992) proposed a coarse recession criterion, whose input is merely streamflow data without other hydrology information. The stream flow under drying sequence is the recession. The streamflow with negative *dq/dt* are baseflow recessions. In contrast to the Vogel method, Brutsaert proposed to filter the stream flow data on a rule-based procedure considering precipitation event impacts (Brutsaert 2008). The Brutsaert criterion eliminates the streamflow data severely impacted by precipitation and recharge. The data points with positive and zero values of *dq/dt* are filtered out. Considering the duration of recharge, the two points before *dq/dt* becomes positive are removed and three points after last positive and zero *dq/dt* are eliminated. Three data points after major precipitation events are eliminated as well. Another detailed criterion takes evapotranspiration into account. For the recession limb of the hydrograph, the criterion based on hydrology

inequality is introduced. If $\frac{|P-AET|}{Q} < 0.1$, the discharge is defined as drought flow because the contribution from precipitation and evapotranspiration to streamflow is negligible, which is quantified as a ratio of 0.1 (Stoelzle et al. 2013). P is the precipitation, AET is the actual evapotranspiration while Q is the streamflow. This inequality is only checked for the recession limb with negative *dq/dt*. For simplicity, this criterion is referred to in this thesis as the hydrology inequality criterion. Furthermore, Shaw and Riha (Shaw and Riha 2012) scrutinizes the recession flow quantitatively and constrains the recharge events' duration. The first 30% of every recession period is removed to omit the impact of potential storm runoff events on streamflow recession.

In this thesis, the hydrology inequality recession criterion and the classic Brutsaert recession criterion are both applied for recession analysis and their impacts for the recession analysis are reported and analyzed.

The classic baseflow recession analysis is based on a cloud of recession points filtered based on the recession criteria (Brutsaert and Nieber 1977). An example of the recession analysis for the gauging station 5338500 is shown below (Figure 6). To produce this plot, the recession rate, denoted as *dq/dt*, against the discharge is plotted. Values of $\frac{q_{i-1}-q_{i+1}}{2}$ are plotted against q_i in a log-log space (where i refers to the daily flow on i-th day). Allowing for the unavoidable error from the raw data, such as the measurement error in low flow periods, a straight line with the fixed slope is established after keeping five percent of the points below it (Brutsaert 2008). This slope value corresponds to the b value in equation (20) as the form of classic recession analysis. Although b can be determined as a range of values from various Boussinesq solutions, $b = 1$ corresponding the late time domain is determined since the impact of recharge events on the prepared recession data have been removed. The slope of the straight line is fixed to be 1. Consequently, the

intercept of the straight line is calculated and represents K. For the gauging station 5338500, K is calculated as $10^{1.664}$ days, or 46 days.

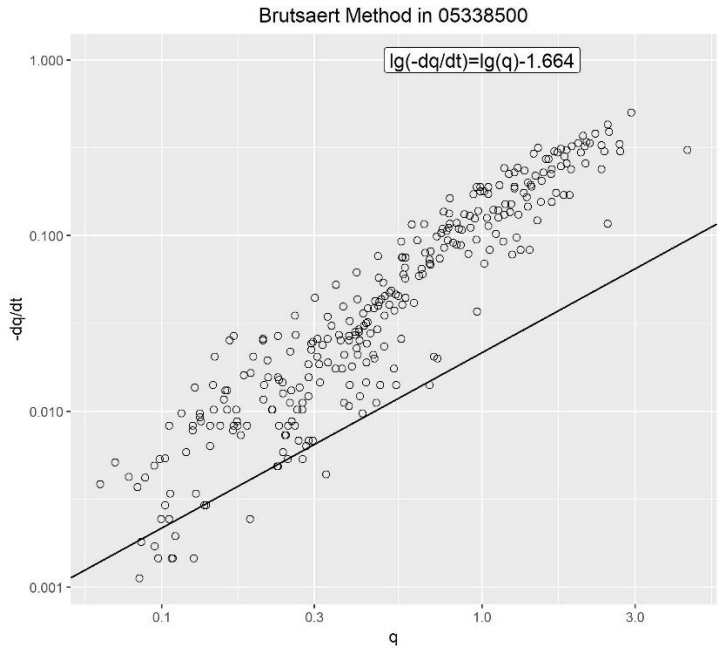

Figure 6. Baseflow recession analysis for the gauging station 5338500 as an example to illustrate the recession analysis procedure. Data clouds for the recession flow are plotted. A straight line by fixing the slope to be 1 is plotted to find the intercept, which is the characteristic drainage timescale. (Units of discharge (q): mm)

4.2. Multivariate Analysis

To answer the intriguing question mentioned in chapter 1, a multivariate analysis is conducted to attempt to find influential characteristics that impact *K* on a catchment scale. Recharge events impact catchment drainage characteristics and could potentially change the magnitude of drainage timescale under extreme rainfall events (Rupp and Selker 2005, 2006). Instead of investigating the relationship between recharges and *K*, this thesis focuses on catchment characteristics that might impact *K*. The theoretical expression of *K*, as indicated from the Boussinesq equation, provides guidelines to select those potentially influential catchment variables (Brutsaert 2008; Troch et al. 2013). As the groundwater discharge solution to the Boussinesq equation varies across various drainage scenarios specified by boundary and initial conditions, the scope of Boussinesq solutions is limited to the late time domain so that the impact of recharge events is minimized. Therefore, the *K* expressed theoretically in a form of equation (21) and (22) is valuable for selecting independent variables in the multivariate analysis.

A multiple linear regression model is utilized for analyzing the response of watershed characteristics to the basin drainage timescale. The independent variables are aquifer transmissivity *T*, aquifer saturated thickness *D*, bedrock slope α, stream length *L* and watershed area *A*. Aquifer transmissivity was extracted from a transmissivity raster from the National Water Availability and Use Program in USGS (Bayless et al. 2017). Aquifer thickness was the vertical difference between DNR water table map (Adams 2016) and the statewide bedrock topology (Olsen, Bruce M.; Mossler 1982). It was assumed that aquifer saturated thickness remained constant from 2002 to 2015. For the bedrock slope, the slope for each pixel cell in the bedrock topology data was calculated first and an average slope for the entire watershed pixel cell raster represents the watershed bedrock slope. For geomorphic features, watershed area was the enclosed area of each delineated catchment polygon. Stream length was the summation of all linear perennial stream features from MNDNR hydrography datasets. Following the watercourse naming dictionary

requirements in MNDNR (Zeb Thomas 2014), the perennial stream features consist of perennial streams, perennial ditches and the centerline of rivers. Due to the difficulty of estimating drainable porosity, the drainable porosity was not included as an independent variable in the analysis.

4.3. Ground Water Storage Computation

As one innovation of this thesis, the groundwater storage was computed for validating the applicability of the Brutsaert method to infer groundwater storage change from *K*. It is worth emphasizing that only a small portion of groundwater storage is hydrologically active with surface components. In contrast, deep groundwater has very limited hydrological communication with surface water components. Because the Brutsaert method infers the groundwater storage change from the drought flow characteristics, the change in deep groundwater storage is out of the scope that Brutsaert method is capable to estimate. Therefore, the Brutsaert method's applicability for groundwater storage change is evaluated by computing the active groundwater storage change instead of total groundwater storage change. Active groundwater storage is computed based on annual water table interpolation (for simplicity, 'WT method' is used for the statement of the hydrologic components calculated from the water table interpolation) and annual porosity raster estimation.

4.3.1. Water Table Interpolation

Instead of interpolating the water table elevation, an innovative interpolation scheme was applied to capture the dynamic fluctuation of the water table surface by interpolating the deviation for each well's water level relative to a reference value. An annual water table map was then produced for each year by overlaying the interpolated deviation surface over the water table surface base map, which is a state-wide water table elevation map published by MNDNR. Details about this base map is expanded in the section 4.3.1.

$\delta u_{z,t}$, the temporal deviation of the water table from a reference value as expressed in equation (27), is interpolated across the study area. Let $u_{z,t}^{0}$ denote the

water table elevation measured at location *z* and time t. Location *z* represents a two-dimensional coordinate (*x*, *y*) in the landscape. The reference value is the temporal maximum of $u_{z,t}^0$ within the period of the record.

$$\delta u_{z,t} = u_{z,t}^0 - \max\{u_{z,t}^0\} \quad (27)$$

Interpolation is based on $\delta u_{z,t}$ instead of $u_{z,t}^0$. $\delta u_{z,t}$ is negative except for the period of water table record maximum, which is 0. A collection of varying water table data includes abundant data measured at wells and lakes. The water table deviation $\delta u_{z,t}$ is only calculated if *z* is situated at wells or lakes. Another hydrological constraint is that water levels are imposed for stream levels. Assuming the stream levels are invariant across the time, $\delta u_{z,t}$ is always 0 when *z* is at stream channels.

Kriging, Thiessen polygon and inverse distance weighting methods are widely adopted for water table interpolation (Longuevergne, Florsch, and Elsass 2007; Masoumi, Rezaei, and Maleki 2019). The inverse distance weighting method is applied in this thesis to be consistent with the method that MNDNR uses to produce the water table map (Adams 2016). A weighted average from adjacent measurements are calculated as the prediction.

$$\delta u_z = \begin{cases} \dfrac{\sum_{i=1}^{N} w_{z_i} \delta u_{z_i}}{\sum_{i=1}^{N} w_{z_i}}, d(z, z_i) \neq 0 \\ \delta u_{z_i}, d(z, z_i) = 0 \end{cases} \quad (28)$$

$$w_{z_i} = \frac{1}{d(z, z_i)^m} \quad (29)$$

where δu_z is the predicted water table deviation geo-located at *z*, and $d(z, z_i)$ is the distance between the interpolated point *z* and the point wise measurement at z_i. The power term *m* in the inverse distance weighting scheme is set as a default value of

2. The limit for the number of adjacent points accounted for the interpolation grid is 50.

Based on the inverse distance weighting scheme, the deviation spatial grid is generated. Adding the interpolation grid of this water level deviation to the MNDNR baseline water table map produces the annual water table map. The annual water table map is generated for each year from 2002 to 2015 with a spatial resolution of 30 meters.

4.3.2. Active Groundwater Computation

The computation described previously is on an annual basis. Annual active groundwater is defined as below:

$$V_{active_t} = (W_t - W_0) * \varphi \qquad (30)$$

where V_{active_t} is the active groundwater volume at time t, W_t is the water table elevation at time t, W_0 is the temporal minimum base map of the water table elevation, and φ is the porosity. The vertical thickness between W_t and W_0 is the active saturated zone, which oscillates significantly for each year. For a stack of water table elevations during the period of record, W_0 is the baseline elevation map of water table on a grid cell basis. Let $W_{0,z}$ denote the grid value of W_0 located at a specified grid location *z*, then

$$W_{0,z} = \min\{W_{t,z}\} - d \qquad (31)$$

A buffer zone, denoted as d, is created underneath the temporal minimum water table surface to account for the potential active saturated thickness, which might not be characterized by the spatial water table measurements owing to information reduction. Water levels data were preprocessed such that measurements at a specific location *z* were guaranteed to include at least one measurement per year. Water level measurements that did not satisfy this requirement was eliminated and regional water level information was reduced accordingly (Nieber 2020). d was empirically selected as 5 feet for this study. For each watershed, the active

groundwater storage is computed as the spatial mean of groundwater storage raster within the corresponding watershed.

Aquifer porosity is estimated based on surficial geology, the spatial coverage of which might not reach far down the base of the aquifer. However, because the focus is on the active ground storage, the porosity deep in the aquifer will have no significant effect on the estimation of change in storage. The active groundwater storage calculation is based on water table elevation, and the interpolation across the landscape will then inevitably include surface water storage at locations where water table meets the landscape at lakes and wetlands. However, this surface water storage is eliminated from the active groundwater storage by accounting for the spatial distribution of open surface water and setting the porosity of the areas covered by lakes and streams to be zero. The spatial distribution of surface water bodies is supplied by LANDSAT data via the Global Surface Water Project (European Commission 2018; Jean-Francois Pekel, Andrew Cottam, Noel Gorelick 2016). For the groundwater volume below the surface water bodies this assumption of zero porosity will lead to a small underestimation of groundwater volume, but with regard to the calculation of the change in groundwater storage this assumption will not produce any error.

5. Data

The study area covers 17 HUC-8 watersheds in central Minnesota. This section introduces the data available for conducting the recession analysis, water storage change analysis and the multivariate analysis to interpret K. Except for the watershed re-delineation steps executed in ArcMap, other spatial and non-spatial data were processed in Rstudio 3.5.3. The raster data extraction step was completed with the R package 'exactextractr'. Rasterization procedure was executed with the R package 'fasterize'.

5.1. Study Area

This study focuses on the regional hydrology from 2002 to 2015. The annual precipitation for the study area from 2002 to 2015 ranges from 610 mm to 950 mm. The annual actual evapotranspiration for the study area from 2002 to 2015 ranges from 480 mm to 580 mm (Nieber 2020).

The study area originally includes 17 HUC-8 watersheds in central Minnesota as shown in Figure 7. Gauging stations are not placed exactly at the pour point of each HUC-8 watershed, which poses difficulties for interpreting recession analysis results, especially for the 4 watersheds crossed by the Mississippi River as shown in Figure 7. Drainage characteristics analyzed from recession analysis is derived on the streamflow data, which reflects the drainage area where downstream streamflow is accumulated. If the analyzed gauging station is not situated at its watershed mouth, then the spatial scope, which is recognized between the drainage area enclosed by this gauging station and the watershed boundary, should be excluded for interpreting the recession analysis result. This insight brings the necessity to re-delineate the drainage boundaries for each downstream gauging station in the study area for a comprehensive understanding of recession analysis.

The watershed re-delineation was executed in ArcMap 10.6.1. The Arc toolbox from Arcmap requires DEM data and user specified pour points for the delineation. DEM data are published by MNDNR derived from Lidar data. DEMs are standardized to 30 meter regular grid cells (Adams 2016).

Pour points, flow direction and flow accumulation grids, which are processed from DEMs, are prepared for the final watershed delineation step. Flow accumulation grids identify the number of upstream cells for each grid. Due to digital errors of DEMs, it is possible that user specified pour points are not placed at the highest flow accumulation grid nearby in the downstream direction, which is risky for the watershed delineation. Accounting for this geo placement error of pour points, snap points are defined based on a user defined distance that connects them to the closest cell of highest flow accumulation. The program searches for the highest flow accumulation cell in a search region centered at the pour point with the radius of the user defined distance. After trial and error testing, this distance was determined to be 900 meters such that the delineated watershed boundary was not overly reduced or expanded. The delineated watershed is named by the corresponding gauging station ID. As exhibited in Figure 8, the updated watershed boundary shows obvious discrepancies against the HUC-8 watersheds whose downstream gauging stations are not at the outlet, especially for the Mississippi River (Twin Cities) watershed. But for the watersheds whose outlet coincides with the gauging station, like the Wild Rice River Watershed, the newly delineated watershed boundary did not differentiate significantly from the original boundary.

Figure 7. Original 17 HUC-8 watersheds in central Minnesota (gauging stations are exhibited where red dots are downstream gauging stations while yellow dots are upstream gauging stations in the catchment).

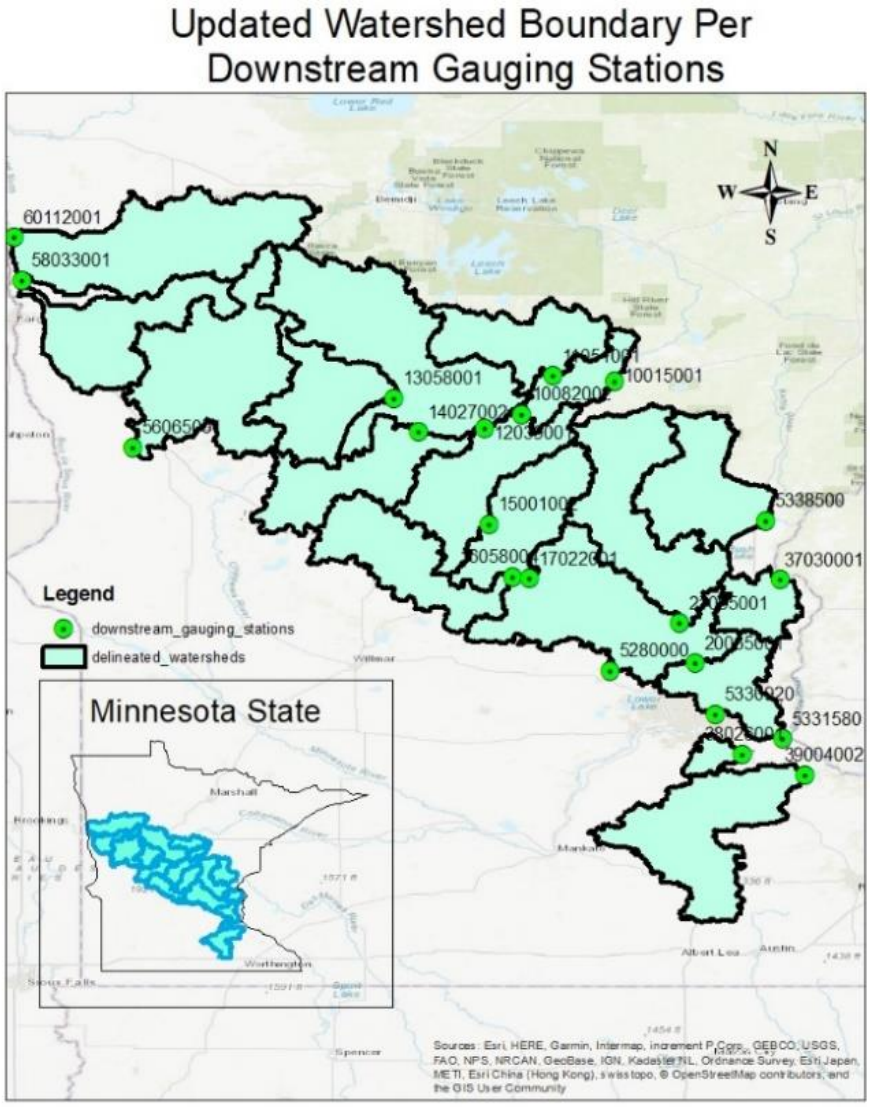

Figure 8. Updated watershed boundary, delineated in ArcMap 10.6.1 using Arc toolbox. Each watershed is re-delineated based on the watershed outlet gauging station IDs.

5.2. Recession Analysis Data

5.2.1. Precipitation and AET

Daily precipitation data were acquired from Daymet raster data. It supplies the daily gridded precipitation for the North American continent as a precipitation interpolation product (Thornton, P.E., M.M. Thornton 2018). The spatial resolution is 1 km. For each catchment, the daily precipitation was set to the mean of the precipitation raster values in the catchment polygon. Note that Daymet data treats every year as common year. Therefore, the February 29th will not occur from 2002 to 2015. Assumptions are made that the daily precipitation on Feb 29th on a leap year is the same as that on Feb 28th.

Actual evapotranspiration (AET) data is published by the Center for Integrated Data Analytics (CIDA) from USGS. The AET data is generated on a monthly basis with a 0.009 degree by 0.009 degree spatial resolution. AET is derived from an energy balance model, meteorological data and Moderate Resolution Imaging Spectroradiometer (MODIS) remote sensing thermal images. The operational Simplified Surface Energy Balance (SSEBop) model (Senay et al. 2013) is applied for producing AET in North America based on the reference ET estimated from MODIS. It combines a unique parametrization scheme from meteorological information (Senay et al. 2013; Velpuri et al. 2013).

5.2.2. Streamflow

The gauging stations and associated watershed boundaries are shown in Figure 8. Streamflow data are available from MNDNR (Minnesota Department of Natural Resources) and USGS (U.S. Geological Survey). Daily discharge data are a data product collected by the MNDNR, the MPCA (Minnesota Pollution Control Agency), the National weather service and the USGS. The geolocation and drainage area of the gauging stations are available as well.

A summary table about stream flow data is attached below to indicate their temporal coverage. In some cases, the DNR and USGS assigned different station IDs. In such cases, the DNR naming system is given priority. The discharge data

were prepared from 2002 to 2015 to match the study period for most gauging stations. A complete day counts from January 1st 2002 to December 31st 2015, yielding a total of 5113 days for most gauging stations. However, data gaps were recognized. Observations for the ice period are missing in certain stations. Some gauging stations instruments were installed after 2002. Then we removed from analysis all time periods when discharge was identified as affected by measurement error or unreliable interpolations. Therefore, the maximum number of day counts in the data was found to be 5113 days while the minimum day counts was 1671 days for (station 11051001).

Table 1. Stream flow data summary table

STATION ID	LONGITUDE	LATITUDE	PERIOD OF RECORD (days)	DRAINAGE AREA (km^2)
05331580	44.7458	-92.8478	4372	1530
05338500	45.8416	-92.9335	5113	2506
10082002	46.3778	-94.1838	5110	1013
11051001	46.5714	-94.0278	1671	2099
12039001	46.3050	-94.3775	5113	5155
13058001	46.4568	-94.8414	2795	2201
14027002	46.2883	-94.7158	1955	2368
15001002	45.8262	-94.3562	5111	2608
16058004	45.5598	-94.2338	5113	2540
17022001	45.5500	-94.1467	5111	2249
20065001	45.1268	-93.2965	5109	4263
21095001	45.3275	-93.3728	5113	3613
37030001	45.5443	-92.8588	2057	980
38026001	44.6668	-93.0553	5113	332
39004002	44.5645	-92.7317	5113	3479
56065001	46.2098	-96.1848	5113	4448
58033001	47.0498	-96.7537	2085	2513
60112001	47.2667	-96.7969	5113	4316

5.3. Water Storage Change Analysis Data

5.3.1. Water Table Interpolation

Section 4.3.1 explained how water table elevation was interpolated. This section introduces the data resources for the interpolation. The annual water table elevation is an overlay of the water table reference surface and the interpolation of water levels temporal anomalies for a certain year.

The reference map, which was published by MNDNR, is the state-wide water table elevation map across the Minnesota state derived from LiDAR. DNR water table map is capable to serve as the basis for regional hydrological study requiring detailed local data (Adams 2016). Detailed and cumbersome water table modeling work has been incorporated into the DNR water table map. Water levels data collected from the County Well Index database were incorporated directly for mapping the water levels in regions sufficient well data were available. Water levels in surface water bodies were assembled from statewide DEM data derived using LiDAR data. In regions with limited number of well data, water table elevation in saturated soils was evaluated from Natural Resources Conservation Service (NRCS) soil surveys. For the time varying well data, point measurements of water table level were collected from monitored observation wells and lake levels. Well data are a collection of the data from Minnesota County Well Index database, USGS, MNDNR and MDA. Lake level data were acquired from the USGS. For stream levels, they were assumed to be immutable. Consequently, in the preparation of data for the water level interpolation, temporal anomalies to water levels in streams, denoted as $\delta u_{z,t}$ in section 4.3.1, were fixed to be 0 (Nieber 2020). The spatial distribution of streams is published and is included in the DNR hydrography dataset as the stream confluence and flow direction dataset (https://mnnaturalresourceatlas.org/metadata/dnr_hydro_features_all.html).

5.3.2. Porosity Data

Raster porosity data was created by assigning porosity values based on digitized surficial geology texture. The surficial geological texture data is published by the MGS (Minnesota Geology Survey) as a compilation of previous maps, including the county geology atlas, surficial geology plates assessed from regional hydrogeological investigation and other MGS statewide maps (Gobbs and Goebel, 1982). As the final product by combining different data products, the sediment texture classification is created uniquely based on USDA terminology. The current surficial geology map has been revised for the discrepancy among textural classification in adjacent areas from previous maps although it is noted by the MGS that the database probably contains inaccurate information and is still undergoing editing. This contributes some uncertainty in the analysis of water storage change.

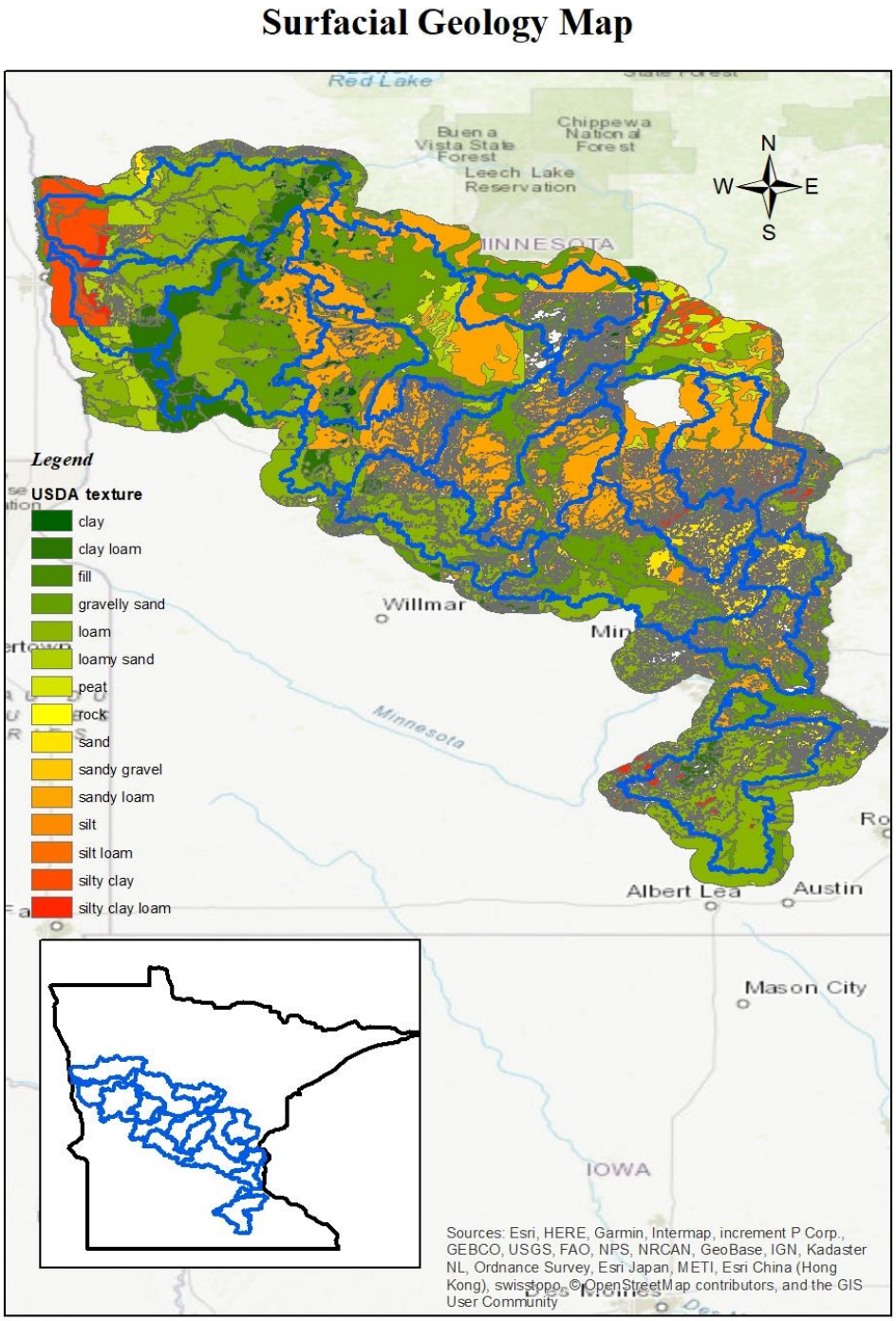

Figure 9. Surficial geology map covering the study area

A unique relation of porosity against the corresponding texture classification is constructed (Table 2). Approaches to estimate soil porosity differentiates for various soil textures. The porosity for peat is 0.8, which is the empirical value for undecomposed peat with active drainage status (Rezanezhad et al. 2016). The porosities of gravelly sand, rock and sandy gravel are empirical values determined from the porosity value table designed for structural engineering purposes (https://structx.com/Soil_Properties_006.html). Porosity estimates for other textures are calculated from dry bulk density and soil particle density using the following equation:

$$\theta = 1 - \frac{\rho_{bulk}}{\rho_{soil}} \qquad (32)$$

where θ is the porosity, ρ_{bulk} is the dry bulk density, and ρ_{soil} is the density of the soil solid. Dry bulk density and solid density for each soil texture category is obtained from soil survey data, published by natural resources conservation service in USDA database (https://www.nrcs.usda.gov/wps/portal/nrcs/detail/soils/survey/office/ssr10/tr/?cid=nrcs144p2_074844). The bulk density from USDA provides estimates for moderately consolidated soils. The derived porosity is defined as an upper bound and lower bound since the bulk density is given in a range of values. Therefore, the average of the derived porosity is used for assigning the porosity.

The surficial geology map covering the study area is shown in Figure 9. A large portion of the study area is covered by clay, gravel sand and loam. Sand and silt dominate the surficial geology in central and east part of the study area. A minority of catchments in the northwest part in the study area are covered by silt clay loam soil. The open water impacts are not involved in the surficial geology data. Even though, with the assistance of the global surface water dataset (Jean-Francois Pekel, Andrew Cottam, Noel Gorelick 2016), the porosity for the subsurface below lakes and streams is forced to be 0 in order to eliminate surface water storage contribution to the groundwater storage change. The change of groundwater in the

saturated layer below open water is negligible compared to the change of groundwater in the subsurface below the land surface where open water is absent. Therefore, it was also assumed that the saturated layer below the open water body, such as the saturated layer below the streambed, lake bottom, etc, does not store water components. Since the global surface water dataset maps the open water distribution every year, the generated porosity raster also varies somewhat over the years due to changes in the area of surface water.

Table 2. Porosity assignment table, rows corresponding to the USDA surficial texture definition.

USDA Texture	Porosity
clay	0.52
clay loam	0.49
gravelly sand	0.33
loam	0.43
loamy sand	0.39
peat	0.8
rock	0.15
sand	0.38
sandy gravel	0.27
sandy loam	0.41
silt	0.48
silt loam	0.46
silty clay	0.49
silty clay loam	0.47

5.3.3. Global Surface Water

Global surface water dataset is available as part of the Joint Reearch centre's Global Surface Water Dataset and is freely downloadable (https://global-surface-water.appspot.com/download). This dataset maps annual open water occurrences globally from 1984 to 2018 with the assist from remote sensing images. Three million Landsat satellite images were used to quantify and map the global surface water at 30 meter resolution (Jean-Francois Pekel, Andrew Cottam, Noel Gorelick 2016). In this dataset, the global surface is classified into four types, which are 'no observations', 'not water', 'seasonal water', and 'permanent water'. Including lakes and streams, open water's spatial distribution is represented by 'seasonal water' and 'permanent water' classes. Derived from occurrences and the spatial distribution of open water, both water history data and water occurrences data are available, which are supplied for both monthly scale and annual scale. For this thesis, the yearly history water data was used for correcting the porosity distribution to remove surface water contribution to the groundwater analysis. Porosities are modified to be 0 for calculating groundwater storage in the areas where the open water is present as indicated by the yearly global surface water history data. Consequently, surface water storage components are removed in calculating the groundwater storage change.

5.4. Multivariate Analysis Data

5.4.1. Transmissivity

Transmissivity is obtained from the National Water Availability and Use Program in USGS. A series of geospatial raster data sets for each hydrogeology variable are accessible (Bayless et al. 2017). The spatial coverage of this program is the glaciated United States. The study area presented in this thesis is included within this spatial coverage. The spatial resolution of those grids is 800 meters.

The National Water Availability and Use Program collects and standardizes the water-well drillers' records that are managed by states and are varying in size, formats and legal requirements. The hydrogeological data elements from this program include total thickness of coarse-grained sediment, equivalent transmissivity and hydraulic conductivity estimation. The hydrogeological raster data are derived with customized processing methods and an interpolation scheme (Arihood 2009). Although data quality is not guaranteed in states with too few water-well driller data, the satisfactory spatial density of water-well driller records in the study area assures reliable hydrogeological information.

Bayless estimated the transmissivity with two approaches, either from glacial sediment texture or from specific capacity. The background for his estimation approaches is summarized below. Texture based estimates standardize the water-well driller records and categorizes into 'aquifer' or 'non-aquifer' material based on USGS lithology codes. Transmissivity was then assigned numerically with generally representative values, which are assumed to distinguish between aquifer and non-aquifer materials for convenience. It is recommended in the report that users evaluate this data product by aquifer tests for applications to avoid potential scaling issues (Bayless et al. 2017). Specific capacity based estimation derives transmissivity by using a modified version of the Theis equation (Theis 1935). Based on the estimated transmissivity, a numerical iteration approach is applied to calculate the conductivity (Arihood 2009; Bayless et al. 2017).

The transmissivity raster estimated from the specific capacity is used for the study area to avoid the potential scaling issues noted in the texture based products (Bayless et al. 2017).

The transmissivity map shown in Figure 10 reflects the geologic structure within the study area. Unconsolidated sediments deposited by glaciers and lakes cover central Minnesota (Kanivetsky 1979). The northwest part in the study area, where the transmissivity is high, is characterized by buried sand aquifers and relatively extensive surficial sand plains as part of a thick layer of unconsolidated sediments overlying the bedrock. In this region, sand and gravel aquifers are common with thick glacial deposits (MNDNR 2016). For the central part in the study area, regional transmissivity is low. Loamy and silty soil with poor hydraulic conductivity is mostly observed. This area is also underlain by hard fractured bedrock that typically has limited groundwater yield (Kanivetsky 1979; Rader 2014). For the southeast part in the study area, the Mississippi River (Twin Cities) watershed (gauging ID 5331580), the Vermillion River Watershed (gauging ID 38026001) are underlain by sedimentary bedrocks with good aquifer properties, which represents a locally permeable aquifer pattern. In the Cannon River Watershed (gauging ID 39004002), the transmissivity is relatively low since the glacial sediments are typically clayey and contain to a limited extent surficial sand aquifers (Kanivetsky 1979).

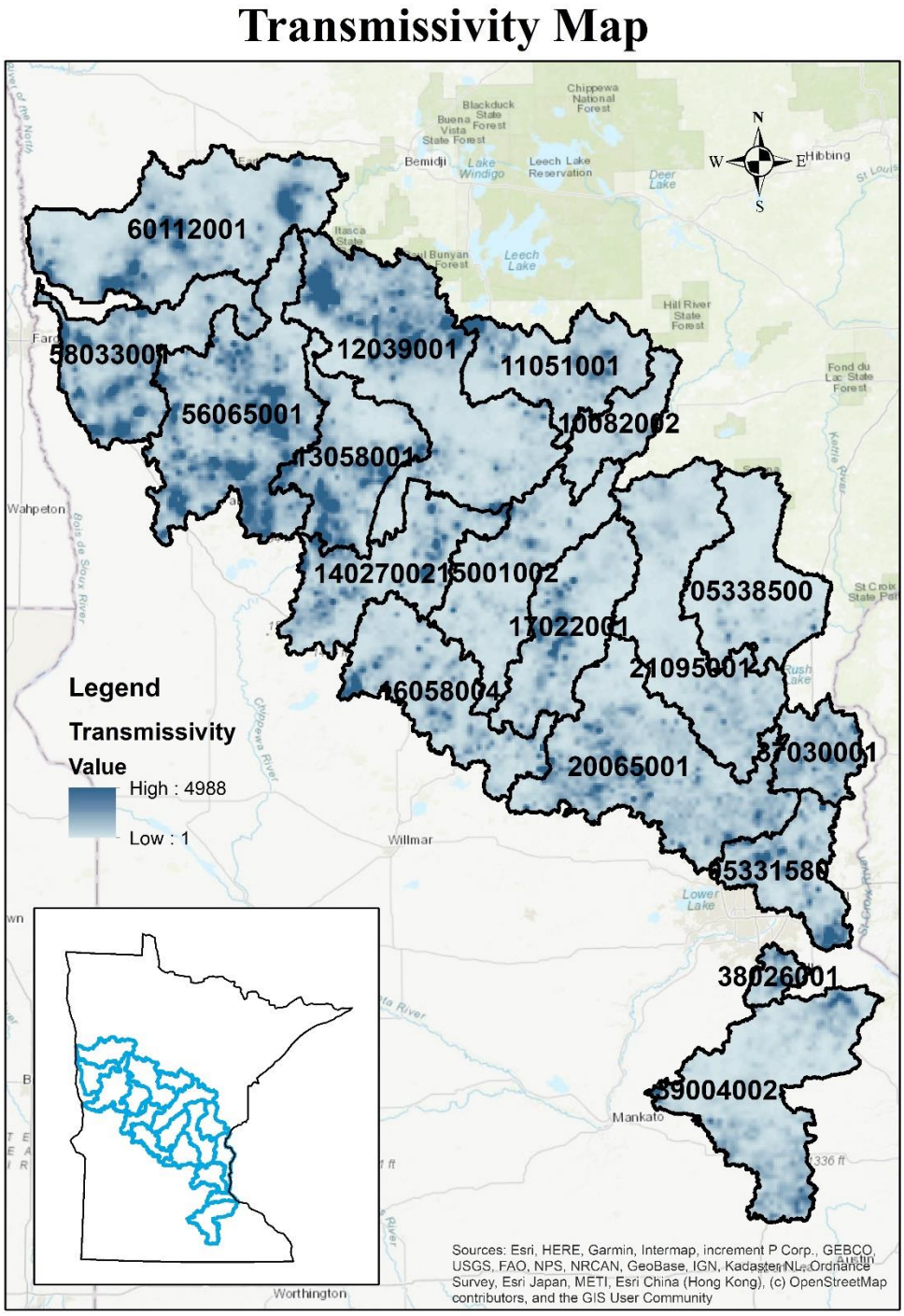

Figure 10. Transmissivity map covering the study area. (units: square meters per day)

5.4.2. Bedrock

The bedrock topography was acquired from S-15 geologic map series published by MGS (Minnesota Geological Survey). The raster data series describes the statewide bedrock geology and topology (Olsen, Bruce M.; Mossler 1982). The spatial resolution is 250 meters. As shown in Figure 11, topography data in the region south of St. Cloud and west of the Elk River are missing. The general bedrock topography elevation line is recognized from the northwestern part of the study area to the southeastern part of the study area. The topographic elevation of bedrock increases around 300 meters from the northwestern part of the study area, where Wild Rice River, Buffalo River joins the North Dakota State, to the central part of the study area, where the Mississippi River (Sartell) watershed and the Sauk River Watershed are located. Relatively low bedrock is observed at the confluence of the Mississippi River and the Minnesota River. The bedrock elevation is also shallow around tributaries in the Twin City Metropolitan Area and the St Croix. River on the Wisconsin border. In the region south of the Cannon River, bedrock topology elevation increases again.

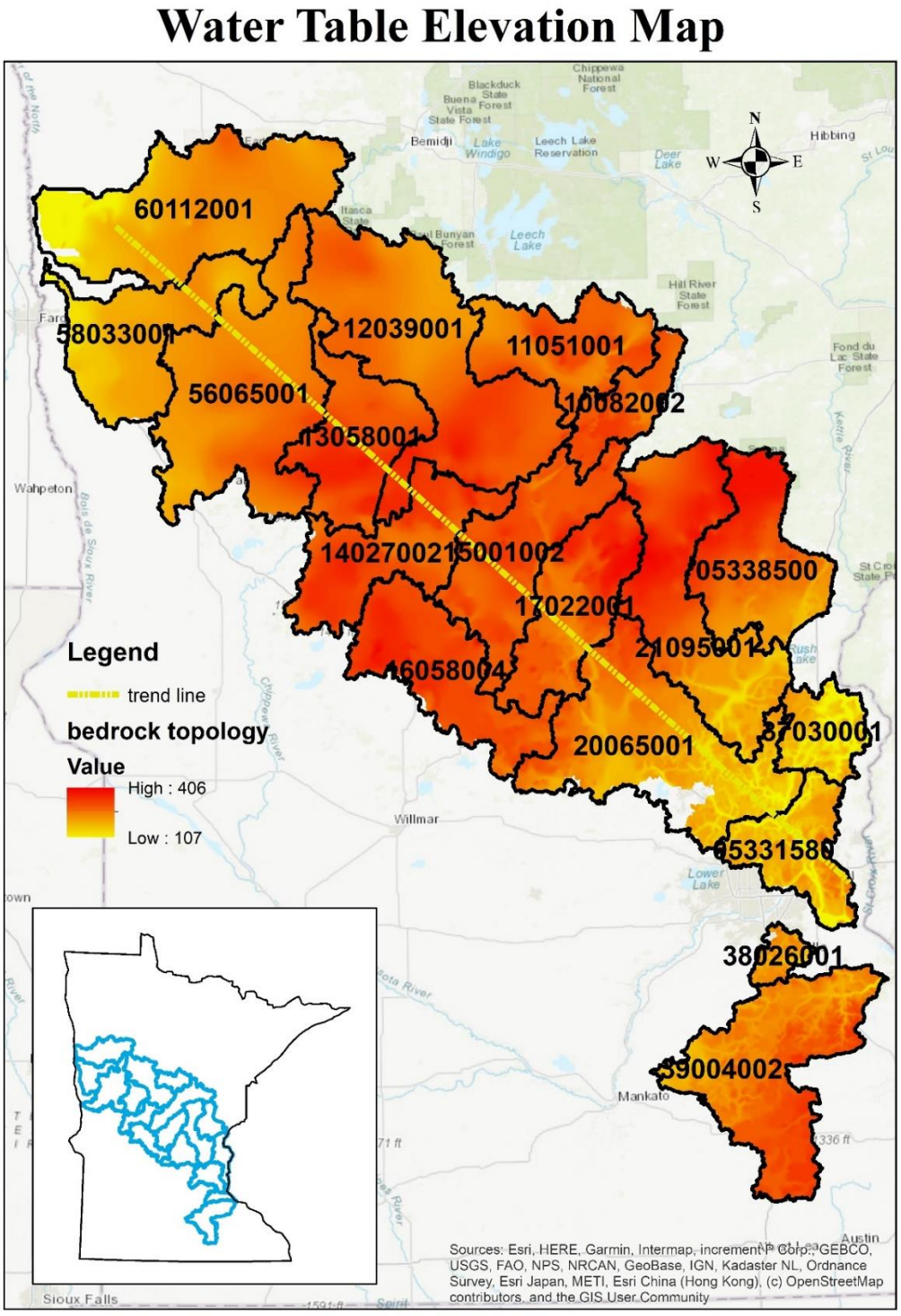

Figure 11. Bedrock topology map covering the study area. (units: meters)

5.4.3. DNR hydrography dataset

The streamline features in the study area were published from the MNDNR hydrography datasets. Current data was updated in 2014. Overall watercourse geometry characters are well characterized by including all water body types (Zeb Thomas 2014). The perennial or intermittent inland waterbodies are denoted as the linear features representing statewide hydrographic features, including streams, lakes, wetlands, rivers and ditches. Particularly, for open water objects whose shape is hard to linearize, such as lakes and wetlands, a set of radial lines from their centers to banks approximate linear shapes. Originally developed from the MNDOT (Minnesota Development of Transportation) base map, the current hydrography datasets are enhanced with assistance from aerial images and informed MNDNR stream management to support hydrology research and management.

5.4.4. Water table elevation

The water table elevation map produced from the MNDNR is a statewide water table information source for groundwater resources management (Adams 2016). It collects abundant water level data from multiple resources. The well data are assembled from DNR monitoring wells, Natural Resources Conservation Services (NRCS) and state County Well Index (CWI) database. The water levels for surface water are derived from statewide 30 meters DEM data using Light Detection and Ranging (LIDAR) data (Adams 2016). The DNR water table map is a spatial interpolation product based on point-wise water table measurements by implementing the inverse distance weighting algorithm. Although site investigations are suggested for local projects with local information supplement, the data quality satisfies the regional hydrology analysis requirement on a watershed scale and therefore was considered valid to be used in our study area. The depth to the water table is generally 3 to 10 meters below the land surface in our study area.

As shown in Figure 12, the water table level is 580 meters above mean sea level in the White Earth State Forest, situated in the junction region among the Wild Rice River watershed, the Buffalo River watershed, the Otter Tail River watershed

and the Crow Wing River watershed. The water table level encompassing the White Earth State Forest decreases to the south part and west part of the study area. As the Mississippi River flows through the study area from Brainard to the Twin Cities, the water table elevation decreases moderately. In the Mississippi River (Twin Cities) watershed, the water table elevation is less than 200 meters along tributaries within the Twin City Metropolitan Area.

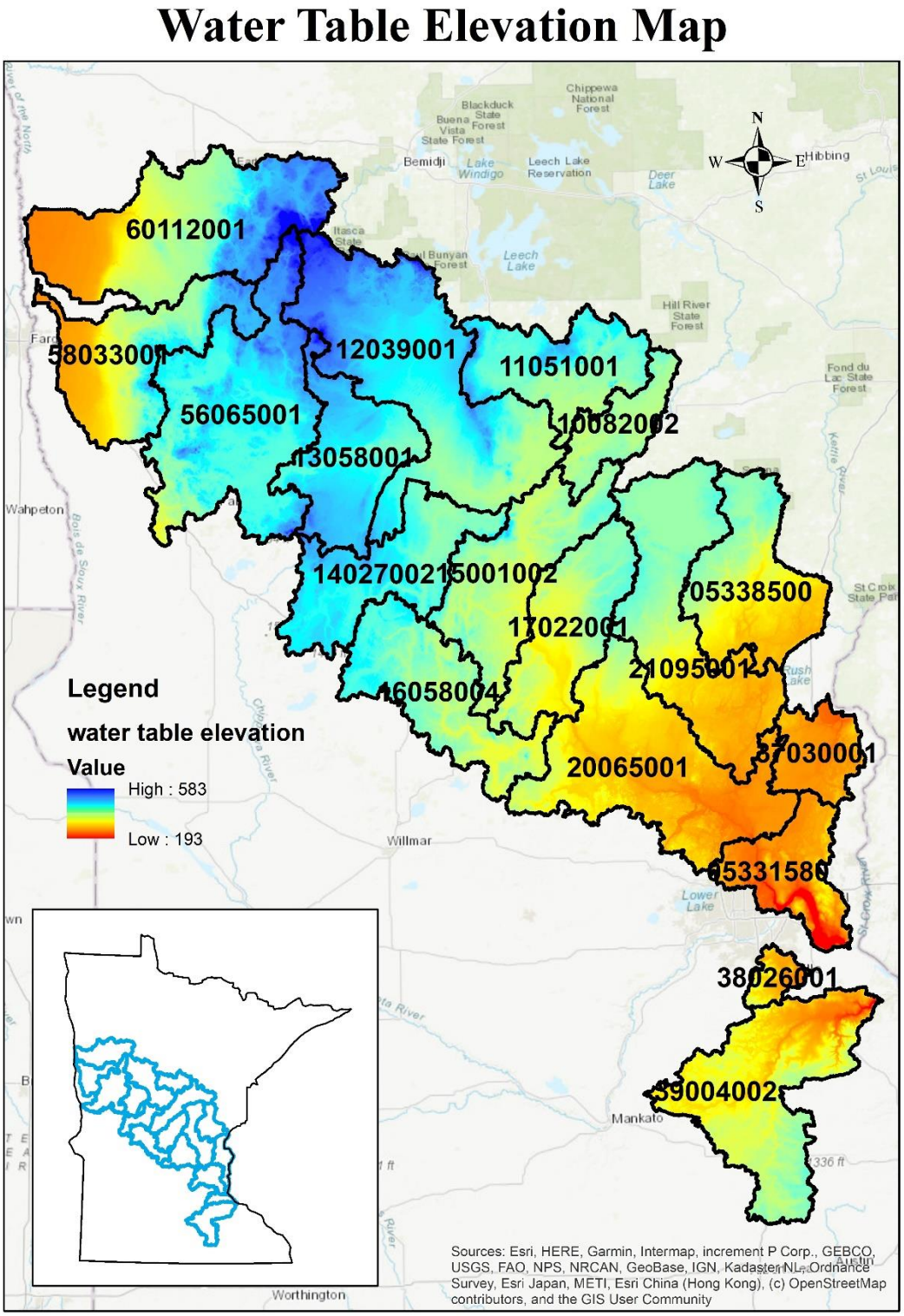

Figure 12. Water table elevation map covering the study area. (Units: meter)

6. Results

This chapter summarized results of this thesis. The results include two products analyzed based on the characteristic drainage timescale *K*, which is derived from the Brutsaert-Nieber recession analysis. The first section lists the derived *K* results. *K* is estimated based on two criteria for selecting recessions from discharge data. These criteria result in different *K* estimates in terms of the magnitude. With the guidance of the theoretical physics equation to express *K* (equations (21) and (22)), a multivariate analysis of *K* was conducted and the result is given in section 6.2. In addition, based on *K* and low flow characteristics, calculation results of the annual groundwater storage change is given in the section 6.3. This annual groundwater storage change estimation from *K* is compared against the actual active groundwater storage change based on the annual water table interpolation product.

6.1. Brutsaert-Nieber Recession Analysis

The drainage timescale is estimated from the Brutsaert-Nieber method. Two recession criteria were applied as stated in section 4.1.2 to extract recession period from the catchment stream flow. The subsequent recession analysis is conducted for those two sets of recession flow separately to each catchment in the study area. Recession analysis results are exhibited in figures that show data points *-dq/dt* plotted against *q* in the Appendix chapter, where *q* is the recession selected based on each recession criterion. Particularly, the recession plot for the gauging station 12039001 is shown in Figure 13 for illustration purposes.

For the hydrology inequality criterion, the implementation requires daily AET to determine the recharge impacts relative to discharge on a daily basis. Assuming a uniform distribution of daily AET, the monthly AET is averaged daily to implement the hydrology inequality criterion. The recessions of the daily flow time series are determined when $\frac{|P - AET|}{Q} < 0.1$ is satisfied. Based on these recession data, *K* was derived by conducting the Brutsaert-Nieber recession analysis. The resulting *K* values for all 18 watersheds are reported in the Table 3.

The magnitude of the *K* estimated from the hydrology inequality criterion ranges from 40 to 900 days. The average *K* values were 180.3 ± 216.5 days for all 18 catchments. Compared to the typical value of 45 ± 15 days (Brutsaert 2008), this result shows large variance and larger values of *K*. The average number of drought flow points identified from the hydrology inequality criterion were merely 60.

The recession plot for the gauging station 12039001 is shown in Figure 13(a). Recession periods are plotted in red, they are mostly in the winter flow season, such as in November and January, when the catchment drainage is inactive compared to the warm seasons of the year. Only 36 points were selected for implementing the recession analysis for the catchment.

Insight is given after investigating the recession periods to examine the *K* value. Drought sequences of streamflow in the winter period is more likely to be included in the recessions defined by the hydrology inequality criterion. The number of recession points selected are also relatively sparse in the log-log space of $-dq/dt$ against q. *K* was estimated by excluding 5 percent of the points with the slowest recession rate before drawing the line with a fixed slope. If recession data cloud points are too few for the analysis, the five percent exclusion will not remove low recession impacts for the recession analysis since the exclusion points are too few accordingly. The estimated *K* will be larger since the slowest recession rates are included for the analysis. In the worst case at the gauging station 58033001 with extremely few points of recessions, the hydrology inequality criterion selects merely 7 points for the recession analysis. The 5 percent exclusion will not remove any points. Similar scenarios are observed for the recessions filtered from the hydrology inequality criterion at the gauging station 13058001 and 37030001.

Applying the Brutsaert criterion to select recessions, the magnitude of the derived *K* estimated ranges from 20 to 150 days as shown in Table 3. The average *K* values were 59.8 ± 36.1 days, which is very close to the typical value of 45 ± 15 days (Brutsaert 2008). For a few catchments in the study area, the *K* estimate exceeds 60 days, which is the upper bound to the typical value (Brutsaert 2008). But

this exceedance is acceptable because the similar magnitude exceedance over 100 days was also reported by other. Recessions were analyzed in the small catchments in Oregon and California, with the K values covering a wide range between 26 and 100 days (Tague and Grant 2009). For 19 catchments in Australia, *K* estimates ranged from 25 to 101 days (Zhang et al. 2014). For 9 catchments in the Kilombero Valley in Tanzania, the average *K* value was estimated to be 203 ± 139 days. This large variance is explained by the variety in the selected watershed scale, which ranged from 175 to 34230 km^2, and due to seasonal evapotranspiration impacts (Lyon et al. 2015). Meanwhile, additional results of *K* also confirm the typical value of *K*. For the cases of two large river basins in Illinois, *K* was estimated as 46 and 37 days (Brutsaert 2008). For 38 selected catchments in the Loss Plateau in China, *K* was estimated in a range of 29 ± 16 days (Gao et al. 2015).

Recognized from the Brutsaert recession criterion, there are 136 baseflow recession points averaging over all 18 catchments. More selected baseflow recession points allow the recession analysis to derive the drainage characteristics comprehensively since it encompasses recessions from all seasons. This complete seasonal pattern is illustrated in Figure 13(b), which exhibits the Brutsaert method implementation for the catchment with the gauging station 12039001. At this gauging station, the recessions encompass complete seasonal patterns rather than just winter periods, which is the recession period that the hydrology inequality criterion selects.

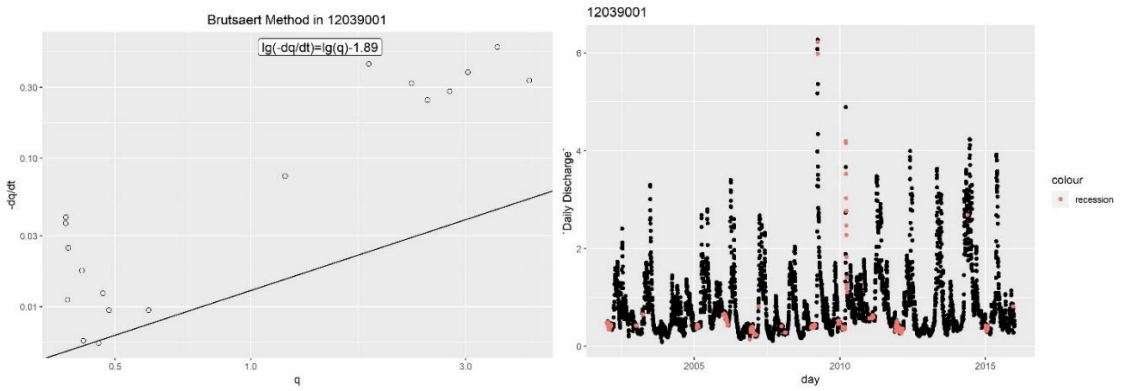

a. Baseflow recession analysis based on hydrology inequality criterion.

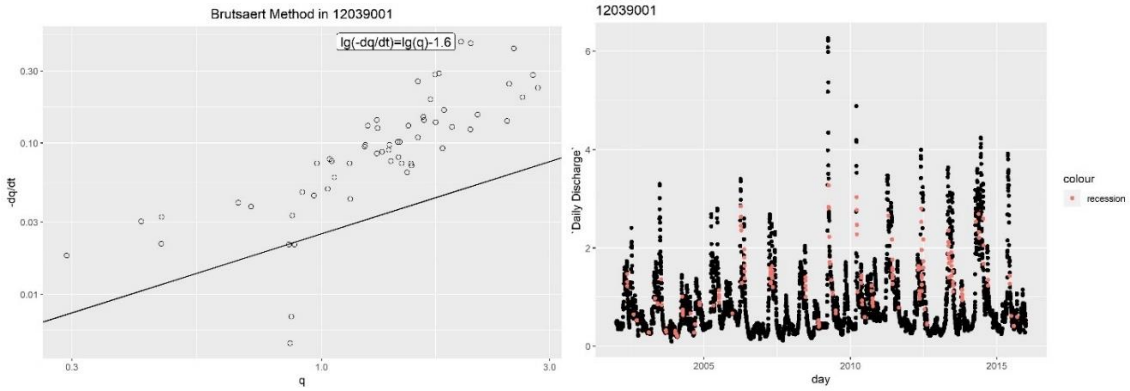

b. Baseflow recession analysis based on the Brutsaert criterion.

Figure 13. Evaluating the different performance of the recession analysis performance difference by two recession criteria: a) hydrological inequation criterion. Red points are recession flows, which feed the recession analysis. b) Brutsaert criterion that filters recession manually from precipitation.

For all of the remaining catchments, it is observed that the *K* estimated from two sets of recessions are consistent in certain cases but are drastically inconsistent under the other scenarios. For cases when *K* estimates exhibit a significant discrepancy, seasonal patterns on recessions is proposed as alternative explanations. For gauging station 13058001, the *K* estimate is 57 days based on the recessions from the Brutseart criterion while the recessions from the hydrology inequality criterion yields an estimate of *K* to be 984 days. It is recognized that the number of recession points decrease drastically from 198 to 20 when the recession criterion changes from the Brutsaert criterion to the hydrology inequality criterion. Those 20 points in the recession cover merely the winter season. For gauging station 16058004, the *K* estimate changes from 103 to 392 days when altering the recession criterion from the Brutsaert criterion to the hydrology inequality criterion.

In cases when *K* is consistent between the estimates from these two criteria, the recessions selected encompass similar seasonal patterns. Although the number of points in the data varies, the flow regimes of selected recessions based on these two recession criteria approximately agree with each other. For gauging station 10082002, as shown in Figure 19, recessions selected based on both criteria include the portion of recession limbs where drainage occurs actively with quick recession rate instead of selecting merely the drought period. For gauging station 11051001 and 58033001, although the number of recession points prepared for the baseflow recession analysis decreases when the hydrology inequality criterion is applied, the estimated *K* values are in relative agreement because selected recession drainage patterns are relatively complete to characterize basin drainage characters.

Table 3. Recession analysis results table. *K* value and the number of data cloud points for the recession analysis (denoted as #) for each gauging station are shown. 'Brutsaert' means the Brutsaert criterion by manually filtering the rainfall data. 'Hydrology inequality' is the hydrology inequality criterion. The figure number to each graphic result is referenced in 'FIGURE NUMBER' column. '*K* COMPARISON ' column summarizes the comparison performance between the *K* derived from these two recession criteria.

GAUGING STATION ID	K COMPARISON	BRUTSAERT		HYDROLOGY INEQUALITY		FIGURE NUMBER
		***K*(days)**	**#**	***K*(days)**	**#**	
5331580	Extremely different estimates. the hydrology inequality criterion selects recessions in the drought flow periods.	95	63	101	119	17
5338500		46	300	127	119	18
12039001		26	61	145	36	13
13058001		57	198	984	20	21
15001002		45	49	114	85	23
16058004		103	280	392	39	24
20065001		44	43	79	59	26
21095001		92	391	168	163	27
37030001		70	100	33	21	28
38026001		72	187	137	86	29
56065001		151	36	340	79	31
60112001		120	290	270	36	33
10082002	Consistent estimates. Seasonal patterns on recession do not vary between the recession criteria. Minor differences are tolerated.	55	18	67	21	19
11051001		92	93	100	19	20
14027002		124	108	135	31	22
17022001		20	19	30	41	25
39004002		108	145	79	95	30
58033001		59	72	46	7	32

It should be noted that this insight is just a preliminary explanation to account for the different *K* estimation performance as a result of selecting recessions based on the Brutsaert criterion or the hydrology inequality criterion. This hypothesis still merits further research to examine its validity. Other potential influential factors might include the quality of data, such as the discharge and precipitation. During the low flow periods such as the ice period in the winter season, streamflow estimates are likely not as accurate as in the summer. Precipitation data also contribute uncertainties for the recession analysis. When analyzing on a catchment scale, the aggregated precipitation data from the Daymet grids, are probable to miss local extreme rainfall events patterns. If recessions are not excluded when rainfall events are present, the derived drainage timescale will be underestimated.

The impact of these two recession criteria over selected recessions is out of the scope of this thesis. But it is suggested to conduct theory guided research to validate which criterion selects the baseflow recession from discharge data objectively. Currently these two criteria select baseflow recession empirically by removing rainfall and other recharge impacts without being compared to the actual baseflow, which is difficult to measure. Obtaining baseflow from the discharge means to remove other surface water fluxes from the discharge, which is challenging to remove completely considering the interaction involved between surface water and groundwater. Among various approaches to obtain baseflow from the discharge, geochemical mass balance methods use source water chemical signatures to separate baseflow from discharge. If the accurate baseflow is separated from the discharge, such as by the geochemical approach, then a comparison between this accurate baseflow in the recession period against the recession criterion derived baseflow will be of the great importance to assess the accuracy of recession criterion regarding the baseflow selection. This routine might be of interest for guiding future research to evaluate the recession criteria.

As an attempt to investigate the *K* estimates, it is still recognized that the selected recessions derived from the Brutsaert criterion encompass relatively

complete seasonal patterns. Because of this the *K* derived from those recessions are considered to be more representative for characterizing the catchment drainage compared to the *K* estimates derived based on the hydrology inequality criterion. Therefore, for the multivariate analysis and the groundwater storage change analysis, the *K* estimated from the Brutsaert criterion instead of the hydrology inequality criterion is used.

6.2. Regression Analysis

Based on the theoretical expressions for the drainage timescale, *K* given by equations (21) and (22), it is hypothesized that the drainage timescale derived empirically should be correlated with aquifer transmissivity, watershed area, stream length, aquifer slope, and aquifer depth. To test this hypothesis the empirically derived *K* is regressed against the watershed geomorphic parameters and the aquifer hydraulic parameters as expressed in the multivariate equation.

$$\log(K) = \beta_1 + \beta_2 \log T + \beta_3 \log D + \beta_4 \log(\tan\alpha) + \beta_5 \log L + \beta_6 \log A \qquad (33)$$

The aquifer drainable porosity also appears in equations (21) and (22) but was not included in the regression relationship because that parameter is difficult to estimate. As will be seen in the following results, the influence of drainage porosity will be implied in the unexpected sign of the regression coefficient for the aquifer depth.

The regression results are summarized in Table 5. The regression coefficients except for the intercept are all statistically significant at the 0.05 level. There is significant relationship observed at 0.005 levels of significance of stream length (L) and watershed area (*A*). Transmissivity (*T*), aquifer thickness (*D*) and aquifer slope ($\tan\alpha$) are statistically significant at the 0.05 levels of significance. The intercept is interpreted as the coefficient accounting for unit conversion in the regression model. The regression coefficients for the stream length and the drainage area are statistically significant at 0.01 level. The p value of the regression model is 0.036. The R^2 is 0.59. A large portion of the system variance is explained by this multivariate regression model. Stream length (*L*), watershed area (*A*), transmissivity (*T*), aquifer thickness (*D*) and aquifer slope ($\tan\alpha$) are confirmed as explanatory variables to quantify the variability of characteristic drainage timescale (*K*). These variables are not completely linearly independent and are correlated as indicated by Table 6. Watershed area is highly correlated with stream length because the spatial

scope of watershed area increases the complexity of river network. Aquifer thickness is also correlated with the transmissivity.

A scatter plot of the residuals is presented in Figure 14. Residuals are the deviation of the model prediction from the actual *K*, which is derived from baseflow recession. As indicated from Figure 14, the residuals are normally distributed around zero. It confirms that the normality assumption for a regression model is not violated. This multivariate regression analysis estimates the coefficients for each independent variables. The equation could be expressed with or without log form (equation (34) and (35)).

$$\log(K) = -2.33 - 0.95\log T + 1.19\log D + 0.61\log\tan\alpha - 1.87\log L + 1.71\log A \qquad (34)$$

$$K = 10\,\wedge\, 2.3\frac{D^{1.19}\left(\tan\alpha\right)^{0.61} A^{1.71}}{L^{1.87}T^{0.95}} \qquad (35)$$

Table 4. Calculated drainage timescale (days) from Brutsaert-Nieber recession analysis, other geomorphic variables and hydrology variables included in the multivariate analysis.

Station ID	K (days)	Transmissivity (m^2/day)	Aquifer thickness(m)	Slope	Drainage area (km^2)	Stream length (km)
5331580	95	261	38	0.0815	1530	299
5338500	46	48	22	0.0182	2506	818
10082002	55	89	54	0.0198	1013	432
11051001	92	186	93	0.0179	2099	668
12039001	26	232	116	0.0083	5155	1635
13058001	57	305	95	0.0109	2201	627
14027002	124	221	79	0.0137	2368	546
15001002	45	94	44	0.0174	2608	817
16058004	103	175	41	0.0147	2540	604
17022001	20	160	31	0.0228	2249	576
20065001	44	194	42	0.0377	4263	1434
21095001	92	81	34	0.0229	3613	1036
37030001	70	243	65	0.0781	980	420
38026001	72	250	41	0.0621	332	95
39004002	108	128	34	0.0436	3479	803
56065001	151	357	136	0.0079	4448	673
58033001	59	316	116	0.0074	2513	561
60112001	120	215	126	0.0088	4316	837

Table 5. Regression summary table for the drainage timescale.

VARIABLES	COEFFICIENTS	STANDARD ERROR	t VALUE	PROBABILITY ($>\|t\|$)
INTERCEPT	-2.33	1.91	-1.22	0.245
TRANSMISSIVITY (*T*)	-0.94	0.39	-2.47	0.030
AQUIFER THICKNESS (*D*)	1.19	0.42	2.83	0.015
BEDROCK SLOPE ($\tan\alpha$)	0.61	0.24	2.48	0.029
STREAM LENGTH (*L*)	-1.87	0.51	-3.69	0.003
DRAINAGE AREA (*A*)	1.72	0.48	3.57	0.004

Table 6. Correlation matrix for the transmissivity, aquifer thickness, slope, stream length and drainage area.

	Transmissivity	*Aquifer Thickness*	*Slope*	*Stream length*	*Drainage area*
Transmissivity	1	0.69	0.06	-0.2	0.06
Aquifer thickness		1	-0.48	0.16	0.42
Slope			1	-0.41	-0.52
Stream length				1	0.85
Drainage Area					1

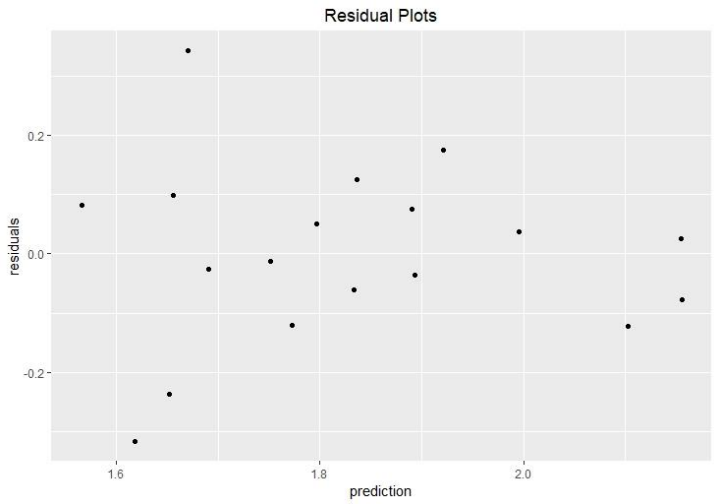

Figure 14. Residual plot for the multivariate analysis

6.3. Groundwater Storage Change Analysis.

Annual groundwater storage change is estimated from the Brutsaert method and the WT method. Capturing the temporal dynamic characteristics of groundwater, active groundwater is calculated for deriving the change of groundwater. It is assumed the active groundwater storage change represents the actual groundwater storage change.

Based on the WT method, the annual groundwater storage change is computed as the difference of the active groundwater storage between two consecutive years from 2002 to 2015. The annual active groundwater storage change from the WT method is compared to the Brutsaert storage change analysis. The unit for storage change is meter per year. The comparison is illustrated in Figure 15. Since the annual Brutsaert storage change analysis is based on stream flow data, the availability of discharge data impacts the analysis period. For the gauging stations 11051001, 14027002, 37033001 and 58033001, the period of record of the streamflow data does not completely cover 2002 to 2015. Small gaps in discharge data for other sites, like the discharge of the site 5331580, also exist, which impacts the comparison evaluation. The magnitude of orders of the groundwater storage change from both approaches is consistent with each other.

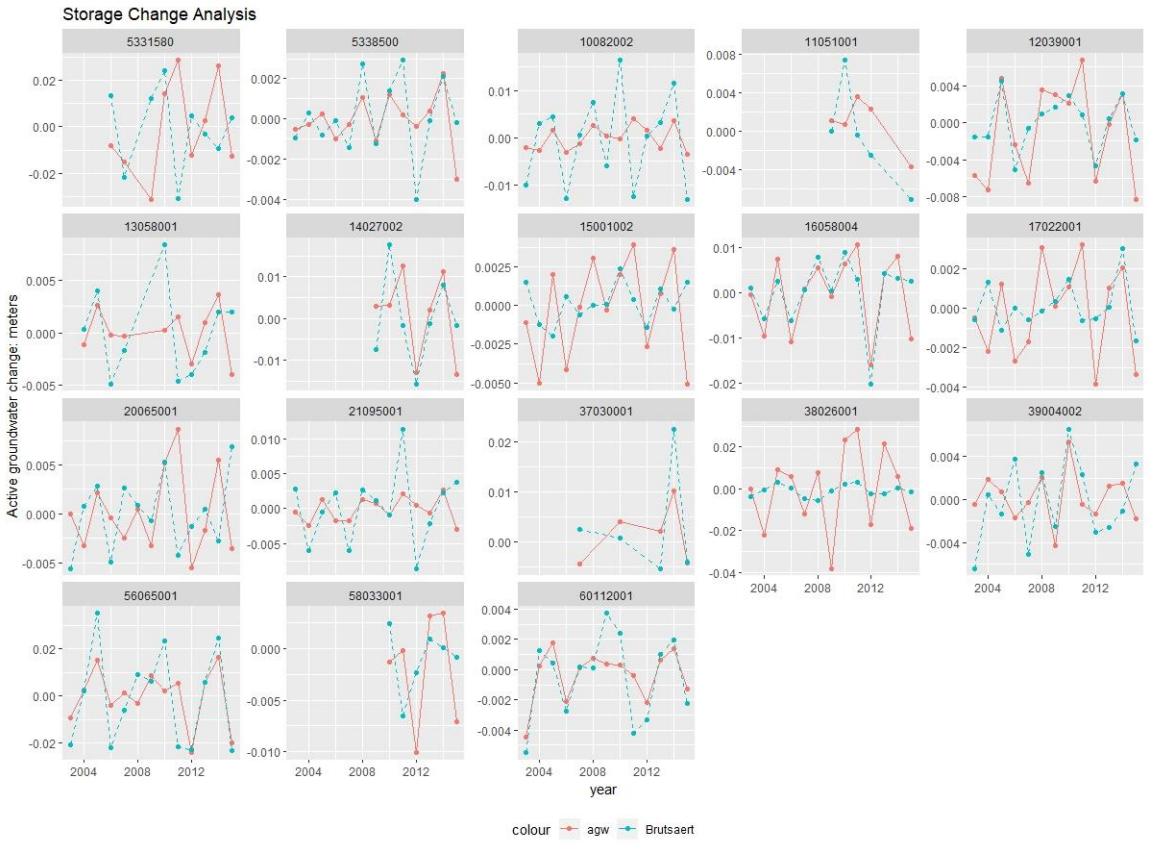

Figure 15. Groundwater storage change analysis comparison between Brutsaert estimate and the active groundwater storage calculation based on WT method. (Units of groundwater storage change: meters)

The agreement between groundwater storage change results is evaluated by three metrics, the Nash-Sutcliffe coefficient (NSE), the absolute bias and the Pearson correlation coefficient (r_{X_m,X_o}). Their calculation formulas are given below.

$$NSE = 1 - \frac{\sum_{t=1}^{n}(X_m^t - X_o^t)^2}{\sum_{t=1}^{n}(X_o^t - \overline{X_o})^2} \quad (36)$$

$$r_{X_m,X_o} = \frac{\sum_{t=1}^{n}(X_m^t - \overline{X_m})(X_o^t - \overline{X_o})}{\sqrt{\sum_{t=1}^{n}(X_m^t - \overline{X_m})^2}\sqrt{\sum_{t=1}^{n}(X_o^t - \overline{X_o})^2}} \quad (37)$$

$$Bias = \frac{1}{n}\sum_{t=1}^{n}\left|X_m^t - X_o^t\right| \quad (38)$$

where X_m^t is the modeled time series variable at timestamp *t* and X_o^t is the observed time series variable at timestamp *t*. $\overline{X_m}$ is the mean of the X_m^t, $\overline{X_o}$ is the mean of the X_o^t.

NSE is a popularly used metric to evaluate the prediction performance of a hydrologic model. The prediction error, which is squared difference between the prediction and observation, is normalized by the observation series. It leads to a preference of NSE to overestimate the model performance during high observation periods. On the contrary, for the periods with low observation values, NSE is not very sensitive to systematic model over- or underprediction (Krause, Boyle, and Base 2005).

In this study, either the Brutsaert method derived groundwater storage change estimate or the groundwater storage change calculated from the WT method can be the X_m^t since they're both modeled results. In other words, either of them can be denoted as the X_o^t. As for answering which of them is the ground truth data

for calculating the NSE will depend on the systematic variance involved, which normalizes the prediction error. Besides, to overcome the disadvantage noted in the NSE metric, which overestimates the model performance for high observed values, the one with lower groundwater storage change averages from those two groundwater storage change methods is selected as the X_o^t.

These calculated metrices are shown in Table 7. The table provides a quantitative comparison of the storage change analysis. NSE calculated is between -1.38 to 0.61. The bias is at a magnitude of order of 0.001 meters. The correlation between the two results for each site ranges from -0.3 to 0.8. An overall satisfactory agreement of the storage change calculated from the Brutsaert method and the WT method is observed. As presented in the magnitude and trend, the storage change analysis from the Brutsaert method for watersheds with gauge ID 60112001, 16058004, 56065001, 12039001 is highly correlated with that computed from the WT method. This satisfactory agreement is also confirmed from their NSE statistics, which is above 0.4. The correlation for only three watersheds, the gauge IDs of which are 13058001, 20065001, and 5331580, shows a poor agreement. For five watersheds with negative NSE, such as the catchment with stations 11051001, 13058001, 15001002, 20065001 and 5331580, their comparisons about storage change estimation do not yield a satisfactory agreement, either.

Table 7. Metrics to evaluate the annual storage change analysis from the WT method and the Brutsaert method. Metrics include the Nash-Sutcliffe Efficiency, bias and the Pearson correlation coefficient.

site	NSE	*Bias*	r_{X_m,X_o}
60112001	0.61	0.001	0.8
58033001	0.18	0.005	0.22
11051001	-0.29	0.004	0.45
10082002	0.11	0.007	0.34
56065001	0.54	0.01	0.76
12039001	0.46	0.003	0.73
13058001	-0.09	0.003	0.18
14027002	-0.01	0.009	0.49
5338500	0.19	0.001	0.48
15001002	-0.15	0.003	0.02
17022001	0.01	0.002	0.28
16058004	0.61	0.004	0.79
37030001	0.23	0.006	0.74
20065001	-1.22	0.005	-0.21
5331580	-1.39	0.024	-0.37
38026001	0.09	0.016	0.38
39004002	0.08	0.003	0.39
21095001	0.13	0.004	0.37

7. Discussion

7.1. Multivariate Regression Analysis

From the multivariate analysis, the regression coefficients for the independent variables, *L*, *A*, *D*, *T*, $\tan\alpha$ were determined. The dominant influence of geomorphic features and hydraulic variables over K is tested by the statistical model. For *L*, *A*, *T* and $\tan\alpha$, not only their significant levels but also the regression coefficients are in accordance with K expressions derived from the solutions to the linearized Boussinesq equation. The equations (21) and (22) are repeated here for convenience.

$$K = \frac{\varphi A^2}{\pi^2 p_B k D L^2} \qquad (39)$$

$$K = \frac{\varphi A^2}{\pi^2 p_B k D L^2 \cos\alpha[1+(\frac{D}{\pi p_B})^2]} \qquad (40)$$

From the geomorphic perspective, the regression coefficient of *L* is negative while that of *A* is positive. As indicated by equation (21) and (22), the theoretical exponential terms are 2 for both of them. 1.87 and 1.72 are reliable estimates for the exponents of A and L respectively considering the spatial scope and the inevitable errors introduced from the data. Bedrock slope impacts K much less compared to *A* and *L*. Equation (22) shows that $\cos\alpha$ decreases K. When α is less than $\frac{\pi}{2}$, $\cos\alpha$ decreases monotonically with α while $\tan\alpha$ increases monotonically with α. Therefore the phreatic zone above a steep aquifer is drained slowly comparatively to a relatively flat aquifer. The sign for the bedrock slope in the regression model is positive and is in accordance with formula (22) because slope increases monotonically with α.

From the hydraulic perspective, the transmissivity *T* characterizes the groundwater drainage flow rate under a unit hydraulic gradient. The transmissivity integrates the hydraulic conductivity over the vertical space and is expressed as

$p_B kD$ in the equation (21) and (22). The coefficient is -0.94 and is approximate to the theoretical value -1 as implied by equation (21) and (22).

Another independent variable is the aquifer thickness *D*. Although the regression coefficient sign of D is opposite from the expression (equation (21) and (22)), which indicates that *K* is monotonically decreasing with *D*, the regression coefficient of 1.19 with a *p* value of 0.0015 is still an unremovable and critical variable for its statistical significance in the multivariate system. Given that the drainable porosity φ is missing and the transmissivity *T* has included *D* for the multivariate analysis, an initial hypothesis is proposed to interpret the reversed behavior of *D* in the multivariate analysis as a mixing effect in combination with the missing φ. Based on the regression analysis, *D* increases *K* in a way similar to φ, which increases *K* as indicated by the Boussniesq groundwater theory. Groundwater discharge movement is driven by the drainable storage during the drop of the water table as a response to the hydraulic gradient, which is the scenario when solutions to the Boussinesq equation are derived (see the initial and boundary condition specified in the equation (5) and (9)) . A longer drainage timescale is expected as a response to more drainable storage, which is denoted as $D\varphi$. Consequently, since φ is excluded in the independent variables, *D* functions as the drainable storage and is therefore a surrogate of the missing φ, which is recognized in the multivariate regression and results the regression coefficient of *D* to 1.19. The difficulty for estimating the drainable porosity φ makes it hard to test this hypothesis.

The *K* expression in a form of recession analysis from the Boussinesq equation's solution is tested by this regression analysis. The statistical significance indicates the fact that including these independent variables are of the great importance for interpreting K. The conformity between the magnitude of regression coefficients of selected independent variables with those coefficients

from the expression of theoretical K also indicates that these environmental variables impact the *K* significantly.

7.2. Groundwater Storage Change Analysis

The groundwater storage change based on the WT method serves as the ground truth against which the Brutsaert groundwater storage change analysis is compared. An overall good agreement between them is observed (Figure 15) but anomalies in the storage change comparison were found and will be discussed in this section.

The applicability of K for groundwater storage change is proved successful for gauging stations 60112001, 16058004, 56065001, and 12039001. The correlation between the groundwater storage change based on those two approaches are above 0.7. Particularly, the storage change for gauging station 16058004 and 60112001 is almost identical between the two estimates. This agreement preliminarily confirms the applicability of using drainage timescale to infer groundwater storage change.

For other watersheds, the correlation is around 0.4 and is still acceptable considering the fact the analysis is based on the HUC-8 scale, which might introduce unavoidable error to the analysis scope. It should be mentioned that the Brutsaert estimate is heavily dependent on the annual drought flow statistics. If the variation of the annual discharge is not well characterized by the available discharge record, the Brutsaert estimation will be severely impacted. Temporal coverage of the daily discharge data affects the annual lowest seven-day flow. For instance, if the discharge covers merely the warm season period, it will inevitably influence the storage change estimation. In that case, it will biasedly overestimate the storage change for the current year and underestimates the storage change for the following year. In alternative fashion, for a discharge record that covers only the cold season, the method will underestimate the storage change for the current year and overestimate the storage change for the subsequent year. In general, estimates of

storage change will be biased whenever the discharge record has strong seasonal flow patterns and when the flow records are incomplete.

For illustration of this problem consider station 13058001. For this station the discharge data is sparse in year 2005 and 2010. As shown in Figure 16, in year 2005 and 2010 at station 13058001, the gauging station records the discharge in early or late summer. Consequently the annual lowest seven-day flow is overestimated without considering low flow in winter periods. This explains the overestimation of the groundwater storage increase that was detected in 2005 and 2010. Consequently, the following year's storage change in 2006 and 2011, is underestimated when applying the Brutsaert method. In 2006, the WT method calculates an increase of groundwater storage change of 0.0098 m while the Brutsaert method estimates a decrease of groundwater storage change of 0.0049 meters. In 2010, the WT method estimates a groundwater storage increase of 0.0140 meters, and the Brutsaert method estimates a groundwater storage decrease of 0.0046 meters.

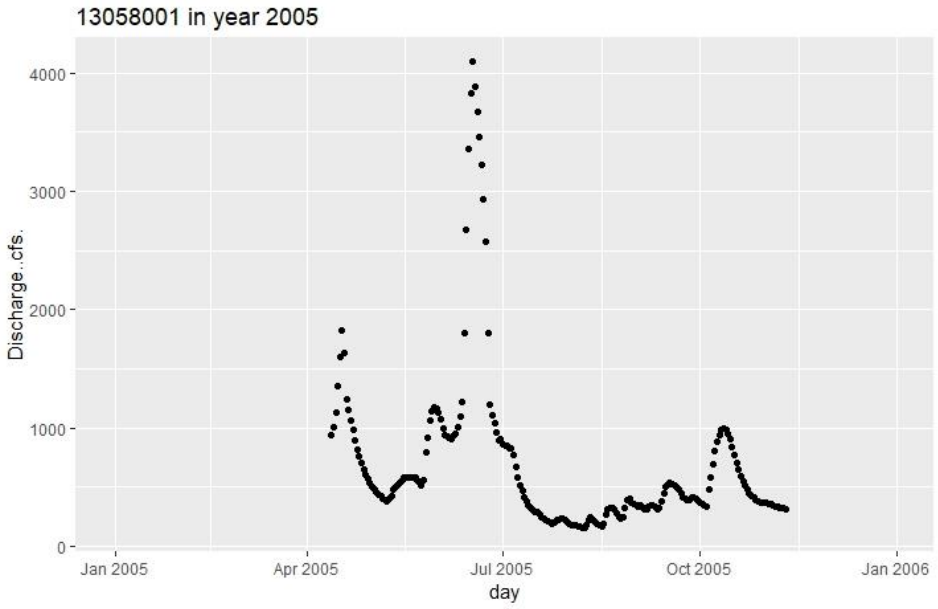

a. discharge data for the gauging station 13058001 in 2005

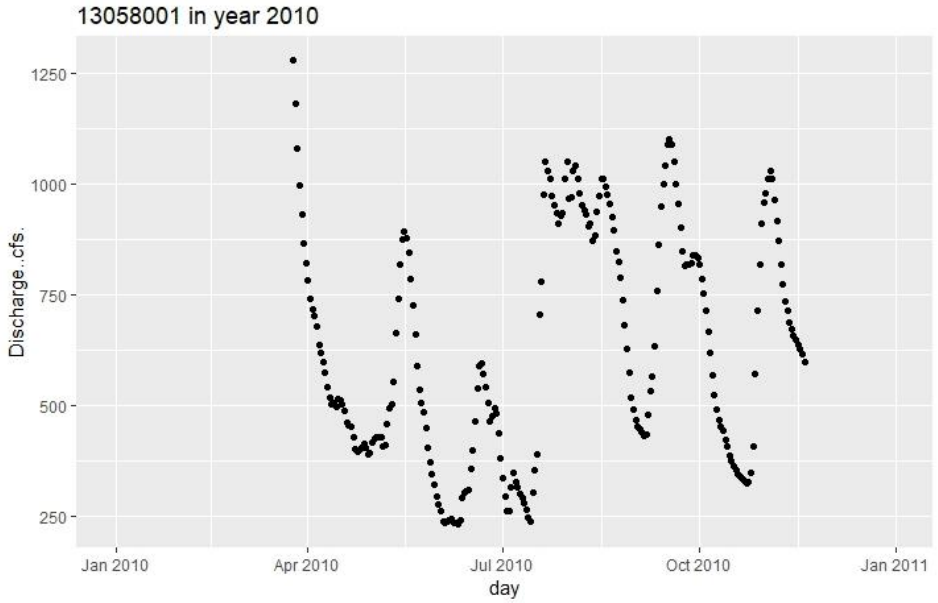

b. discharge data for the gauging station 13058001 in 2010

Figure 16 Temporal coverage for the discharge at gauging station 13058001 in 2010 (a) and 2005 (b).

The magnitude of the storage change estimated from Brutsaert method is consistent with the actual storage change calculated from the WT method for all watersheds in the study area. As for the watersheds crossed by the Mississsippi River, this observation confirms the success to remove the upstream discharge for the watersheds whose pour point gauging station might record extra runoff from tributaries outside the watershed. Otherwise, the storage change from the Brustaert method would have overestimated the actual storage change as extra discharge is included. Nevertheless, for the watersheds with gauging stations 17022001 and 15001002, the discrepancy between the storage estimation and actual storage change still merits further research for the investigation.

Three watersheds, whose gauging station is 15001002, 20065001, 5331580, are observed with poor comparative performances. The stream flow networks in these three watersheds are more intricate than the other watersheds in the study area, each of which have only one main stream. Two main streams meet with each other within these watersheds. Complex river networks obstruct the applicability of *K* for inferring the groundwater storage change. For the Mississippi River (Twin Cities) watershed with gauging station 5331580, the Minnesota River merges into the Mississippi River before it reaches the gauging station 5331580. Similarly, the confluence of the Crow Wing River and the Mississippi River is located within the watershed with gauging station 15001002. The Crow River meets the Mississippi River before it flows into the gauging station 20065001, located in the Mississippi River (St. Cloud) watershed.

As mentioned before, the annual variation of the pour point discharge impacts the implementation of the Brutsaert method. The occurrence of confluence of river network merits further examination of the preprocessed discharge data. In the discharge preprocessing step, the discharge from these two main streams have been removed separately from the downstream discharge. However, for the river channel segment at the downstream of the confluence, the redundant upstream discharge elimination assumes these two rivers flow independently without

converging. This misrepresentation of flow network assumption is likely to introduce errors to the analyzed drainage system. Whether this failed assumption underestimates or overestimates the processed pour point discharge is not answered in this thesis but it is one alternate explanation for the unsatisfactory estimation results for those three gauging sites. This observation points to the need to design a further complicated algorithm for eliminating upstream discharge to account the for complex river networks.

Instead of estimating long-term record of groundwater storage change, the Brutsaert method is applied to estimate groundwater storage change on an annual scale. In our study area, inferring annual groundwater storage change is applicable for a majority of the watersheds, four of which yielded satisfactory comparison results against actual groundwater storage change. In addition, for a few watersheds with complicated river network and relative incomplete discharge data, the cause of this inconsistency still merits further research. The Brutsaert method estimates the groundwater storage change based on discharge data, which implies that the estimation is sensitive to the quality of stream flow data. This dependency to stream flow data also indicates that Brutsaert method could not be applied to ungauged basins, which limits its applicability.

Recent advances in remote sensing data collection indicates the potential and breakthrough for investigating the change of storages on a watershed scale. The GRACE (Gravity Recovery and Climate Experiment) satellite was launched in 2002 to monitor the spatial temporal variation of the total terrestrial water storage change on a monthly scale. The predictability of the GRACE signal for groundwater storage change has been confirmed regionally (Biancamaria et al. 2019; Scanlon, Longuevergne, and Long 2012). Although the spatial resolution of GRACE signal is poor, GRACE signal is updated monthly. This temporal scale makes it possible to track groundwater storage change on a monthly basis. Nevertheless, anomalies and local mismatching patterns are identified between GRACE data and large scale hydrological models. Validating the GRACE signal across various scales is one of

the challenging tasks considering the spatial heterogeneity. For hydrological insight into regional ungauged watersheds, the GRACE monitoring mission provides numerous investigation opportunities for hydrological studies, which are unachievable using the Brutsaert method due to its dependency on discharge data availability. Discussion about power of GRACE data to monitor groundwater storage change is outside the scope of this thesis. But for the Brutsaert method, applicability of the *K* in annual groundwater storage change analysis is meaningful for leveraging GRACE data for monitoring the earth's hydrological system. Will these two approaches develop collectively for investigating the drainage characteristics and the groundwater storage change for both gauged and gauged catchments? There is great potential for continued applications of the Brutaert method with the assistance of GRACE data to obtain scientific insights into groundwater storage change analysis.

8. Conclusion

This study conducted baseflow recession analysis for HUC-8 watersheds. The characteristic basin drainage timescale is estimated from the classic Brutsaert-Nieber method. Comparisons of K estimated from two recession criteria are discussed. Considering the seasonal effects on recessions, K evaluated from the Brutsaert recession criterion is assessed for multivariate analysis and annual storage change analysis. Within the study area, K ranges from 30 days to 120 days across the catchments.

The agreement between the drainage timescale theoretical expression form yielded from the Boussinesq equation and that from the empirical Brutsaert-Nieber method is satisfactory. The strength of the regression relationship among variables is characterized by the coefficient of determination and statistical significance. The striking feature of the regression analysis is that the regression coefficient sign and their magnitudes approximate to the relations as expressed from Boussinesq groundwater theory. The interpretation of K by stream length, watershed area, aquifer transmissivity and aquifer slope from both theory and data perspective are confirmed to be almost identical statistically. But this agreement is not observed for the aquifer thickness. It is tentatively explained by the mixing effect between the drainable porosity and the aquifer thickness, which is introduced by excluding the drainable porosity from the regression analysis. The multivariate statistical analysis confirms that the geomorphology of a groundwater system is dominant in the basin drainage process (Biswal and Marani 2010, 2014; Biswal and Nagesh Kumar 2015).

The annual storage change analysis compares the storage change estimated from the Brutsaert method against the groundwater storage change calculated from the WT method. The groundwater storage change from the WT method is assumed to be represented by the active groundwater storage change. Active groundwater storage change captures dynamic water table fluctuation and is actively connected with the surficial geology, which is used for porosity estimation. The general coherence between the estimated change and the computed change is observed for

all watersheds regarding the storage change trend and the magnitude although the analysis for a few watersheds exhibits inconsistencies. Explanations from insights into the quality of discharge data are provided to attempt to explain the inconsistency. Seasonal patterns and temporal completeness of discharge data, intricate river networks might introduce errors to drainage system when preparing discharge data for the analysis. But a causality to explain the observed inconsistency is not concluded and merits further research.

9. References

Adams, Roberta. 2016. “Water-Table Elevation and Depth to Water Table Minnesota Hydrogeology Atlas Series Atlas HG-03 Minnesota Department of Natural Resources Ecological and Water Resources Division County Geologic Atlas Program.” (June).

Arciniega-esparza, Saúl, Jose Agustín Breña-naranjo, Antonio Hernández-espriú, Adrián Pedrozo-acuña, Bridget R. Scanlon, Jean Philippe, Michael H. Young, Brad D. Wolaver, and Victor Hugo Alcocer-yamanaka. 2017. “Baseflow Recession Analysis in a Large Shale Play : Climate Variability and Anthropogenic Alterations Mask Effects of Hydraulic Fracturing.” 553:160–71.

Arihood, Leslie D. 2009. Processing, Analysis, and General Evaluation of Well-Driller Logs for Estimating Hydrogeologic Parameters of the Glacial Sediments in a Ground-Water Flow Model of the Lake Michigan Basin.

Bayless, E. R., L. D. Arihood, H. W. Reeves, B. J. S. Sperl, S. L. Qi, V. E. Stipe, and A. .. Bunch. 2017. “Maps and Grids of Hydrogeologic Information Created from Standardized Water-Well Drillers’ Records of the Glaciated United States.” U.S. Geological Survey (Scientific Investigations Report 2015–5105):34.

Biancamaria, Sylvain, Moussa Mballo, Patrick Le Moigne, José Miguel Sánchez Pérez, Grégory Espitalier-Noël, Youen Grusson, Roxelane Cakir, Vincent Häfliger, Florian Barathieu, Marhiu Trasmonte, Aaron Boone, Eric Martin, and Sabine Sauvage. 2019. “Total Water Storage Variability from GRACE Mission and Hydrological Models for a 50,000 Km2 Temperate Watershed: The Garonne River Basin (France).” Journal of Hydrology: Regional Studies 24(April).

Biswal, Basudev and Marco Marani. 2010. “Geomorphological Origin of Recession Curves.” Geophysical Research Letters 37(24):1–5.

Biswal, Basudev and Marco Marani. 2014. “‘Universal’ Recession Curves and Their Geomorphological Interpretation.” Advances in Water Resources 65:34–42.

Biswal, Basudev and D. Nagesh Kumar. 2014. “What Mainly Controls Recession Flows in River Basins?” Advances in Water Resources 65:25–33.

Biswal, Basudev and D. Nagesh Kumar. 2015. “Estimation of ‘drainable’ Storage - A Geomorphological Approach.” Advances in Water Resources 77:37–43.

Biswas, Atrayee, Dipanjan Das Majumdar, and Sayandeep Banerjee. 2014. “Morphometry Governs the Dynamics of a Drainage Basin: Analysis and

Implications.” Geography Journal 2014:1–14.

Boussinesq, M. J. 1868. “Mémoire Sur l’influence Des Frottements Dans Les Mouvements Réguliers Des Fluides.” J. Math. Pure Appl. 13:377–424.

Brutsaert, Wilfried. 1994. “The Unit Response of Groundwater Outflow from a Hillslope.” Water Resources Research 30(10):2759–63.

Brutsaert, Wilfried. 2008. “Long-Term Groundwater Storage Trends Estimated from Streamflow Records: Climatic Perspective.” Water Resources Research 44(2):1–7.

Brutsaert, Wilfried. 2010. “Annual Drought Flow and Groundwater Storage Trends in the Eastern Half of the United States during the Past Two-Third Century.” Theoretical and Applied Climatology 100(1):93–103.

Brutsaert, Wilfried and Hassan Ali Ibrahim. 1966. “On the First and Second Linearization of the Boussinesq Equation.” 549–54.

Brutsaert, Wilfried and John L. Nieber. 1977. “Regionalized Drought Flow Hydrographs from a Mature Glaciated Plateau.” Water Resources Research 13(3):637–43.

Daly, Edoardo and Amilcare Porporato. 2004. “A Note on Groundwater Flow along a Hillslope.” Water Resources Research 40(1):1–5.

European Commission, Joint Research Center. 2018. “Global Surface Water - Data Access.”

Gao, Zhaoliang, Lu Zhang, Lei Cheng, Xiaoping Zhang, Tim Cowan, Wenju Cai, and Wilfried Brutsaert. 2015. “Groundwater Storage Trends in the Loess Plateau of China Estimated from Streamflow Records.” Journal of Hydrology 530:281–90.

Hall, Francis R. 1968. “Base-Flow Recessions—A Review.” Water Resources Research 4(5):973–83.

Heaslet, M. A., A. Alksne. 1961. “Diffusion from a Fixed Surface with a Concentration-Dependent Coefficient.” Journal of the Society for Industrial and Applied Mathematics 9(4):584–96.

J.-Y. Parlange, W. L. Hogarth and Govindaraju. 2000. “On an Exact Analytical Solution of the Boussinesq Equation.” Transport in Porous Media 39(1956):339–45.

Jachens, Elizabeth R., David E. Rupp, Clément Roques, and John S. Selker. 2020. “Recession Analysis Revisited: Impacts of Climate on Parameter Estimation.” Hydrology and Earth System Sciences 24(3):1159–70.

Jacob Bear. 1972. Dynamics of Fluids in Porous Media. New York: Dover, Mineola, New York.

Jean-Francois Pekel, Andrew Cottam, Noel Gorelick, Alan S. Belward. 2016. "High-Resolution Mapping of Global Surface Water and Its Long-Term Changes." Nature 540:418–22.

Johnson, E.A. and Dils, R. E. 1956. "Outline for Compiling Precipitation, Runoff, and Ground Water Data from Small Watersheds." US For. Serv. Southeast 68.

Kanivetsky, R. 1979. S-02 Hydrogeologic Map of Minnesota, Bedrock Hydrogeology.

Kirchner, James W. 2009. "Catchments as Simple Dynamical Systems: Catchment Characterization, Rainfall-Runoff Modeling, and Doing Hydrology Backward." Water Resources Research 45(2):1–34.

Krause, P., D. P. Boyle, and F. Base. 2005. "Comparison of Different Efficiency Criteria for Hydrological Model Assessment." Advances in Geosciences 5:89–97.

Langbein, W. B. 1937. Some Channel Storage Studies and Their Applicatin to the Determination of Infiltration.

Lockington, D. A. 1997. "Response of Unconfined Aquifer to Sudden Change in Boundary Head." Journal of Irrigation and Drainage Engineering 123:24–27.

Longuevergne, Laurent, Nicolas Florsch, and Philippe Elsass. 2007. "Extracting Coherent Regional Information from Local Measurements with Karhunen-Loève Transform: Case Study of an Alluvial Aquifer (Rhine Valley, France and Germany)." Water Resources Research 43(4):1–13.

Lyon, Steve W., Alexander Koutsouris, Friedemann Scheibler, Jerker Jarsjö, Rene Mbanguka, Madaka Tumbo, Keven K. Robert, Asha N. Sharma, and Ype van der Velde. 2015. "Interpreting Characteristic Drainage Timescale Variability across Kilombero Valley, Tanzania." Hydrological Processes 29(8):1912–24.

Masoumi, Zohreh, Abolfazl Rezaei, and Jamshid Maleki. 2019. "Improvement of Water Table Interpolation and Groundwater Storage Volume Using Fuzzy Computations." Environmental Monitoring and Assessment 191(6):1–15.

MNDNR. 2016. Procedure for Determining Buried Aquifer and Bedrock Surface Pollution Sensitivity.

Nieber, John L. 2020. "Techniques for Water Storage Estimates in Central Minnesota." Environment and Natural Resources Trust Fund M.K. 2017; Chp.96; Sec. 2; Subd. 04h.

Olsen, Bruce M.; Mossler, John H. 1982. "S-15 Geologic Map of Minnesota,

Bedrock Topography."

Patnaik, Swagat, Basudev Biswal, D. Nagesh Kumar, and Bellie Sivakumar. 2015. "Effect of Catchment Characteristics on the Relationship between Past Discharge and the Power Law Recession Coefficient." Journal of Hydrology 528:321–28.

Polubarinova-Kochina, P. Ya. 1962. Theory of Groundwater Movement. edited by R. J. M. De Wiest. Princeton, N.J.: Princeton University Press.

Rader, Nancy. 2014. Minnesota Geographic Metadata Guidelines.

Rezanezhad, Fereidoun, Jonathan S. Price, William L. Quinton, Bernd Lennartz, Tatjana Milojevic, and Philippe Van Cappellen. 2016. "Structure of Peat Soils and Implications for Water Storage, Flow and Solute Transport: A Review Update for Geochemists." Chemical Geology 429:75–84.

Roques, Clément, David E. Rupp, and John S. Selker. 2017. "Improved Streamflow Recession Parameter Estimation with Attention to Calculation of − DQ/Dt." Advances in Water Resources 108:29–43.

Rupp, David E. and John S. Selker. 2005. "Drainage of a Horizontal Boussinesq Aquifer with a Power Law Hydraulic Conductivity Profile." Water Resources Research 41(11):1–8.

Rupp, David E. and John S. Selker. 2006. "On the Use of the Boussinesq Equation for Interpreting Recession Hydrographs from Sloping Aquifers." Water Resources Research 42(12):1–15.

Scanlon, B. R., L. Longuevergne, and D. Long. 2012. "Ground Referencing GRACE Satellite Estimates of Groundwater Storage Changes in the California Central Valley, USA." Water Resources Research 48(4):1–9.

Senay, Gabriel B., Stefanie Bohms, Ramesh K. Singh, Prasanna H. Gowda, Naga M. Velpuri, Henok Alemu, and James P. Verdin. 2013. "Operational Evapotranspiration Mapping Using Remote Sensing and Weather Datasets: A New Parameterization for the SSEB Approach." JAWRA Journal of the American Water Resources Association 49(3):577–91.

Shaw, Stephen B. and Susan J. Riha. 2012. "Examining Individual Recession Events Instead of a Data Cloud: Using a Modified Interpretation of DQ/Dt-Q Streamflow Recession in Glaciated Watersheds to Better Inform Models of Low Flow." Journal of Hydrology 434–435:46–54.

Shiklomanov IA, Rodda JC. 2003. World Water Resources at the Beginning of the Twenty-First Century. Cambridge University.

Skaugen, Thomas and Zelalem Mengistu. 2016. "Estimating Catchment-Scale

Groundwater Dynamics from Recession Analysis – Enhanced Constraining of Hydrological Models." 4963–81.

Stoelzle, M., K. Stahl, and M. Weiler. 2013. "Are Streamflow Recession Characteristics Really Characteristic?" Hydrology and Earth System Sciences 17(2):817–28.

Tague, Christina and Gordon E. Grant. 2009. "Groundwater Dynamics Mediate Low-Flow Response to Global Warming in Snow-Dominated Alpine Regions." 45(May):1–12.

Tallaksen, L. M. 1995. "A Review of Baseflow Recession Analysis." Journal of Hydrology 165(1–4):349–70.

Theis, Charles V. 1935. "The Relation between the Lowering of the Piezometric Surface and the Rate and Duration of Discharge of a Well Using Ground-Water Storage." Transactions, American Geophysical Union 16(2):519.

Thomas, Brian F., Richard M. Vogel, and James S. Famiglietti. 2015. "Objective Hydrograph Baseflow Recession Analysis." JOURNAL OF HYDROLOGY 525:102–12.

Thornton, P.E., M.M. Thornton, and R. S. Vose. 2018. "Daymet: Daily Surface Weather Data on a 1-Km Grid for North America, Version 3."

Toebes, C., and D. D. Strang. 1964. "On Recession Curves: 1 - Recession Equations." Jounal of Hydrology (New Zealand) 3(2):2–14.

Troch, Peter A., Alexis Berne, Patrick Bogaart, Ciaran Harman, Arno G. J. Hilberts, Steve W. Lyon, Claudio Paniconi, Valentijn R. N. Pauwels, David E. Rupp, John S. Selker, Adriaan J. Teuling, Remko Uijlenhoet, and Niko E. C. Verhoest. 2013. "The Importance of Hydraulic Groundwater Theory in Catchment Hydrology: The Legacy of Wilfried Brutsaert and Jean-Yves Parlange." Water Resources Research 49(9):5099–5116.

Velpuri, N. M., G. B. Senay, R. K. Singh, S. Bohms, and J. P. Verdin. 2013. "A Comprehensive Evaluation of Two MODIS Evapotranspiration Products over the Conterminous United States: Using Point and Gridded FLUXNET and Water Balance ET." Remote Sensing of Environment 139:35–49.

Vogel, Richard M. and Charles N. Kroll. 1992. "Regional Geohydrologic-Geomorphic Relationships for the Estimation of Low-Flow Statistics." Water Resources Research 28(9):2451–58.

W. L. Hogarth, J. Y. Parlange. 1999. "Solving the Boussinesq Equation Using Solutions of the Blasius Equation." Water Resources Research 35(3):885–87.

Zeb Thomas, Jamie Schulz. 2014. "DNR Hydrography Dataset."

Zhang, Lu, Wilfried Brutsaert, Russell Crosbie, and Nick Potter. 2014. “Long-Term Annual Groundwater Storage Trends in Australian Catchments.” Advances in Water Resources 74:156–65.

Appendix – Recession Plot for Implementing the Brutsaert-Nieber Analysis

Graphic results of recession analysis are shown in this appendix. The recession data were selected based on two recession criteria: hydrology inequality criterion and Brutsaert criterion. For each catchment, two sets of recession data were selected from gauging observed discharge, each of which was prepared for conducting the baseflow recession analysis in a form of the Brutsaert-Nieber method. The Brutsaert-Nieber method analyses the data points $-dq/dt$ against q to derive the drainage characteristics, such as K. These data cloud figures for each catchment in the study area, with corresponding selected recessions plotted to identify seasonal patterns, are given in this appendix as the exhibition of graphic results of this thesis. The analysis results to the gauging station 12039001 is not listed in the appendix since it has already been illustrated in Figure 13.

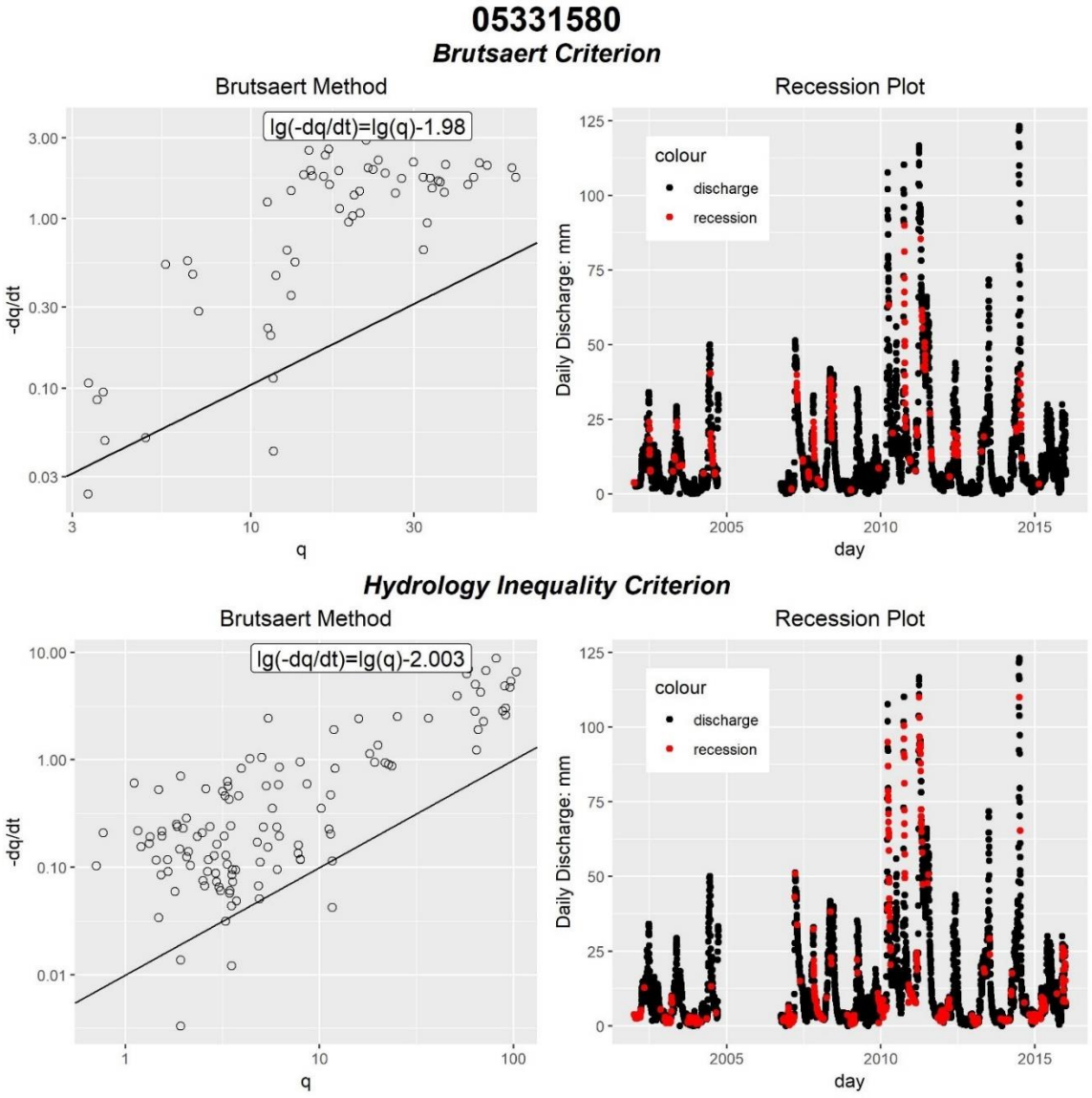

Figure 17. Graphic results after adopting Brutsaert-Nieber method for baseflow recession analysis in the catchment with the gauging station 5331580.

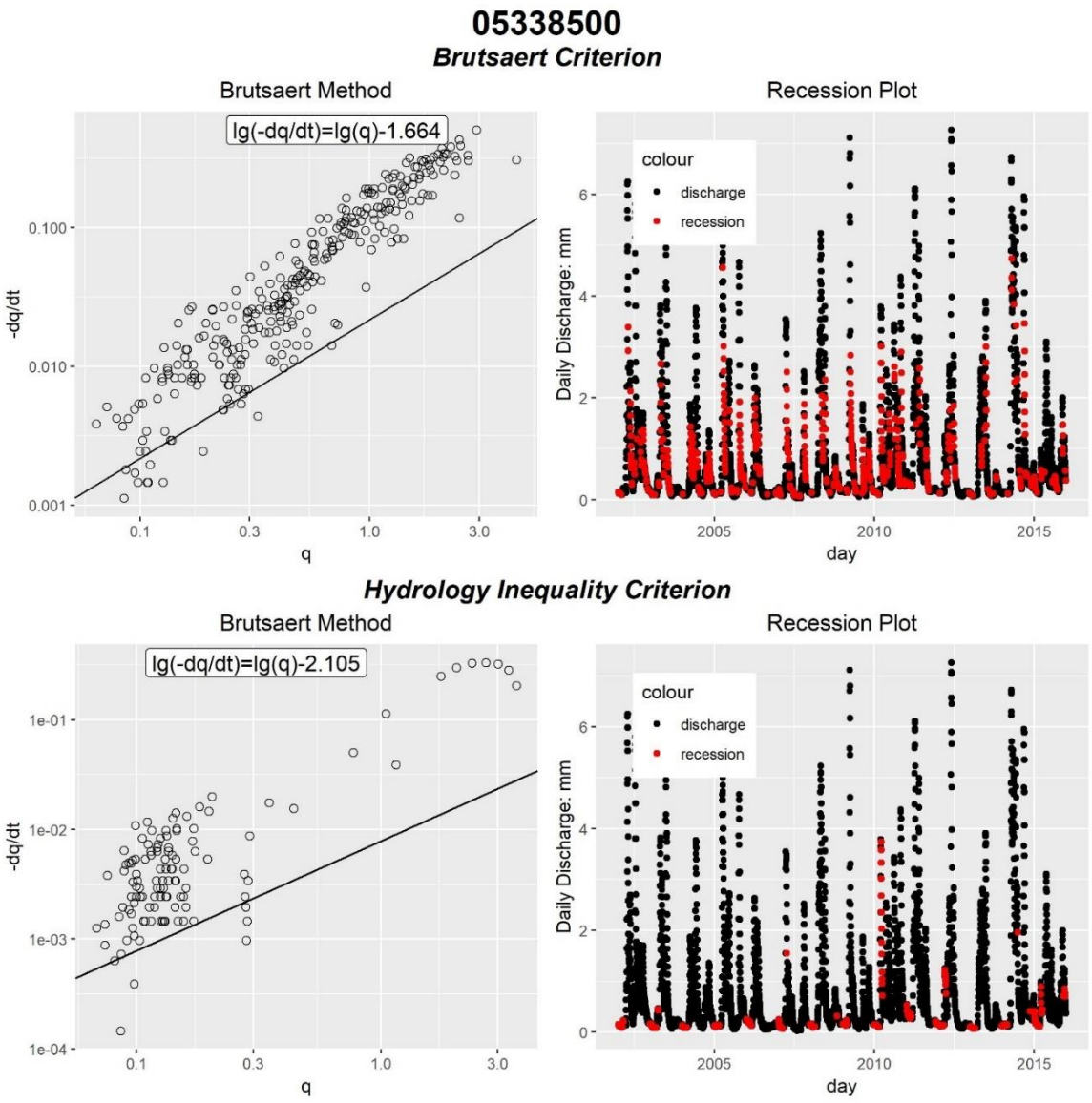

Figure 18. Graphic results after adopting Brutsaert-Nieber method for baseflow recession analysis in the catchment with the gauging station 5335800.

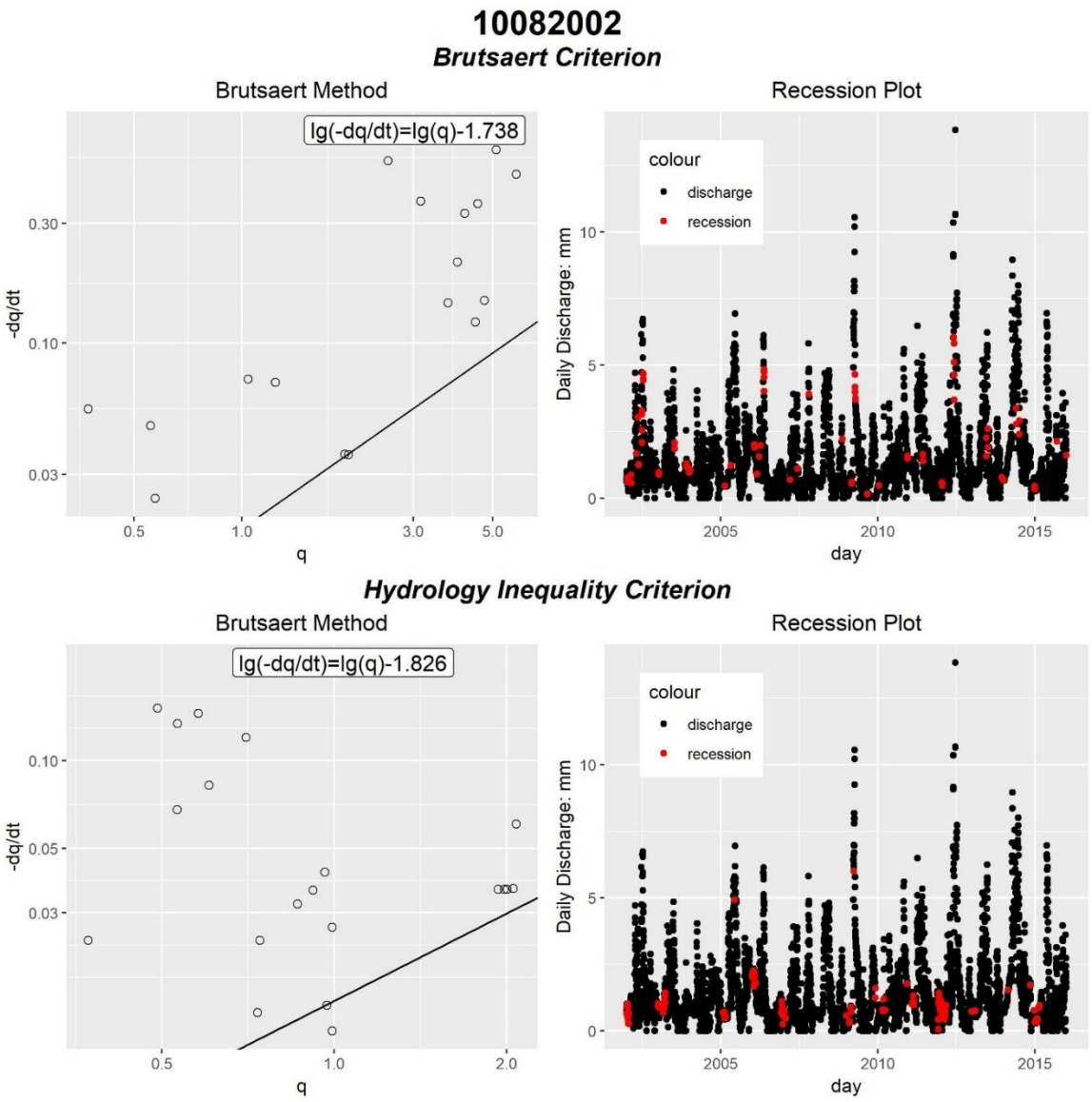

Figure 19. Graphic results after adopting Brutsaert-Nieber method for baseflow recession analysis in the catchment with the gauging station 10082002.

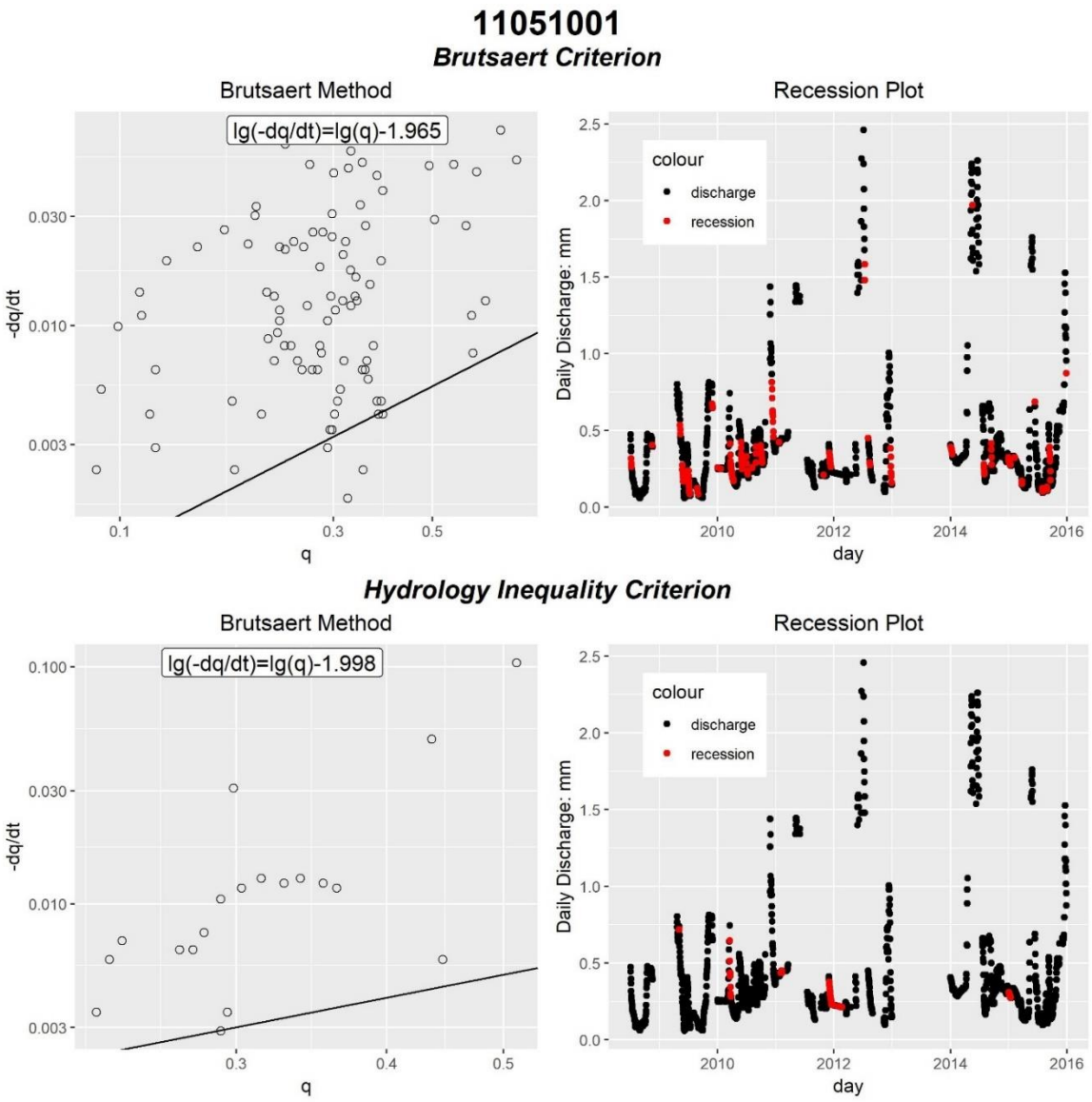

Figure 20. Graphic results after adopting Brutsaert-Nieber method for baseflow recession analysis in the catchment with the gauging station 11051001.

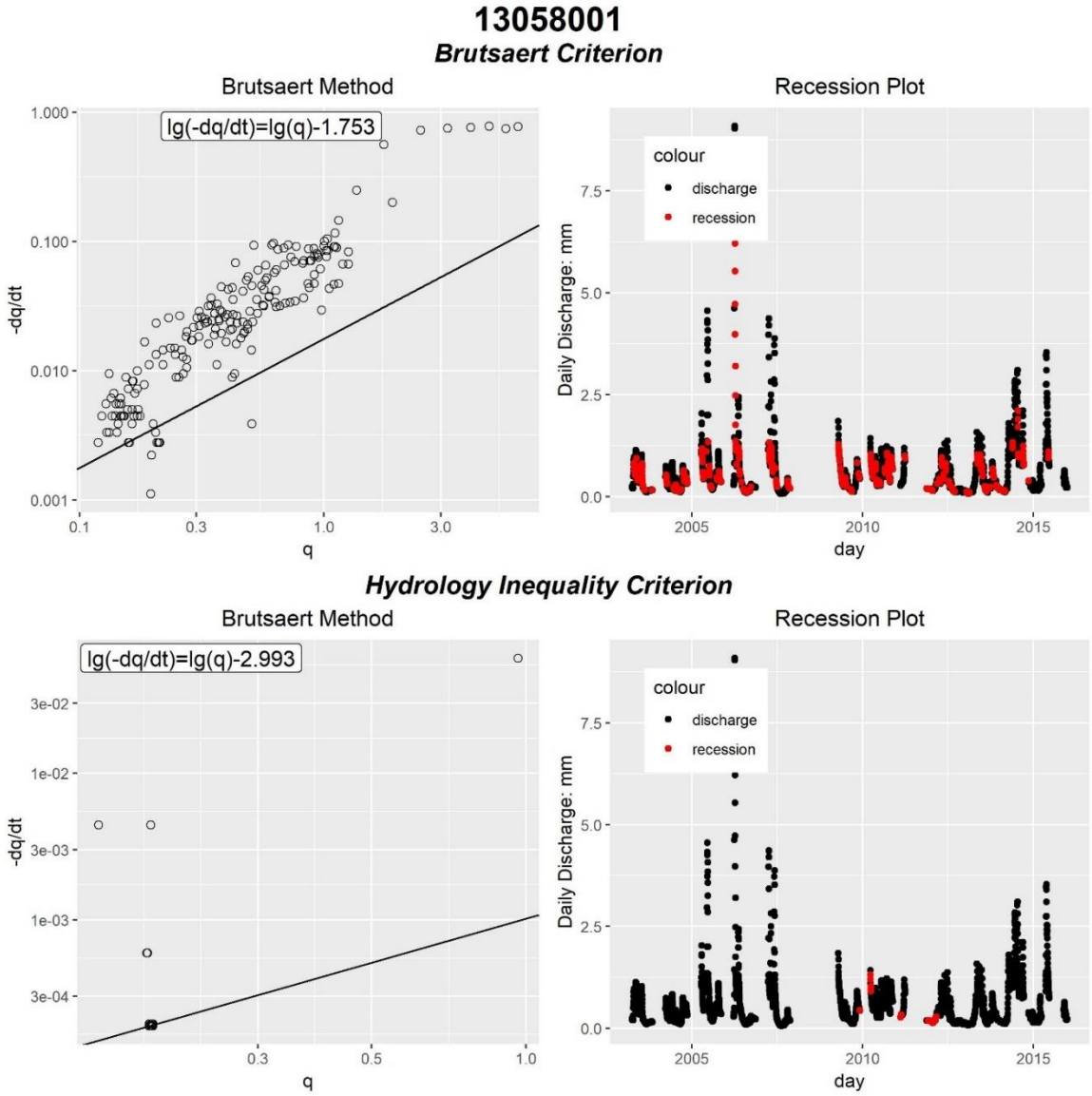

Figure 21. Graphic results after adopting Brutsaert-Nieber method for baseflow recession analysis in the catchment with the gauging station 13058001.

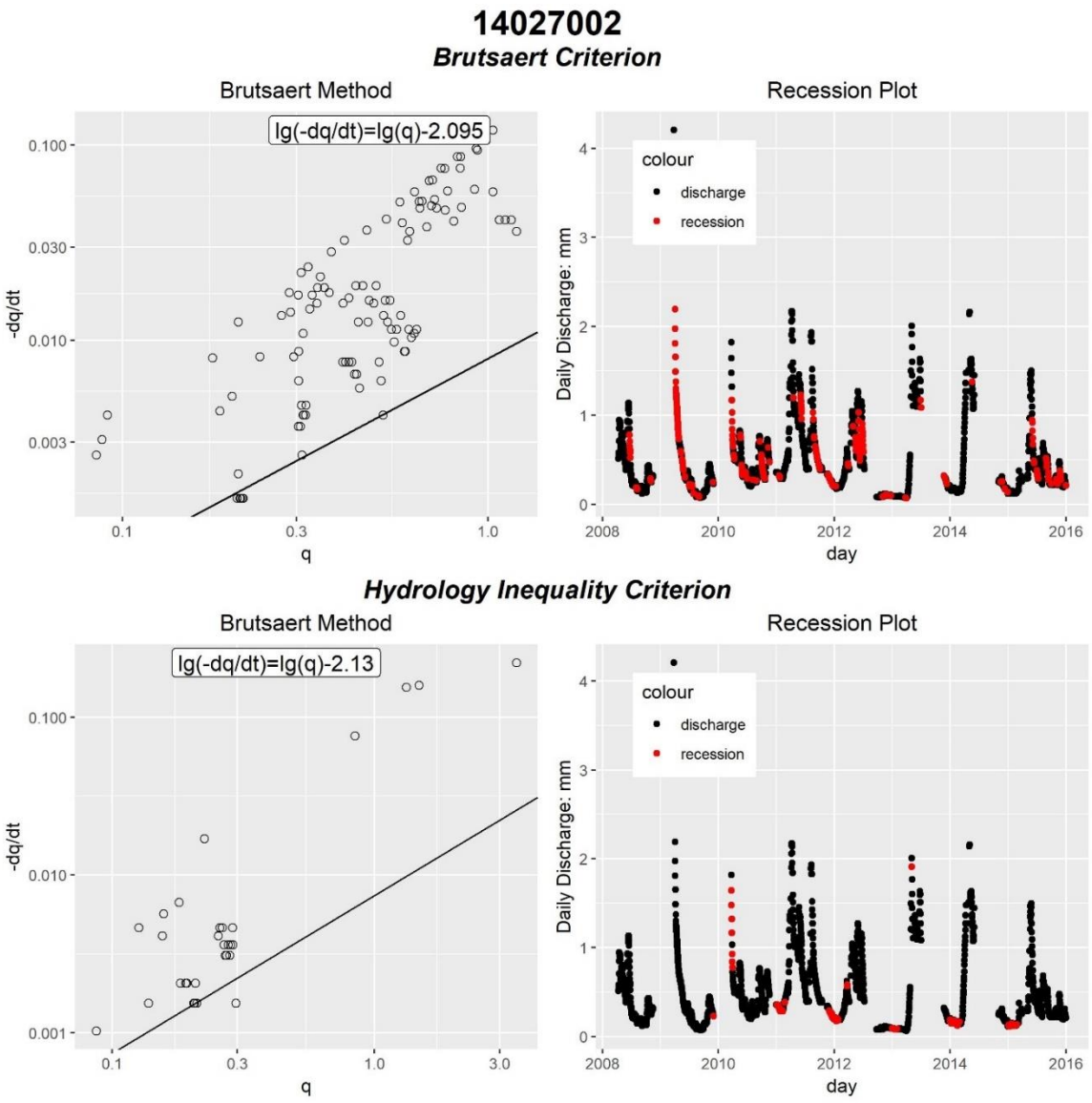

Figure 22. Graphic results after adopting Brutsaert-Nieber method for baseflow recession analysis in the catchment with the gauging station 14027002.

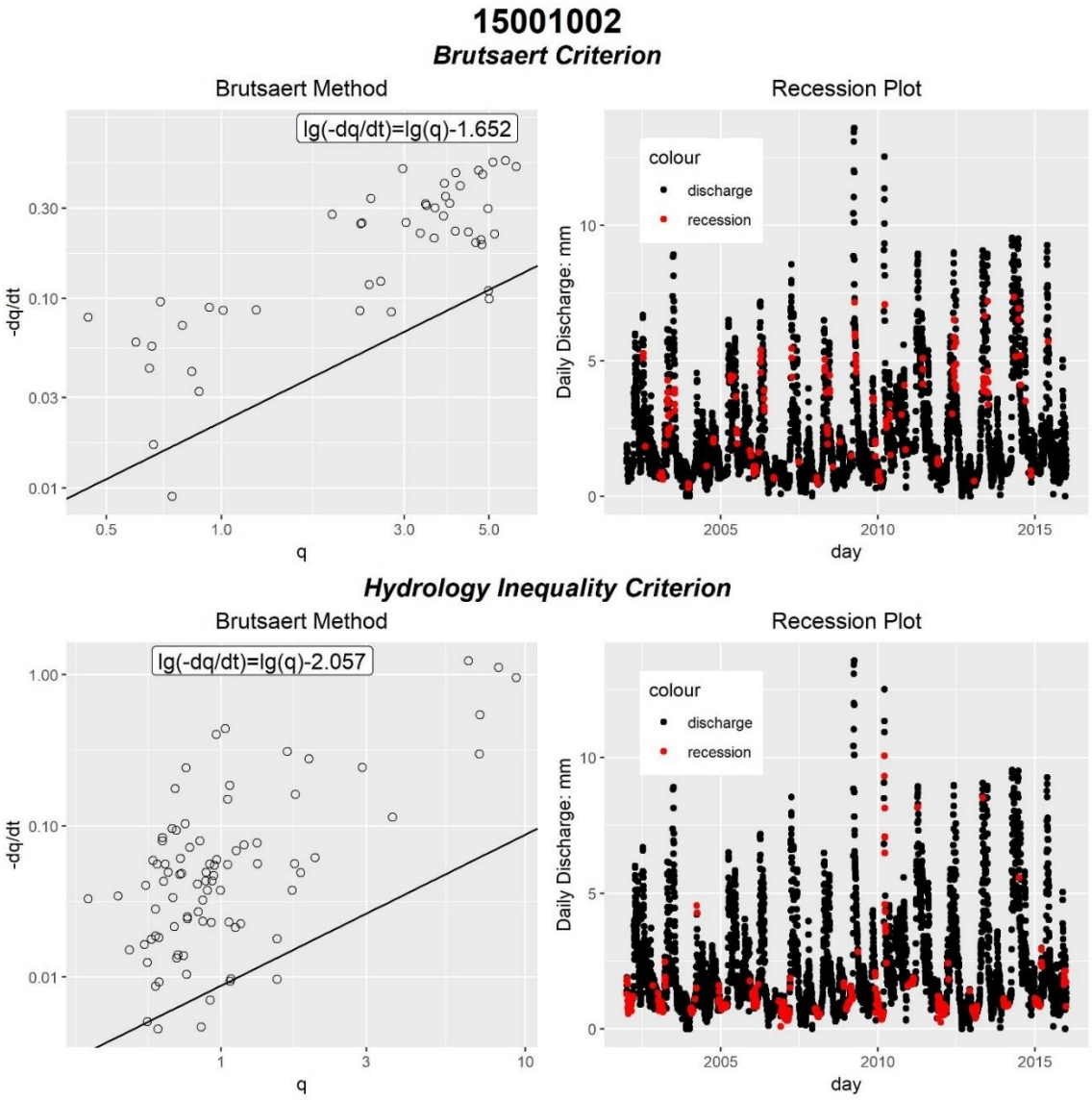

Figure 23. Graphic results after adopting Brutsaert-Nieber method for baseflow recession analysis in the catchment with the gauging station 15001002.

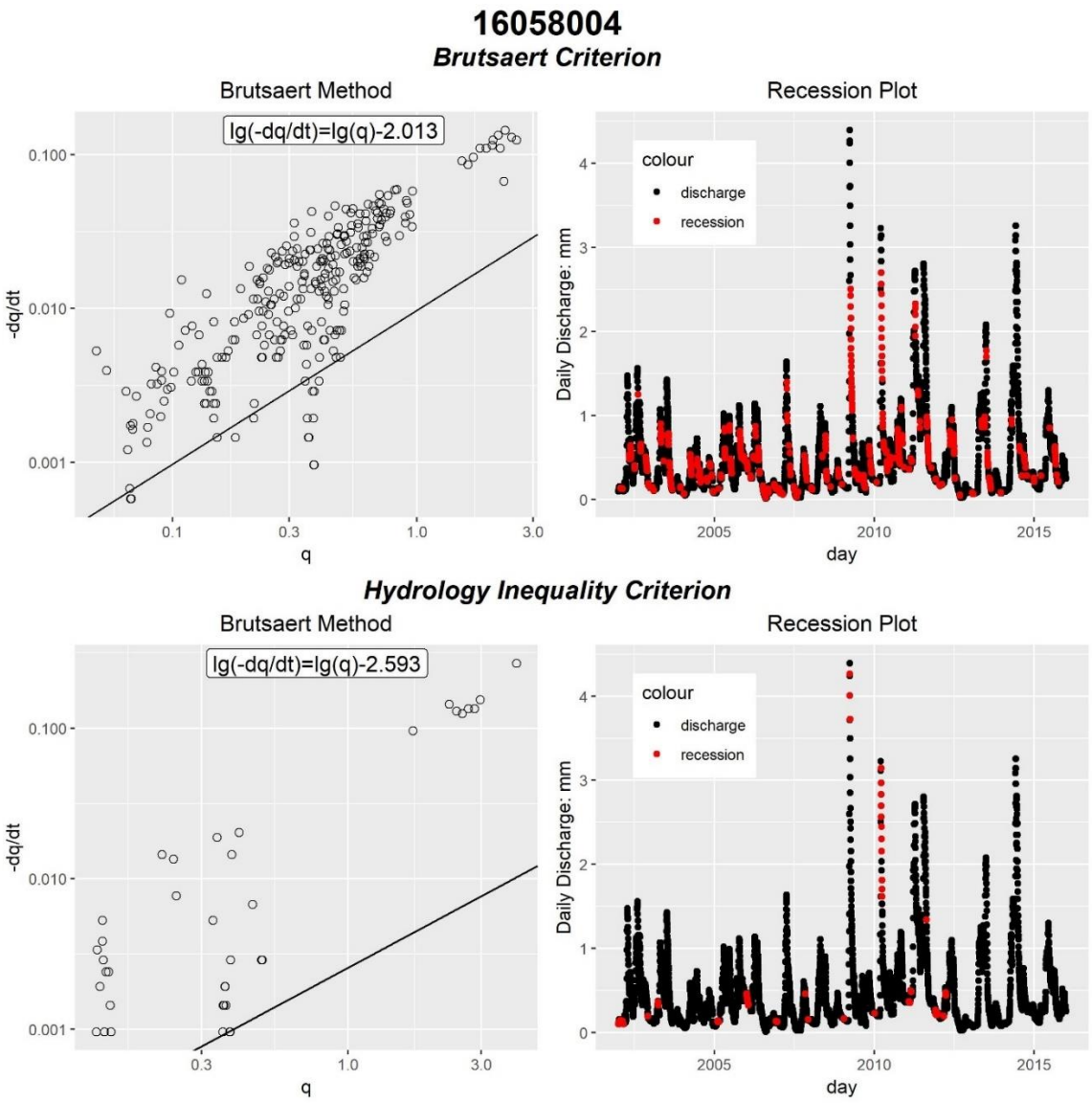

Figure 24. Graphic results after adopting Brutsaert-Nieber method for baseflow recession analysis in the catchment with the gauging station 16058004.

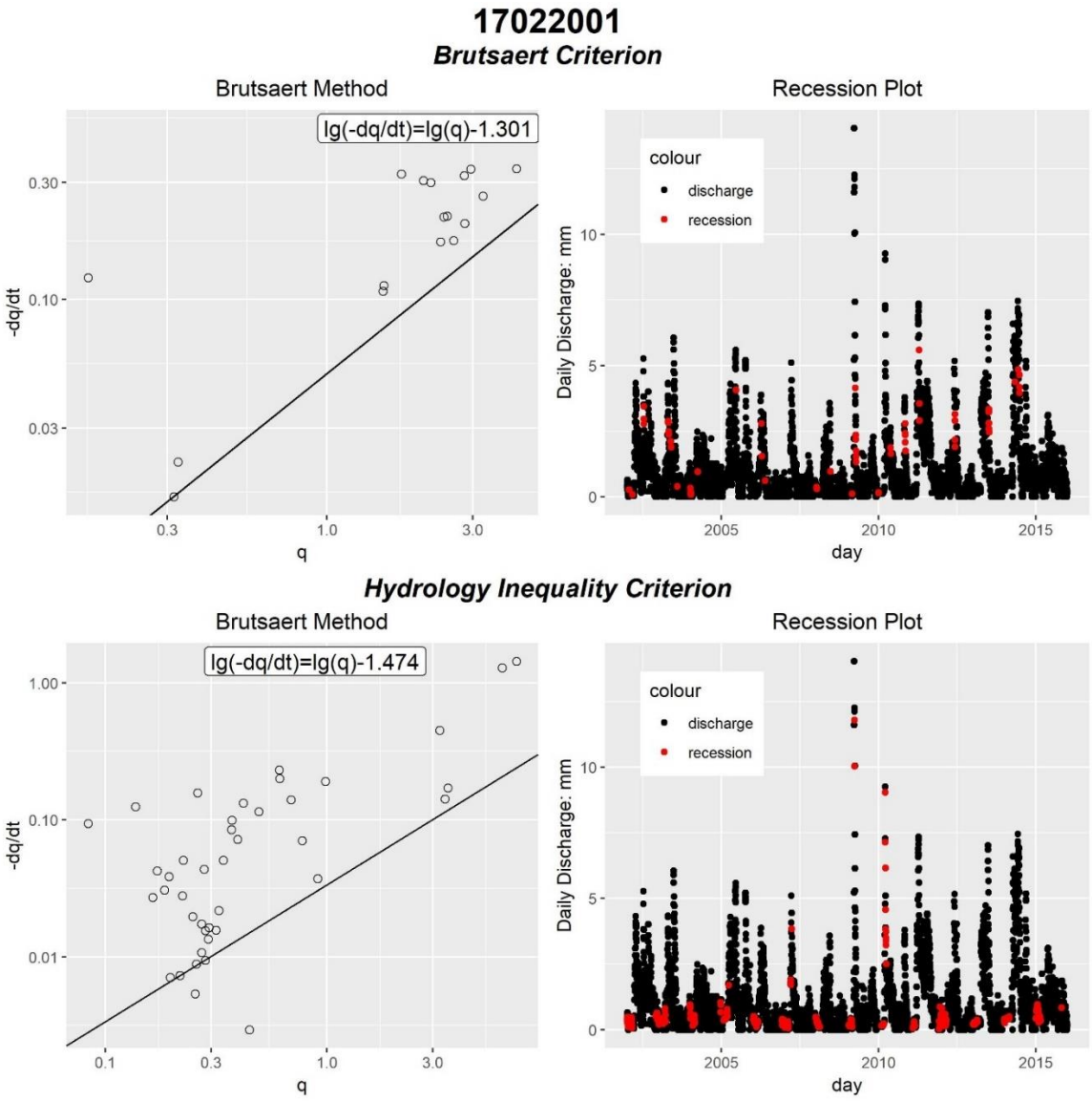

Figure 25. Graphic results after adopting Brutsaert-Nieber method for baseflow recession analysis in the catchment with the gauging station 17022001.

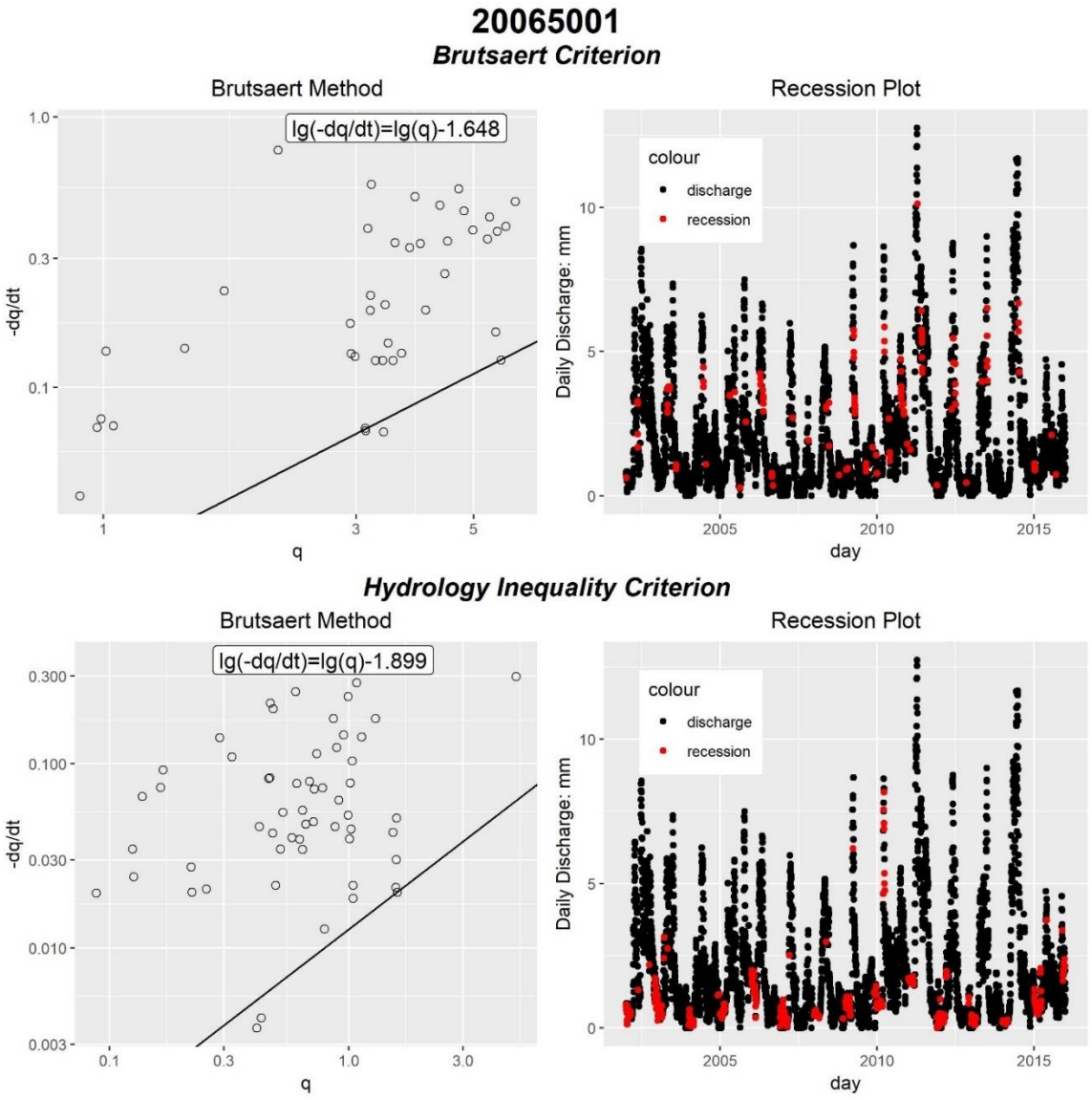

Figure 26. Graphic results after adopting Brutsaert-Nieber method for baseflow recession analysis in the catchment with the gauging station 20065001.

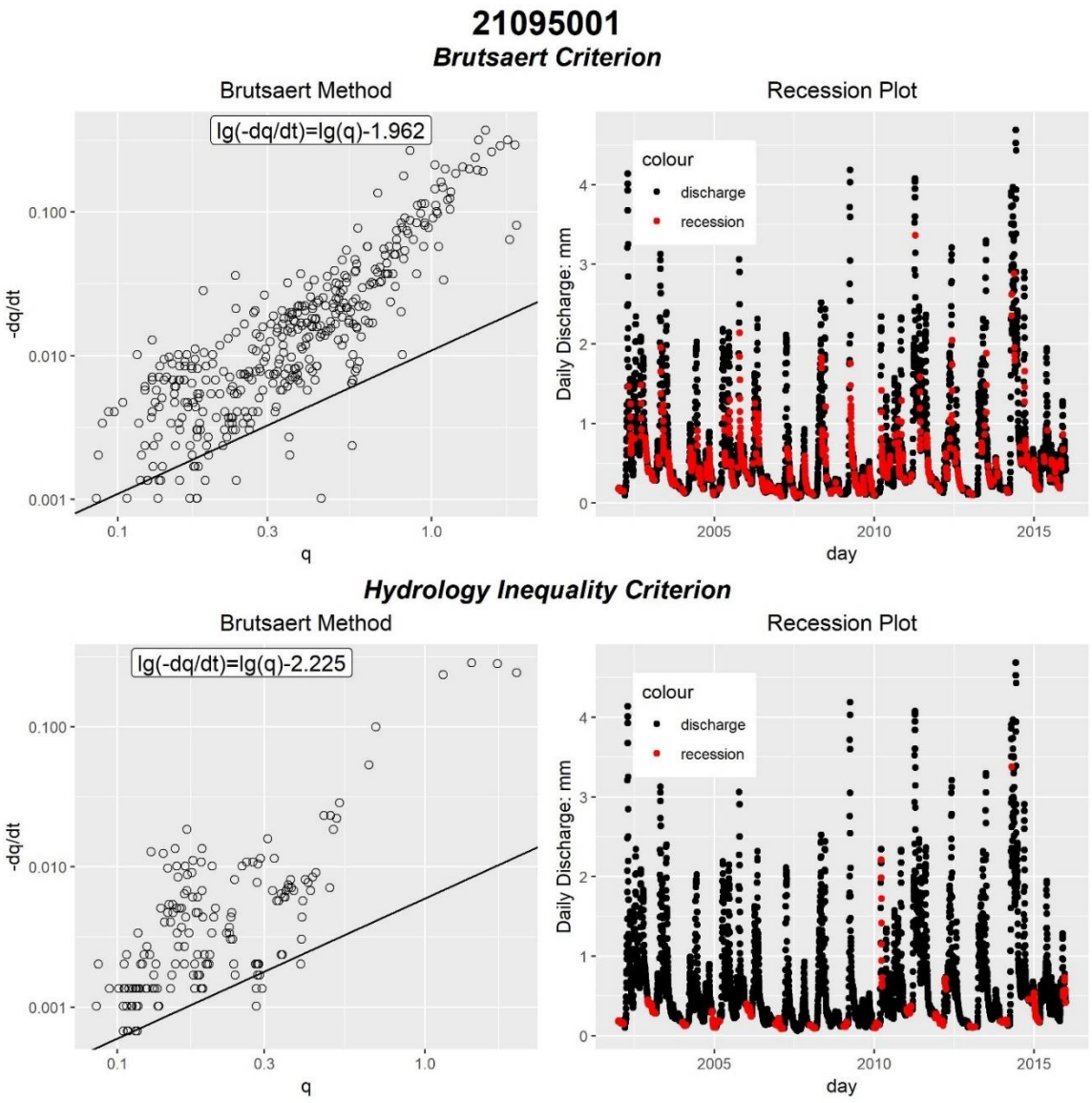

Figure 27. Graphic results after adopting Brutsaert-Nieber method for baseflow recession analysis in the catchment with the gauging station 21095001.

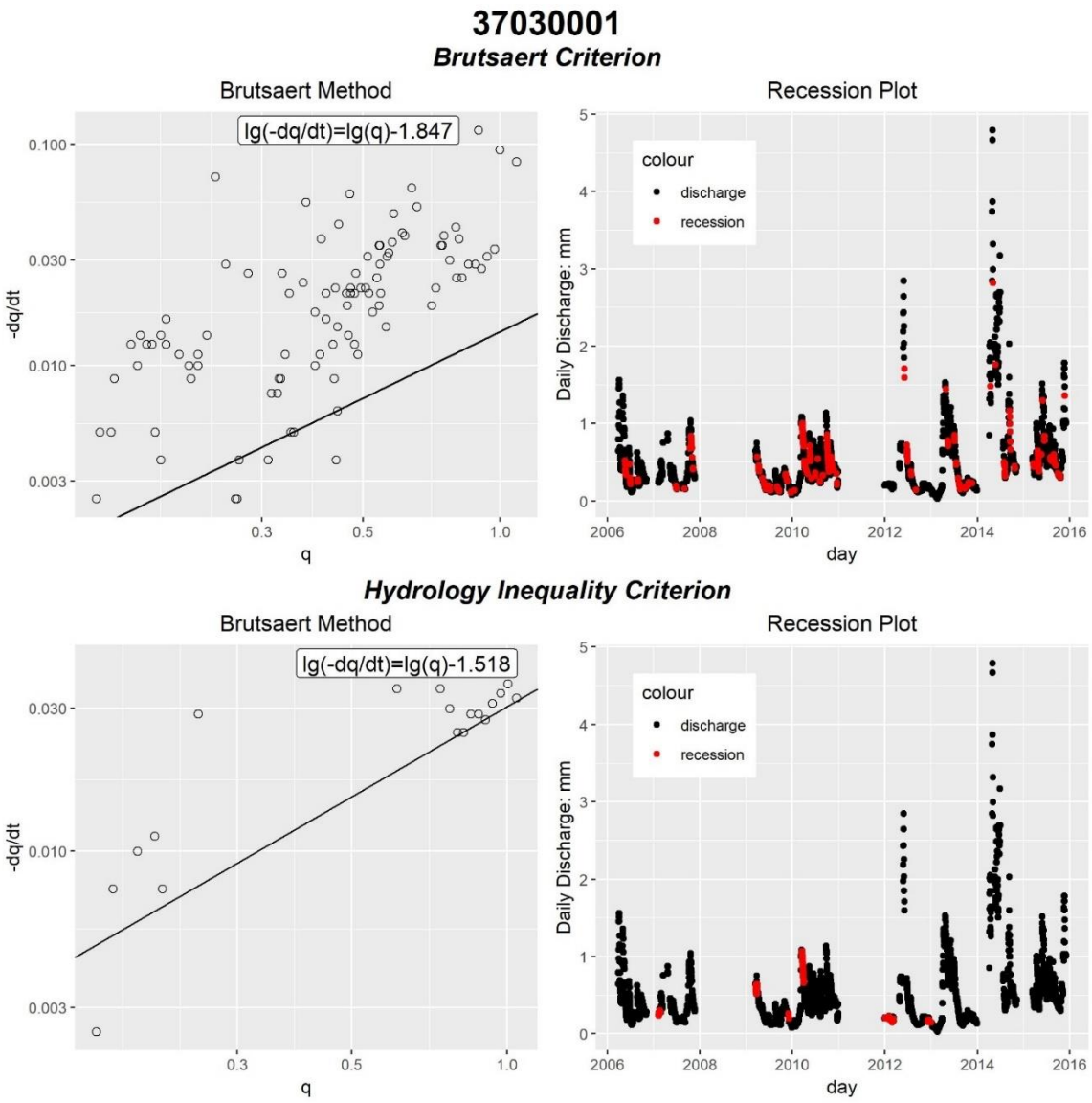

Figure 28. Graphic results after adopting Brutsaert-Nieber method for baseflow recession analysis in the catchment with the gauging station 37030001.

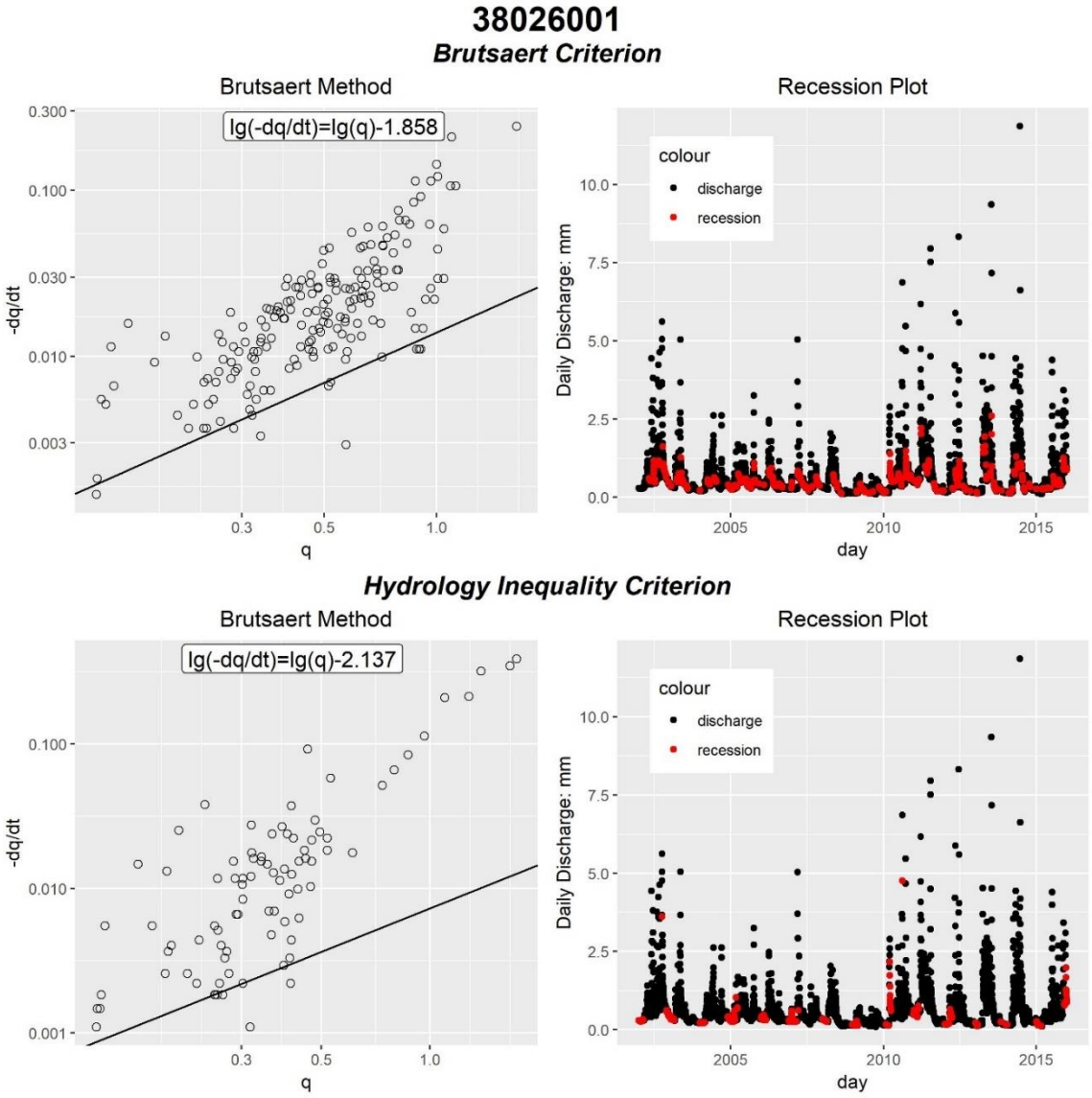

Figure 29. Graphic results after adopting Brutsaert-Nieber method for baseflow recession analysis in the catchment with the gauging station 38026001.

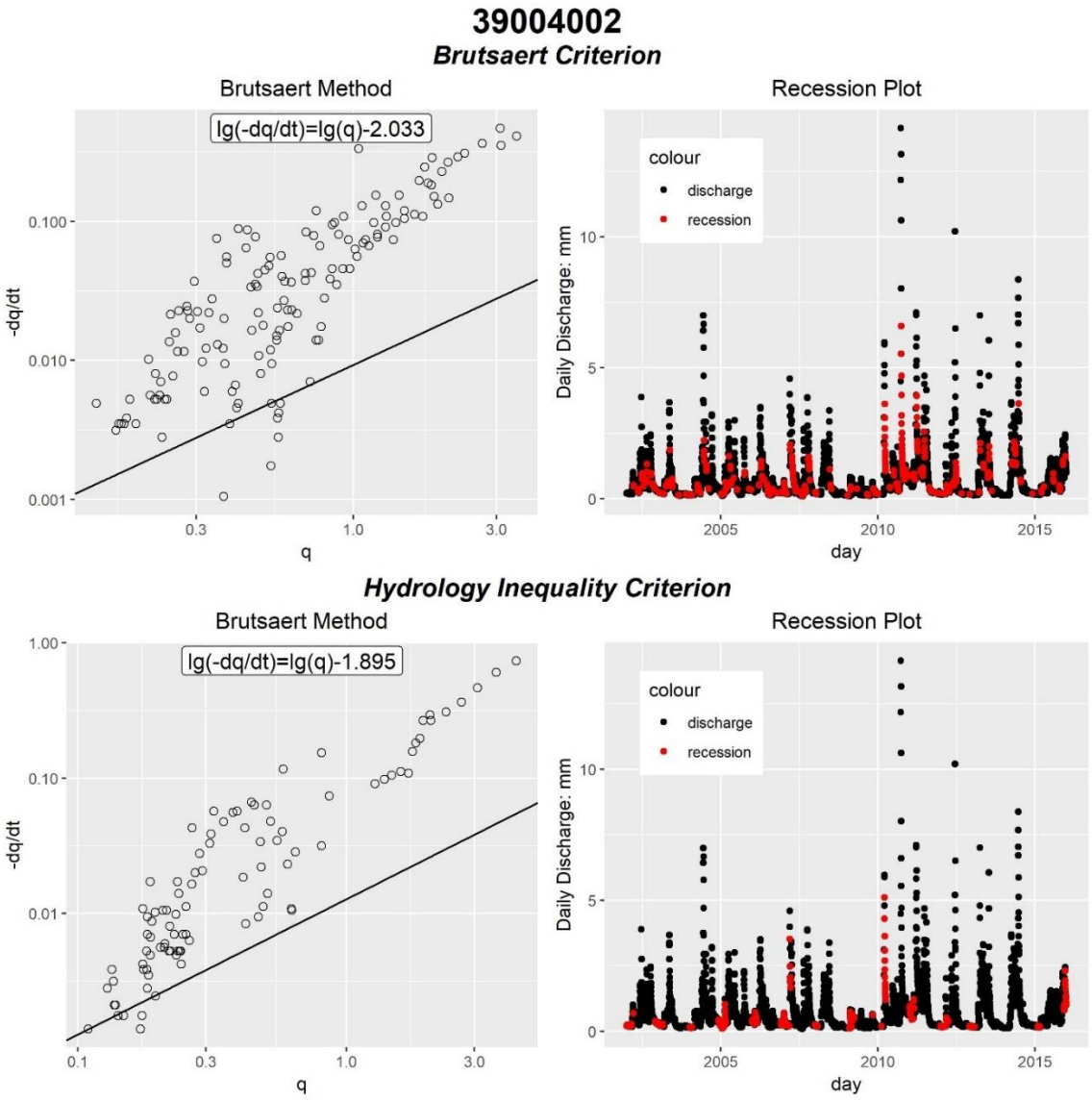

Figure 30. Graphic results after adopting Brutsaert-Nieber method for baseflow recession analysis in the catchment with the gauging station 39004002.

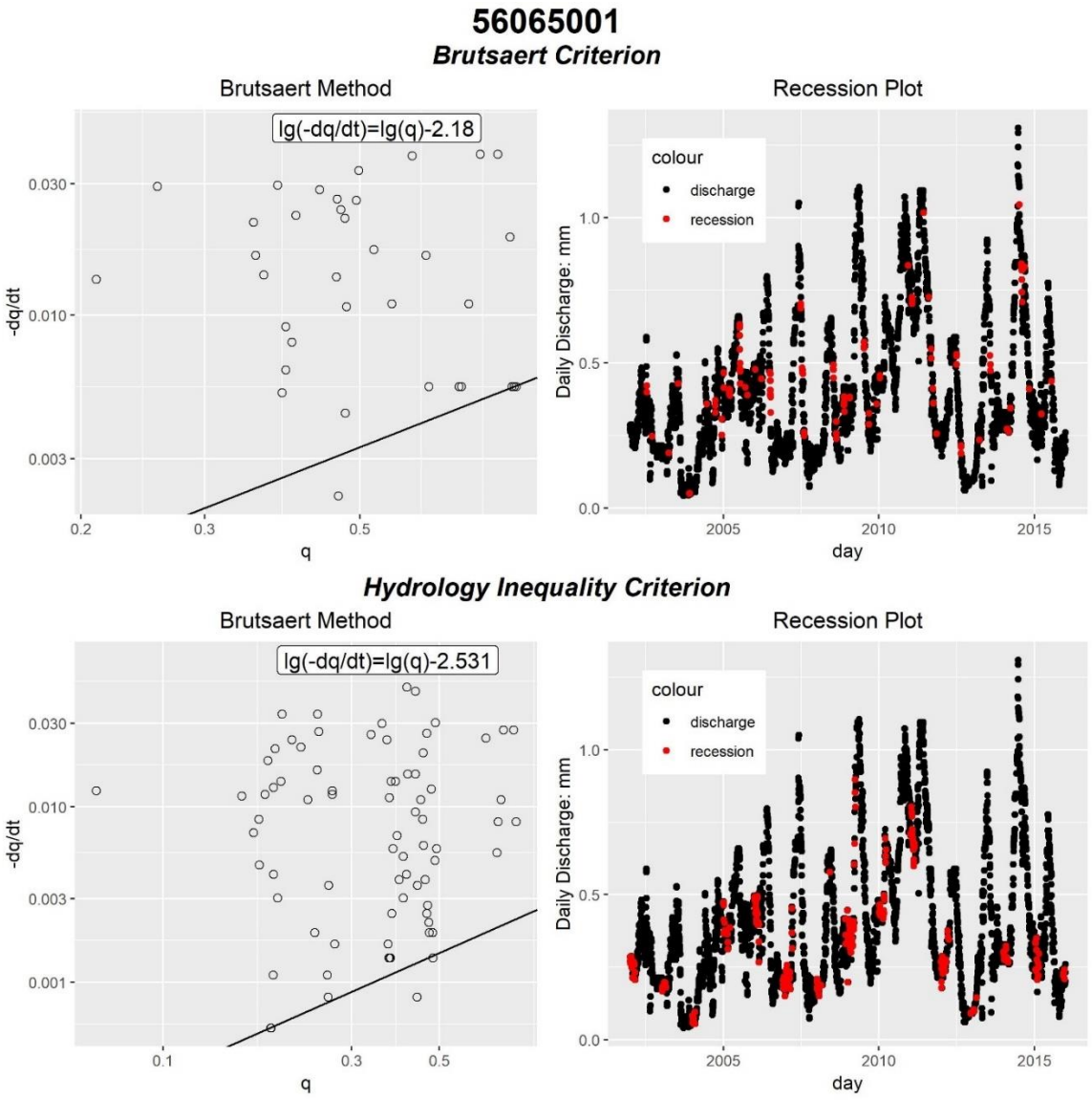

Figure 31. Graphic results after adopting Brutsaert-Nieber method for baseflow recession analysis in the catchment with the gauging station 56065001.

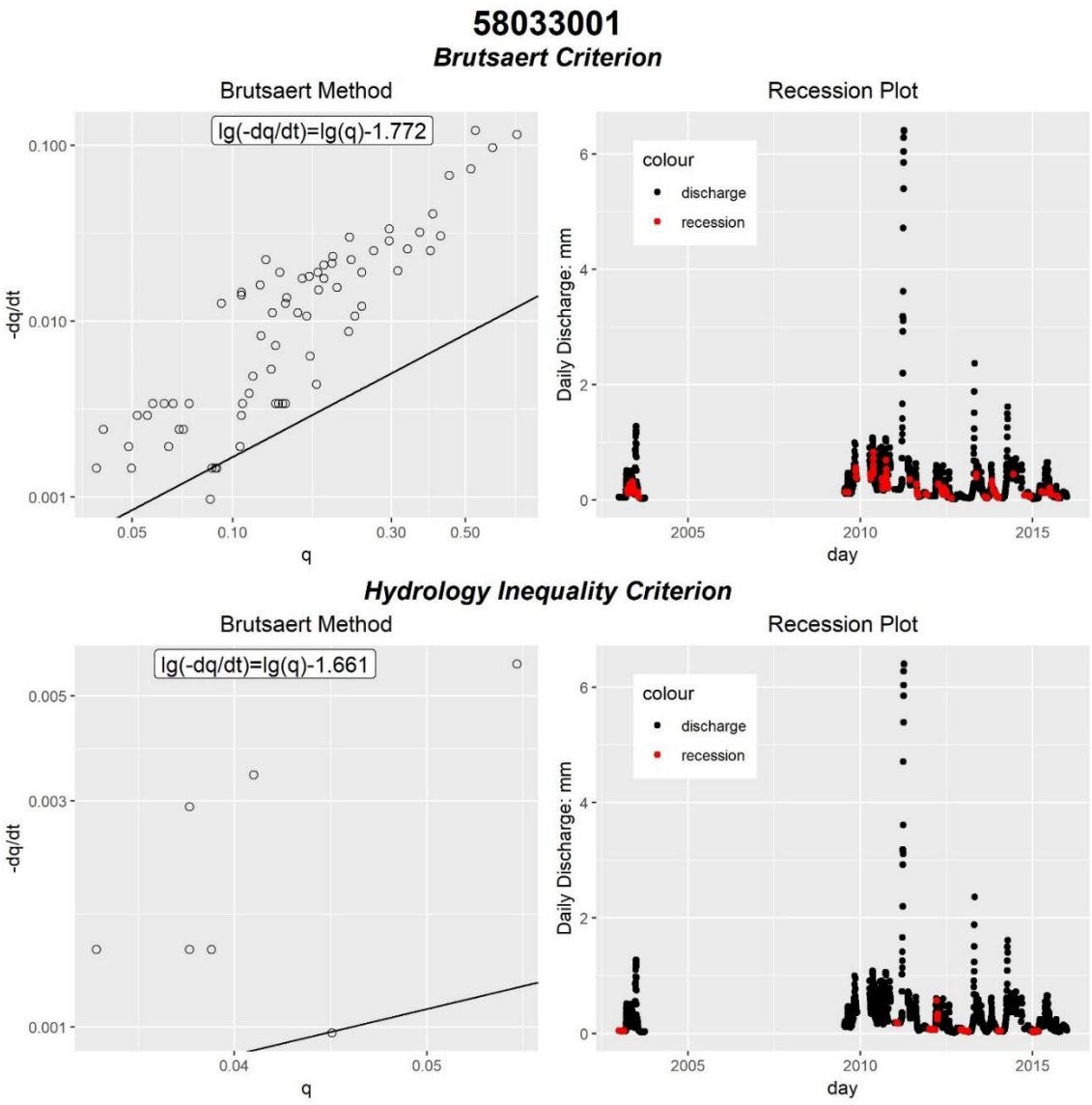

Figure 32. Graphic results after adopting Brutsaert-Nieber method for baseflow recession analysis in the catchment with the gauging station 58033001.

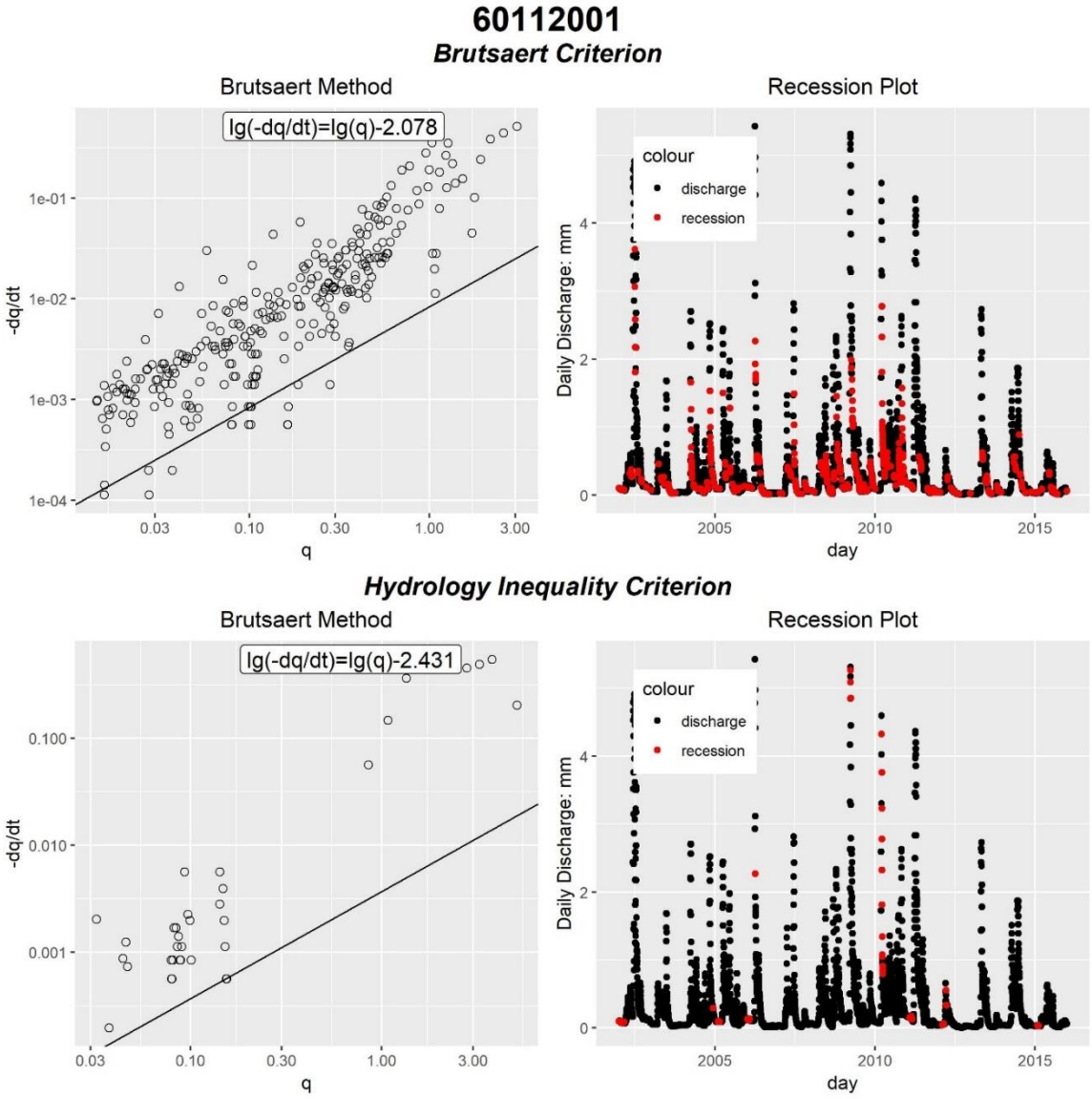

Figure 33. Graphic results after adopting Brutsaert-Nieber method for baseflow recession analysis in the catchment with the gauging station 60112001.